

# Recommendations and guidelines from the ISMIRM Diffusion Study Group for preclinical diffusion MRI: Part 2 — *Ex vivo* imaging

Kurt G Schilling<sup>1,2,#</sup>, Francesco Grussu<sup>3,4</sup>, Andrada Ianus<sup>5</sup>, Brian Hansen<sup>6</sup>, Rachel L C Barrett<sup>7,8</sup>, Manisha Aggarwal<sup>9</sup>, Stijn Michielse<sup>10</sup>, Fatima Nasrallah<sup>11</sup>, Warda Syeda<sup>12</sup>, Nian Wang<sup>13,14</sup>, Jelle Veraart<sup>15</sup>, Alard Roebroek<sup>16</sup>, Andrew F Bagdasarian<sup>17,18</sup>, Cornelius Eichner<sup>19</sup>, Farshid Sepehrband<sup>20</sup>, Jan Zimmermann<sup>21</sup>, Lucas Soustelle<sup>22</sup>, Christien Bowman<sup>23,24</sup>, Benjamin C Tandler<sup>25</sup>, Andreea Hertanu<sup>26</sup>, Ben Jeurissen<sup>27,28</sup>, Lucio Frydman<sup>29</sup>, Yohan van de Looij<sup>30</sup>, David Hike<sup>17,18</sup>, Jeff F Dunn<sup>31,32,33</sup>, Karla Miller<sup>34</sup>, Bennett A Landman<sup>35</sup>, Noam Shemesh<sup>5</sup>, Adam Anderson<sup>36,2</sup>, Emilie McKinnon<sup>37</sup>, Shawna Farquharson<sup>38</sup>, Flavio Dell'Acqua<sup>39</sup>, Carlo Pierpaoli<sup>40</sup>, Ivana Drobnjak<sup>41</sup>, Alexander Leemans<sup>42</sup>, Kevin D Harkins<sup>1,2,43</sup>, Maxime Descoteaux<sup>44,45</sup>, Duan Xu<sup>46</sup>, Hao Huang<sup>47,48</sup>, Mathieu D Santin<sup>49,50</sup>, Samuel C. Grant<sup>17,18</sup>, Andre Obenaus<sup>51,52</sup>, Gene S Kim<sup>53</sup>, Dan Wu<sup>54</sup>, Denis Le Bihan<sup>55,56</sup>, Stephen J Blackband<sup>57,58,59</sup>, Luisa Ciobanu<sup>60</sup>, Els Fieremans<sup>61</sup>, Ruiliang Bai<sup>62,63</sup>, Trygve Leergaard<sup>64</sup>, Jiayang Zhang<sup>65</sup>, Tim B Dyrby<sup>66,67</sup>, G Allan Johnson<sup>68,69</sup>, Julien Cohen-Adad<sup>70,71,72</sup>, Matthew D Budde<sup>73,74</sup>, Ileana O Jelescu<sup>26,75,3</sup>

#Corresponding authors — [kurt.g.schilling.1@vumc.org](mailto:kurt.g.schilling.1@vumc.org), [ileana.jelescu@chuv.ch](mailto:ileana.jelescu@chuv.ch)

<sup>1</sup>Radiology and Radiological Sciences, Vanderbilt University Medical Center, Nashville, TN, USA, <sup>2</sup>Vanderbilt University Institute of Imaging Science, Vanderbilt University, Nashville, TN, <sup>3</sup>Radiomics Group, Vall d'Hebron Institute of Oncology, Vall d'Hebron Barcelona Hospital Campus, Barcelona, Spain, <sup>4</sup>Queen Square MS Centre, Queen Square Institute of Neurology, Faculty of Brain Sciences, University College London, London, UK, <sup>5</sup>Champalimaud Research, Champalimaud Foundation, Lisbon, Portugal, <sup>6</sup>Center of Functionally Integrative Neuroscience, Aarhus University, Aarhus, Denmark, <sup>7</sup>Department of Neuroimaging, Institute of Psychiatry, Psychology and Neuroscience, King's College London, London, UK, <sup>8</sup>NatBrainLab, Department of Forensics and Neurodevelopmental Sciences, Institute of Psychiatry, Psychology and Neuroscience, King's College London, London, UK, <sup>9</sup>Russell H. Morgan Department of Radiology and Radiological Science, Johns Hopkins University School of Medicine, Baltimore, MD, USA, <sup>10</sup>Department of Neurosurgery, School for Mental Health and Neuroscience (MHeNS), Maastricht University Medical Center, Maastricht, The Netherlands, <sup>11</sup>The Queensland Brain Institute, The University of Queensland, Queensland, Australia, <sup>12</sup>Melbourne Neuropsychiatry Centre, The University of Melbourne, Parkville, Victoria, Australia, <sup>13</sup>Department of Radiology and Imaging Sciences, Indiana University, IN, USA, <sup>14</sup>Stark Neurosciences Research Institute, Indiana University School of Medicine, IN, USA, <sup>15</sup>Center for Biomedical Imaging, NYU Grossman School of Medicine, New York, NY, USA, <sup>16</sup>Faculty of psychology and Neuroscience, Maastricht University, Maastricht, Netherlands, <sup>17</sup>Department of Chemical & Biomedical Engineering, FAMU-FSU College of Engineering, Florida State University, Tallahassee, FL, USA, <sup>18</sup>Center for Interdisciplinary Magnetic Resonance, National High Magnetic Field Laboratory, Tallahassee, FL, USA, <sup>19</sup>Department of Neuropsychology, Max Planck Institute for Human Cognitive and Brain Sciences, Leipzig, Germany, <sup>20</sup>USC Stevens Neuroimaging and Informatics Institute, Keck School of Medicine of USC, University of Southern California, Los Angeles, CA, USA, <sup>21</sup>Department of Neuroscience, Center for Magnetic Resonance Research, University of Minnesota, MN, USA, <sup>22</sup>Aix Marseille Univ, CNRS, CRMBM,

Marseille, France, <sup>23</sup>Bio Imaging Laboratory, Faculty of Pharmaceutical, Biomedical and Veterinary Sciences, University of Antwerp, Antwerp, Belgium, <sup>24</sup> $\mu$ NEURO Research Centre of Excellence, University of Antwerp, Antwerp, Belgium, <sup>25</sup>Wellcome Centre for Integrative Neuroimaging, FMRIB, Nuffield Department of Clinical Neurosciences, University of Oxford, United Kingdom, <sup>26</sup>Department of Radiology, Lausanne University Hospital and University of Lausanne, Lausanne, Switzerland, <sup>27</sup>imec Vision Lab, Dept. of Physics, University of Antwerp, Belgium, <sup>28</sup>Lab for Equilibrium Investigations and Aerospace, Dept. of Physics, University of Antwerp, Belgium, <sup>29</sup>Department of Chemical and Biological Physics, Weizmann Institute of Science, Rehovot, Israel, <sup>30</sup>Division of Child Development & Growth, Department of Pediatrics, Gynaecology & Obstetrics, School of Medicine, Université de Genève, Genève, Switzerland, <sup>31</sup>Department of Radiology, Cumming School of Medicine, University of Calgary, Calgary, Alberta, Canada, <sup>32</sup>Hotchkiss Brain Institute, Cumming School of Medicine, University of Calgary, Calgary, Alberta, Canada, <sup>33</sup>Alberta Children's Hospital Research Institute, Cumming School of Medicine, University of Calgary, Calgary, Alberta, Canada, <sup>34</sup>FMRIB Centre, Wellcome Centre for Integrative Neuroimaging, Nuffield Department of Clinical Neurosciences, University of Oxford, Oxford, United Kingdom, <sup>35</sup>Department of Electrical and Computer Engineering, Vanderbilt University, <sup>36</sup>Department of Radiology and Radiological Sciences, Vanderbilt University Medical Center, Nashville, TN, USA, <sup>37</sup>Medical University of South Carolina, Charleston, SC, USA, <sup>38</sup>National Imaging Facility, Melbourne, Victoria, Australia, <sup>39</sup>Department of Forensic and Neurodevelopmental Sciences, King's College London, London, UK, <sup>40</sup>Laboratory on Quantitative Medical imaging, NIBIB, National Institutes of Health, Bethesda, MD, USA, <sup>41</sup>Department of Computer Science, University College London, London, UK, <sup>42</sup>PROVIDI Lab, Image Sciences Institute, University Medical Center Utrecht, The Netherlands, <sup>43</sup>Biomedical Engineering, Vanderbilt University, Nashville, TN, <sup>44</sup>Sherbrooke Connectivity Imaging Lab (SCIL), Computer Science department, Université de Sherbrooke, <sup>45</sup>Imeka Solutions, <sup>46</sup>Department of Radiology and Biomedical Imaging, University of California San Francisco, CA, USA, <sup>47</sup>Department of Radiology, Perelman School of Medicine, University of Pennsylvania, Philadelphia, PA, USA, <sup>48</sup>Department of Radiology, Children's Hospital of Philadelphia, Philadelphia, PA, USA, <sup>49</sup>Centre for Neuroimaging Research (CENIR), Inserm U 1127, CNRS UMR 7225, Sorbonne Université, Paris, France, <sup>50</sup>Paris Brain Institute, Paris, France, <sup>51</sup>Department of Pediatrics, University of California Irvine, Irvine CA USA, <sup>52</sup>Preclinical and Translational Imaging Center, University of California Irvine, Irvine CA USA, <sup>53</sup>Department of Radiology, Weill Cornell Medical College, New York, NY, USA, <sup>54</sup>Key Laboratory for Biomedical Engineering of Ministry of Education, College of Biomedical Engineering & Instrument Science, Zhejiang University, Hangzhou, China, <sup>55</sup>CEA, DRF, JOLIOT, NeuroSpin, Gif-sur-Yvette, France, <sup>56</sup>Université Paris-Saclay, Gif-sur-Yvette, France, <sup>57</sup>Department of Neuroscience, University of Florida, Gainesville, FL, United States, <sup>58</sup>McKnight Brain Institute, University of Florida, Gainesville, FL, United States, <sup>59</sup>National High Magnetic Field Laboratory, Tallahassee, FL, United States, <sup>60</sup>NeuroSpin, UMR CEA/CNRS 9027, Paris-Saclay University, Gif-sur-Yvette, France, <sup>61</sup>Department of Radiology, New York University Grossman School of Medicine, New York, NY, USA, <sup>62</sup>Interdisciplinary Institute of Neuroscience and Technology, School of Medicine, Zhejiang University, Hangzhou, China, <sup>63</sup>Frontier Center of Brain Science and Brain-machine Integration, Zhejiang University, <sup>64</sup>Department of Molecular Biology, Institute of Basic Medical Sciences, University of Oslo, Norway, <sup>65</sup>Department of Radiology, New York University School of Medicine, NY, NY, USA, <sup>66</sup>Danish Research Centre for Magnetic Resonance, Centre for Functional and Diagnostic Imaging and Research, Copenhagen University Hospital Amager & Hvidovre, Hvidovre, Denmark, <sup>67</sup>Department of Applied Mathematics and Computer Science, Technical University of Denmark, Kongens Lyngby, Denmark, <sup>68</sup>Duke Center for In Vivo Microscopy, Department of Radiology, Duke University, Durham, North Carolina, <sup>69</sup>Department of Biomedical Engineering, Duke University, Durham, North Carolina, <sup>70</sup>NeuroPoly Lab, Institute of Biomedical Engineering, Polytechnique Montreal, Montreal, QC, Canada, <sup>71</sup>Functional Neuroimaging Unit, CRIUGM, University of Montreal, Montreal, QC, Canada, <sup>72</sup>Mila - Quebec AI Institute, Montreal, QC, Canada, <sup>73</sup>Department of Neurosurgery, Medical College of Wisconsin, Milwaukee, Wisconsin, <sup>74</sup>Clement J Zablocki VA Medical Center, Milwaukee, Wisconsin, <sup>75</sup>CIBM Center for Biomedical Imaging, Ecole Polytechnique Fédérale de Lausanne, Lausanne, Switzerland

## Abstract

The value of preclinical diffusion MRI (dMRI) is substantial. While dMRI enables *in vivo* non-invasive characterization of tissue, *ex vivo* dMRI is increasingly being used to probe tissue microstructure and brain connectivity. *Ex vivo* dMRI has several experimental advantages including higher signal-to-noise ratio (SNR) and spatial resolution compared to *in vivo* studies, and enabling more advanced diffusion contrasts for improved microstructure and connectivity characterization. Another major advantage of *ex vivo* dMRI is the direct comparison with histological data, as a crucial methodological validation. However, there are a number of considerations that must be made when performing *ex vivo* experiments. The steps from tissue preparation, image acquisition and processing, and interpretation of results are complex, with many decisions that not only differ dramatically from *in vivo* imaging of small animals, but ultimately affect what questions can be answered using the data. This work represents “Part 2” of a series of recommendations and considerations for preclinical dMRI, where we focus on best practices for dMRI of *ex vivo* tissue. We first describe the value that *ex vivo* imaging adds to the field of dMRI, followed by general considerations and foundational knowledge that must be considered when designing experiments. We briefly describe differences in specimens and models and discuss why some may be more or less appropriate for different studies. We then give guidelines for *ex vivo* protocols, including tissue preparation, imaging sequences and data processing including pre-processing, model-fitting, and tractography. Finally, we provide an online resource which lists publicly available *ex vivo* dMRI datasets and dedicated software packages, to promote responsible and reproducible research. In each section, we attempt to provide guidelines and recommendations, but also highlight areas for which no guidelines exist (and why), and where future work should lie. An overarching goal herein is to enhance the rigor and reproducibility of *ex vivo* dMRI acquisitions and analyses, and thereby advance biomedical knowledge.

**Keywords:** preclinical; diffusion MRI; *ex vivo*; best practices; microstructure; diffusion tensor; tractography; acquisition; processing; open science.

<b>1 Introduction</b>	<b>5</b>
<b>2 Added Value</b>	<b>6</b>
2.1 Added value	7
2.2 Ex vivo: Translation and validation considerations	8
2.3 Species differences	11
2.3.1 Murine models (mouse and rat)	11
2.3.2 Primate models	12
2.3.3 Human models	13
2.3.4 Other models	15
<b>3 Acquisition</b>	<b>15</b>
3.1 Standard Protocol - overview	15
3.2 Hardware (species/organ specific)	16
3.3 Fixation	17
3.4 Sample Preparation	20
3.5 MR Scanning	24
3.5.1 Encoding	24
3.5.2 Readout	25
3.5.3 q-t coverage	27
3.5.4 MR Scanning, Monitoring, scan duration	30
3.5.5 Spatial resolution	31
3.5.5.1 Volume equivalent resolutions and pushing the boundaries	32
3.6 Storage	34
3.7 Specifics of ultra-high resolution MRI and MR microscopy	34
<b>4 Data Processing</b>	<b>36</b>
4.1 Pre-processing pipeline	36
4.2 Processing pipelines	38
4.2.1 Ex vivo MRI-histology correlations	39
4.2.2 Ex vivo MRI-histology alignment	41
4.2.3 Where future work should lie	43
4.3 Tractography	44
<b>5 Perspectives</b>	<b>45</b>
5.1 Open science	45
5.1.1 Code/Software	45
5.1.2 Data Sharing & Databases	46
5.2 The future: what should we strive to achieve?	46
<b>6 Acknowledgements and Support</b>	<b>48</b>
<b>7 References</b>	<b>48</b>

# 1 Introduction

Diffusion magnetic resonance imaging (dMRI) is a medical imaging technique that utilizes the diffusion of water molecules to generate image contrast, enabling the non-invasive mapping of the diffusion process in biological tissues. These diffusion patterns can be used to infer and generate maps of tissue microstructure, or can be applied to map tissue orientation to study the structural connections of the brain in a process called fiber tractography. These microstructure and connectivity maps have often been described as a non-invasive ‘virtual histology’ or ‘virtual dissection’ and have found applications widely used in neuroscience, neuroanatomy, and neurology, but also outside the brain with musculoskeletal, whole-body, and organ-specific applications in normal and pathological conditions.

Much like any biomedical research, the use of animal models and *ex vivo* tissue is essential to the field of diffusion MRI. In this work, **we define small animal imaging as imaging performed on a living animal model of human tissue, whereas *ex vivo* we define as covering any fresh excised tissue, perfused living tissue, or fixed tissue.** Small-animal research is highly valuable for investigating the biology, etiology, progression, and treatment of disease; for the field of dMRI specifically, preclinical imaging is essential for methodological development and validation, characterizing the biological basis of diffusion phenomena, and comparative anatomy. While dMRI enables non-invasive characterization of tissue *in vivo*, *ex vivo* acquisitions are increasingly being used to probe tissue properties and brain connectivity. Diffusion MRI of *ex vivo* tissue has several experimental advantages, including longer scanning times and absence of motion. Together, these make it possible to acquire data with significantly higher signal-to-noise ratio (SNR) by sometimes orders of magnitude, traded most often for much higher resolution compared to *in vivo* studies, and with sophisticated diffusion contrasts which may enable better characterization of microstructure and connectivity. Another advantage afforded by *ex vivo* dMRI is the ability to compare diffusion data to histological data, bridging the gap between *in vivo* and histology for methodological validation. Because of these advantages, there have been an increasing number of dMRI studies on *ex vivo* tissue samples.

However, there are a number of considerations that must be made when performing *ex vivo* experiments. The steps from tissue preparation, image acquisition and processing, and interpretation of results are complex, with many decisions that not only differ dramatically from *in vivo* imaging of small animals, but ultimately affect what questions can be answered using the data. This work represents “Part 2” of a 2-part series of recommendations and considerations for preclinical diffusion MRI, where Part 1 presents best practices for preclinical dMRI of *in vivo* tissue. **This work does not serve as a “consensus” on any specific topic, but rather as a snapshot of “best practices” or “guidelines”** from the preclinical dMRI community as represented by the authors. We envision this work to be useful to imaging centers using small animal scanners for research, sites that may not have personnel with expert knowledge in diffusion, pharmaceutical or industry employees who may want to run their own tests and studies, or new trainees in the field of dMRI that are planning their own studies. The resources provided herein may act as a starting point when reading the literature, and understanding the decisions and processes for studying model systems with dMRI.

The manuscript is organized as follows. We first describe the value that *ex vivo* imaging adds to the field of dMRI, followed by general considerations and foundational knowledge that must be considered when designing experiments. We briefly describe differences in specimens and models and discuss why some may be more or less appropriate for different studies. We then give guidelines for *ex vivo* acquisition protocols, including decisions on hardware, sample preparation, and imaging sequences, followed by guidelines for data processing including pre-processing, model-fitting, and tractography. Finally, we give perspectives on the field, describing sharing of code and data, and goals that we wish to achieve. In each section, we attempt to provide guidelines and recommendations, but also highlight areas for which no guidelines exist (and why), and where future work should lie. An overarching goal herein is to enhance the rigor and reproducibility of *ex vivo* dMRI acquisitions and analyses, and thereby advance biomedical knowledge.

## 2 Added Value

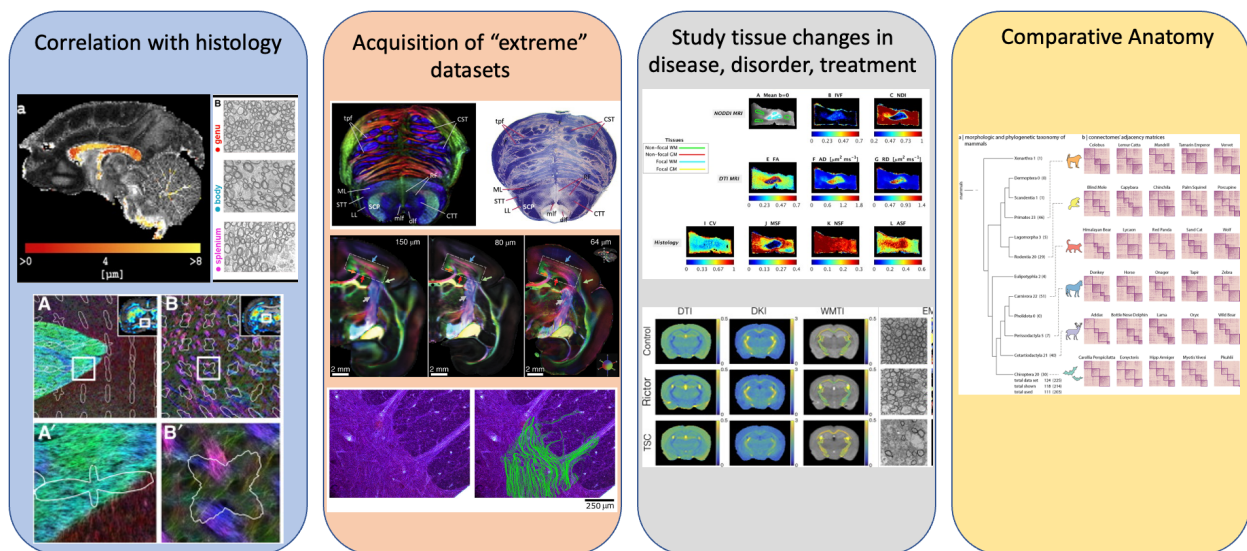


**Figure 1.** Four areas in which preclinical brain imaging adds value to the field of dMRI. It enables: (i) correlation with histology on the same subject/sample, (ii) the acquisition of richer datasets than on clinical systems thanks to more advanced hardware and longer scan times available, (iii) the study of tissue changes with disease and treatment in a more controlled setting, and (iv) comparative anatomy between species. Figures reused and adapted from (i) (Alexander et al. 2010; Seppehrband et al. 2016; Budde and Frank 2012) (ii) (Aggarwal et al. 2013; Liu et al. 2020; Hansen et al. 2011) (iii) (Grussu et al. 2015; Kelm et al. 2016) (iv) (Suárez et al., n.d.)

## 2.1 Added value

*Ex vivo* samples add substantial value to dMRI in much the same way as small animal systems, by acting as supplements, substitutes, translations, and/or validation mechanisms for *in vivo* human studies. Building on the four areas identified in Part 1 in which preclinical MRI adds value to the field of diffusion MRI, here we focus on aspects specific to *ex vivo* experiments (**Figure 1**).

**First, *ex vivo* dMRI allows correlations with histological and other imaging measures** in a more direct way than *in vivo* dMRI, since the tissue has undergone the similar changes related to fixation and other chemical treatments. Through co-registration of microscopy images to MRI images of the same specimens, direct comparisons and correlation of dMRI measures to different quantitative microscopic parameters can be achieved, thus elucidating how different microscopic tissue features influence dMRI contrast, and increase insight into how sub-voxel tissue architecture can be assessed using dMRI techniques. Such validation studies in turn improve our ability to interpret *in vivo* dMRI for both preclinical and clinical studies and open new avenues for diagnostic imaging, disease monitoring and treatment, as well as non-invasive mapping of brain structure and function.

**Second, *ex vivo* imaging allows acquisition of “extreme” datasets** not possible with *in vivo* preclinical or clinical imaging, pushing the boundaries of acquisition and analysis to answer questions about what dMRI is capable of measuring in principle. By “extreme” datasets, we target in particular: advanced diffusion encoding, higher *b*-values, shorter diffusion times, or simply very comprehensive *q-t* coverage that requires very long scan times. Preclinical MRI systems indeed offer four distinct advantages for imaging: higher field strengths, smaller RF coils, stronger and faster switching gradients, and longer scan times. Together these allow to achieve higher signal to noise ratio (SNR), with more advanced diffusion encoding and stronger diffusion sensitization (i.e., higher *b*-values), and in the case of *ex vivo* samples, with no physiological motion compared to *in vivo* imaging. The appeal of **higher fields** is driven by benefits of potentially higher SNR due to increased net magnetization, and changes in relaxation parameters which are not always directly advantageous to diffusion MRI but are uniquely suited or adapted for the enormous flexibility in sequence optimizations and tissue preparation techniques offered by *ex vivo* MRI. *Ex vivo* allows flexibility in **RF coils**, which can be close in proximity to the sample being imaged, further increasing SNR. **Stronger and faster switching gradients** are also an immense asset for dMRI experiments (D. K. Jones et al. 2018), enabling a higher SNR via reduced echo time. Most importantly, stronger gradients facilitate the exploration of broader ranges of diffusion sensitization and diffusion time (i.e. “*q-t* space”) while keeping an acceptable SNR level. In particular, unique insights into tissue microstructure have been brought by exploring a range of *q-t* space only feasible (at the time) on preclinical systems (Does, Parsons, and Gore 2003; Aggarwal, Smith, and Calabresi 2020; Pyatigorskaya et al. 2014; Wu et al. 2014; Assaf et al. 2008), including very short diffusion times, very strong diffusion weightings (Does, Parsons, and Gore 2003; Aggarwal, Smith, and Calabresi 2020; Pyatigorskaya et al. 2014; Wu et al. 2014); (Jespersen et al. 2010; Seppehrband et al. 2016; Dyrby et al. 2013), or more complex diffusion encoding schemes (Xu et al. 2014;

lanuş et al. 2018; Lundell et al. 2019). Finally, the greatest asset enabled by *ex vivo* imaging is a lengthy **scan time**, with the ability to scan over extended periods of time ranging from overnight scans to successful scans of > 10 day periods. Long scanning further facilitates acquisitions across *q-t* ranges, with substantially increased SNR and/or increased spatial resolution. For these reasons, the combination of high magnetic field strengths, fast high-amplitude gradients, and extended scan time enables “extreme” acquisitions currently impossible on clinical scanners, pushing the scientific boundaries of what can be studied with these unique contrasts.

**Third, the use of animal models allows us to study the sensitivity of dMRI to tissue changes in diseases, disorders and treatments in a controlled way.** While not unique to *ex vivo* samples specifically, animal models are critical to biomedical research as they may be biologically similar to humans, susceptible to many of the same health problems, and can be studied throughout their whole life span and across generations. Thus, these models are essential for the discovery of the causes, diagnosis, and treatment of diseases and disorders. *Ex vivo* imaging has the added benefit of bridging the gap between *in vivo* imaging and histology (added value #1) and investigation of new imaging sequences (added value #2) that together spur development and validate new biomarkers for diagnosis and treatment.

**Fourth, the use of *ex vivo* systems enables comparative anatomy.** A key challenge in comparative neuroanatomy is to identify homologous structures and structural boundaries across species. Moreover, the brain undergoes substantial changes through development and aging which hampers comparison of data from different timepoints. High-resolution *ex vivo* structural MRI and dMRI data have provided versatile reference data for creating anatomical atlases for mouse, rat, and primate brains (G. Allan Johnson et al. 2010; Aggarwal, Zhang, and Mori 2011; Ullmann et al. 2013; Liu et al. 2018; Papp et al. 2014; Feng et al. 2017) allowing detection of detailed anatomical systems corresponding to those identified using histological criteria (Kjonigsen et al. 2015; Osen et al. 2019). Comparative neuroanatomical efforts, then, may rely on histological comparisons across species supplemented by high quality imaging acquisitions as a marker of ‘virtual histology’ and ‘virtual brain dissection’.

In the light of the different levels of added value, the ability of *ex vivo* experiments to inform about tissue features or properties that can be extrapolated to humans is variable and greatly depends on the translatability of the specific aspects under study.

## 2.2 *Ex vivo*: Translation and validation considerations

Similar to *in vivo* studies of small animals, scanning *ex vivo* tissue presents both opportunities and challenges when translating and validating experimental findings (G. A. Johnson et al. 1993). This section introduces experimental and biological aspects that must be considered when designing and interpreting *ex vivo* studies. We begin with a very brief summary from Part 1 of considerations in anatomy, disease model, and hardware that are general to all preclinical or animal studies, and finally discuss considerations in the diffusion process that are specific to *ex vivo* imaging. All aspects are covered in more detail in their corresponding sub-sections in *Acquisition* ([Section 3](#)).



## Anatomical considerations

The basic constituents of the brain and other organs are largely preserved across mammalian species, providing the basis for translational MRI studies. Moreover, the constituents of *ex vivo* tissue are largely similar to their *in vivo* counterparts, assuming appropriate perfusion fixation (to preserve 'dead' tissue) or artificial perfusion (to preserve 'viable' *ex vivo* tissue) (Dyrby et al. 2018; Flint et al. 2015). For example, in the central nervous system, the fundamental structure of a long axon wrapped with a myelin sheath is preserved with chemical fixation *ex vivo*. Similarly, tissue complexity is expected to be similar *ex vivo*, both at the microstructure scale of tissue constituents and tissue organization and at the macrostructure scale of cortical folding and organization. Noticeable exceptions to similarity are possible changes in size, volume fractions of tissue compartments, membrane permeability and/or diffusivity drop beyond those that are expected from temperature changes (see *Considerations of microstructure and the diffusion process*, below) (J. Zhang et al. 2012; Shepherd, Thelwall, et al. 2009).

## Considerations in disease/disorder/model

As in small animal studies, a challenge when using *ex vivo* models to study the sensitivity of dMRI to detect changes in disease or treatments is confirming the translational value to human studies. The challenging translational value is related to animal models only replicating a subset of the human disease manifestations, or to reproducing the effect but not the cause leading to it (e.g. producing demyelination in the mouse corpus callosum using cuprizone intoxication, while the mechanism causing demyelination in multiple sclerosis is unclear and cannot be reproduced in animals). Despite this, *ex vivo* imaging of models of stroke, demyelination, traumatic brain injury, spinal cord injury, and tumor models have proven useful to investigate altered microstructure or connectivity in diseased states, and facilitate subsequent histological validation (Budde and Song, n.d.). Clearly, the advantage of small animal imaging for longitudinal studies of development or disease progression in single subjects stops at the *ex vivo* scan, yet the benefits of the high resolution and high SNR scan enable detailed investigations of the *ex vivo* tissue at one specific time point.

## Considerations of microstructure and the diffusion process

The translation of *ex vivo* measurements to *in vivo* should be interpreted with caution, and as both the tissue microstructure and intrinsic diffusivities may be different in *ex vivo* vs *in vivo* tissue (**Figure 2**). To prevent postmortem degradation and to limit uncontrolled changes in tissue microstructure, tissues should be chemically fixed. Nevertheless, even using appropriate **chemical fixation**, the tissue inevitably undergoes changes: intra-/extracellular space volume fraction shifts, cell membrane permeability, relaxation rates and diffusion coefficients, etc. (Wehr et al. 2015; Thelwall et al. 2006; Shepherd, Thelwall, et al. 2009; H. E. D'Arceuil, Westmoreland, and de Crespigny 2007; J. Zhang et al. 2012). The degree to which fixation affects microstructure features is however variable across the literature - see [Section 3.3](#) for details. *Ex vivo* dMRI on fixed tissue at room temperature also distinguishes itself through **lower diffusivity by a factor of 3-4** in the tissue, which cannot be explained by the difference in temperature alone, but is also due to fixation and/or other post-mortem tissue changes (Sun et al. 2005).

These differences will impact the scanning protocol - and the need for higher b-values in particular, as well as the interpretation of results in terms of diffusion distance and probed spatial scales ([Section 3.5.3](#)). Lastly, **temporal drift**, due to both scanner instability and temperature changes in the sample over long scan times need to be considered and accounted for. Over the course of an *ex vivo* dMRI experiment, the tissue temperature might change as an effect of gradient or RF heating. Strategies for mitigating and/or correcting temporal drift are described throughout, and may involve sample preparation ([Section 3.4](#)), controlling temperature during scanning ([Section 3.5.4](#)) and within preprocessing pipelines (Section 4.1).

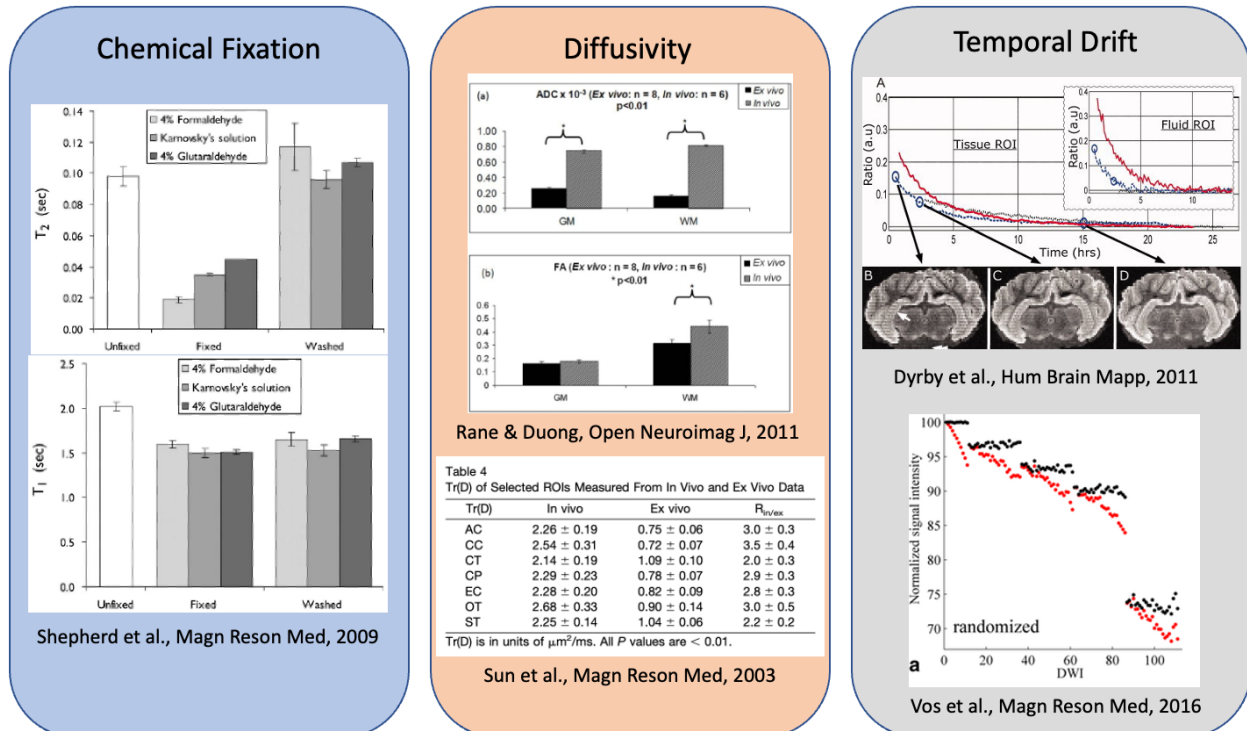


**Figure 2** Considerations in the diffusion process. When performing studies on *ex vivo* tissue, one must consider effects of chemical fixation (changes in geometry, volume fractions, relaxation rates, permeability, diffusion coefficients), changes in diffusivity (which can be ~2-5 times reduced from *in vivo* depending on experimental conditions), and temporal instabilities over long scan times (causing temporal drift or image artifacts).

These effects need to be considered when interpreting *in vivo* dMRI based on *ex vivo* validation studies, especially when considering the validation of biophysical models. A diffusion MRI model that is validated or performs well *ex vivo* may not be valid/validated *in vivo*, and vice-versa, due to modeling assumptions, and potential differences in diffusivities, compartmental volume fractions, and relaxation rates. Nevertheless, *ex vivo* dMRI remains a popular and practical method to compare metrics of microstructure or structural connectivity to those estimated from histology, and thus validate them. Once a non-invasive dMRI method has been validated using *ex vivo* imaging vs histology, it can be applied to *in vivo* imaging (including human imaging) with higher confidence (Flint et al. 2009; C. H. Lee et al. 2015).

## 2.3 Species differences

As discussed in Part 1, diffusion MRI has been utilized in a number of animal models, both *in vivo* and *ex vivo*. The most appropriate species to investigate is ultimately dependent upon the research question, as some species are more appropriate than others for a given study - for example one species may facilitate replication of neurological conditions, whereas another may better reflect the biology or structural connectivity of the human brain. In general, among several possible species that are appropriate models, the one with the least experimental hurdles and the minimum cost will be chosen. Of course, in studies of human anatomy, the postmortem human brain can also be imaged and subsequently dissected, or sectioned for histological analysis. Additionally improved SNR can be achieved and traded for spatial resolution by dissecting just the region of interest from the sample allowing the use of higher magnetic fields and smaller RF coils.

Clearly, different model systems have their own advantages and disadvantages. Below, we list some of the most common (and less common) species studied with *ex vivo* dMRI and briefly describe advantages and disadvantages of each.

### 2.3.1 Murine models (mouse and rat)

Rats and mice have been and continue to be the long-standing preferred species for biomedical research models as they offer a low-cost option with outcome measures widely available and a substantial database of normative data, including behavioral, genomic, and medical imaging. For this reason, the murine models have become popular small animal models in dMRI, both *in vivo* and *ex vivo* (**Figure 3**). In addition to biological advantages, the small physical size offers technical advantages, fitting in the typically smaller bores (and smaller coils) of magnets with larger field strengths. This is particularly advantageous for *ex vivo* imaging, where the small size may facilitate scanning with smaller bore ultra-high field scanners and smaller volume coils or cryogenic probes. While the advantages of the murine models are numerous, it is important to note the multiple anatomical differences from human structures, including smaller size, less gyration, and less white matter.

In summary, murine models are particularly suited for studies for which there are models that replicate human neurological disease, for histological validation of acquisitions and models, and for investigations of single fiber population structures like the corpus callosum. Because of the larger ratio of gray-to-white matter, murine models may also be well-suited for studies of gray matter anatomy. *Ex vivo*, mouse models have found most applications in exploration and development of advanced image acquisition and diffusion encoding, and validation of multi-compartment modeling facilitated through subsequent histology.

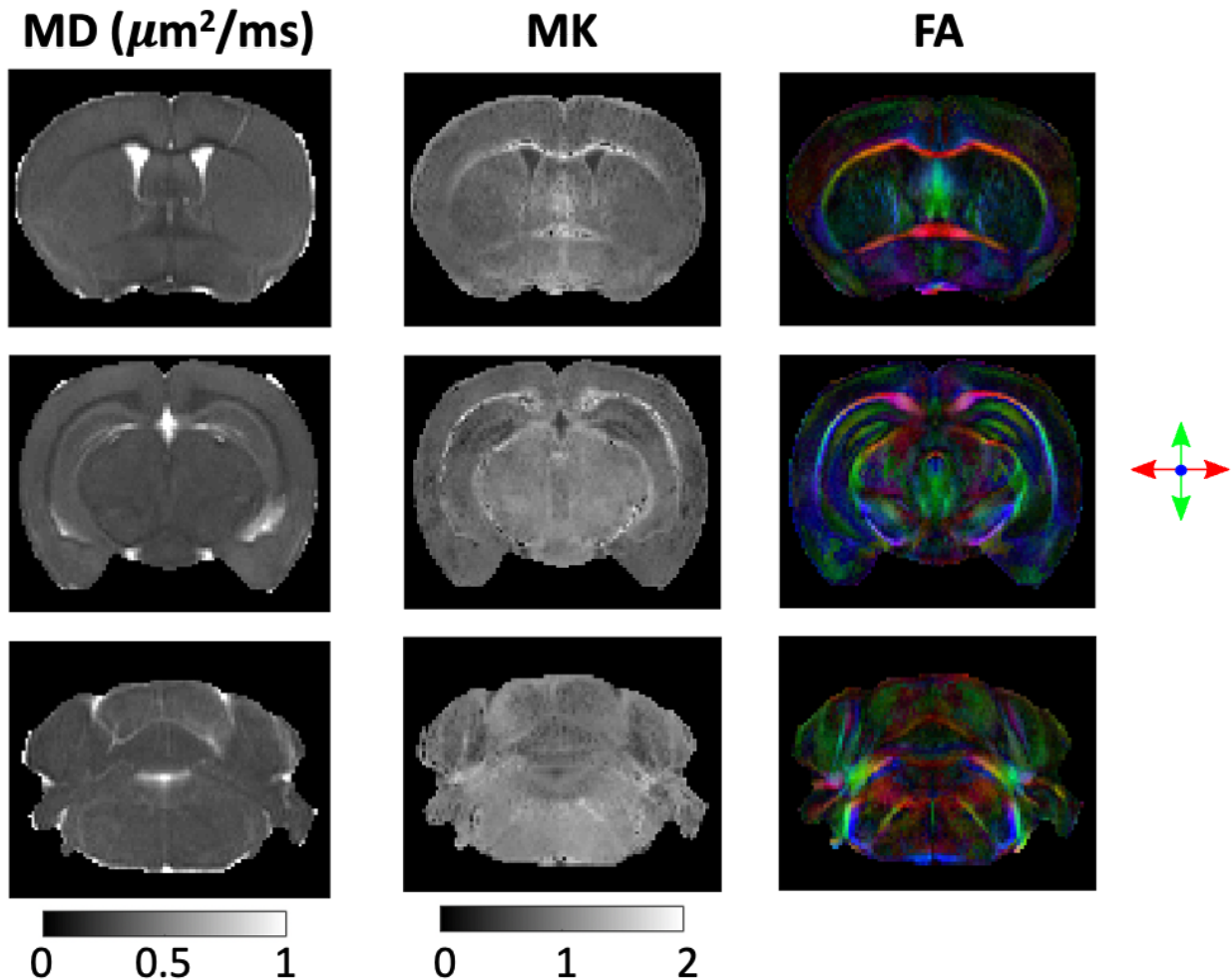


**Figure 3.** *Ex vivo* imaging of mouse models facilitates high resolution, high SNR, dense sampling of  $q$ - $t$  space. Here, a fixed mouse brain was imaged on a 16.4T Bruker Aeon Ascend scanner equipped with a 10-mm birdcage coil and gradients capable of producing up to 3 T/m in all directions. Images show mean diffusivity (MD), Mean Kurtosis (MK), and directionally encoded color (DEC) FA maps (Pajevic and Pierpaoli 2000). All animal studies were approved by the competent institutional and national authorities, and performed according to European Directive 2010/63. Images kindly provided by Andrada Ianus and Noam Shemesh.

### 2.3.2 Primate models

Popular Non-human primates (NHPs) in dMRI literature include marmosets, squirrel monkeys, and macaques. NHPs have been popular in psychological, evolutionary, and biological sciences because they offer a model of tissue microstructure and structural connectivity that is closer to the human than rodents. For example, there are a number of white matter and gray matter regions with homologous counterparts in humans, with evidence for similar function, structure, and tissue constituents (“Nonhuman Primates and Medical Research” 1973; Sibal and Samson 2001; *The Squirrel Monkey in Biomedical and Behavioral Research*

2000; Royo et al. 2021). For these reasons, NHPs are particularly well suited for studies of cortical development, gyrification, and interrogation of complex white matter.

NHPs are also well suited for studies of specific pathways and their structural and functional significance. *Ex vivo* NHP imaging, in particular, is very common after injection of histological tracers, and constitutes a majority of diffusion tractography validation studies (**Figure 4**). As an example, controversies regarding the existence or nonexistence of a pathway, or the location of pathway terminations have been resolved or steered through primate models (Sarubbo et al. 2019; Mandonnet, Sarubbo, and Petit 2018; Panesar and Fernandez-Miranda 2019; K. G. Schilling et al. 2021). A number of tractography validation studies have used tracer studies in *ex vivo* primates, which enables comparisons of tracers to exceptional quality diffusion datasets, in order to identify challenges and limitations in diffusion tractography (K. G. Schilling et al. 2020a; Gutierrez et al. 2020; Girard et al. 2020a; Thomas et al. 2014a; Donahue et al. 2016; K. G. Schilling, Nath, et al. 2019; Yan et al. 2022; Maffei et al. 2022a; Grisot, Haber, and Yendiki 2021a; Ambrosen et al. 2020).

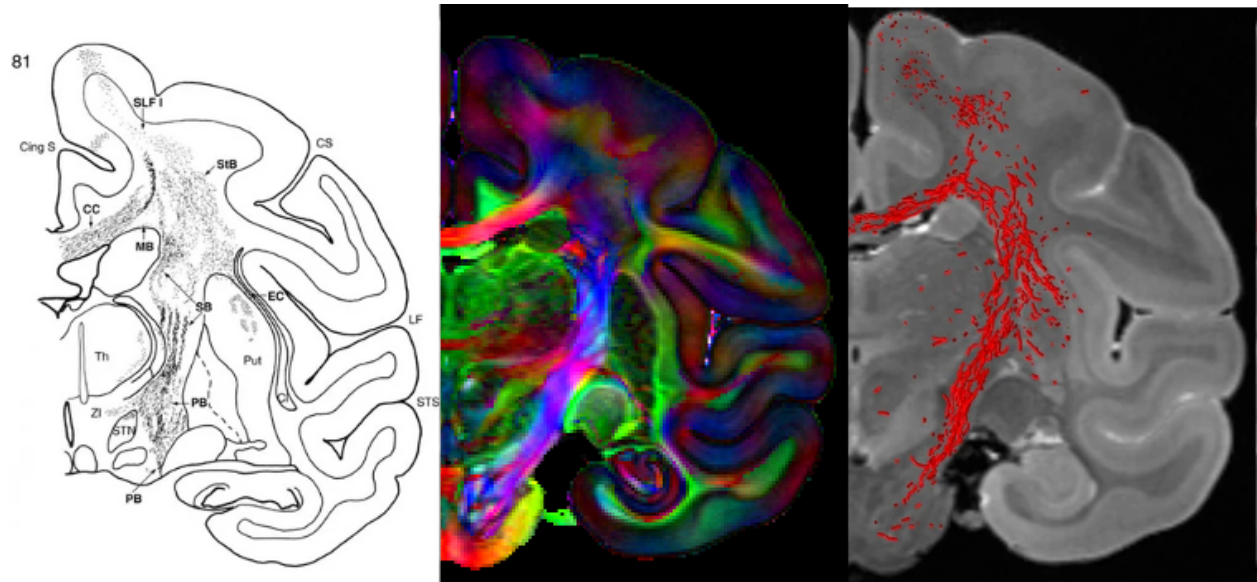


**Figure 4.** Primate models have been used to validate tractography estimates of structural connectivity. *Ex vivo* imaging offers the ability to investigate and compare the anatomical accuracy of high quality and high resolution dMRI datasets against histological tracers, the gold-standard for elucidating brain tractography. Figure adapted from (Schmahmann and Pandya 2009) and (K. G. Schilling et al. 2020b), based on *ex vivo* macaque data acquired by (Thomas et al. 2014b) shows tracer trajectory (left), directionally encoded color map (middle) and tractography streamlines (right).

### 2.3.3 Human models

*Ex vivo* imaging of human brains is also possible (**Figure 5**). Of course, the greatest advantage is the immediate translatability to the *in vivo* human brain. Because of the high resolution and high quality offered by *ex vivo* imaging, in combination with the ability to probe

multiple  $b$ -values at multiple diffusion times, *ex vivo* imaging of the human brain has found a number of neuroanatomical applications (Roebroek, Miller, and Aggarwal 2019) including validation of orientation estimates and tractography (Budde and Annese 2013; R. Jones et al. 2020; Roebroek et al. 2008; Seehaus et al. 2015), mapping of subcortical structures and creation of high resolution atlases and templates (Aggarwal et al. 2013; Adil et al. 2021; Calabrese, Hickey, et al. 2015), and investigation of gray matter laminar structures (Kleinnijenhuis 2014; Dyrby et al. 2011; Aggarwal et al. 2015). Challenges that are specific to human brain samples include limitations to medium-to-large bore systems (that often do not have specialized hardware such as strong gradient sets), and the need for specific sample holders or coils, although small sub-sections of human brains have also been scanned. Additionally, high quality scans are only possible on well-preserved samples, whereby minimizing the post-mortem interval between death and fixation is a necessity (see [Section 3.3 Fixation](#) for detailed discussion of the effects of post-mortem interval on MR-relevant tissue features). Perfusion fixation can sometimes be performed on post-mortem brain tissue using mechanical means (Roebroek, Miller, and Aggarwal 2019; Grinberg et al. 2008).

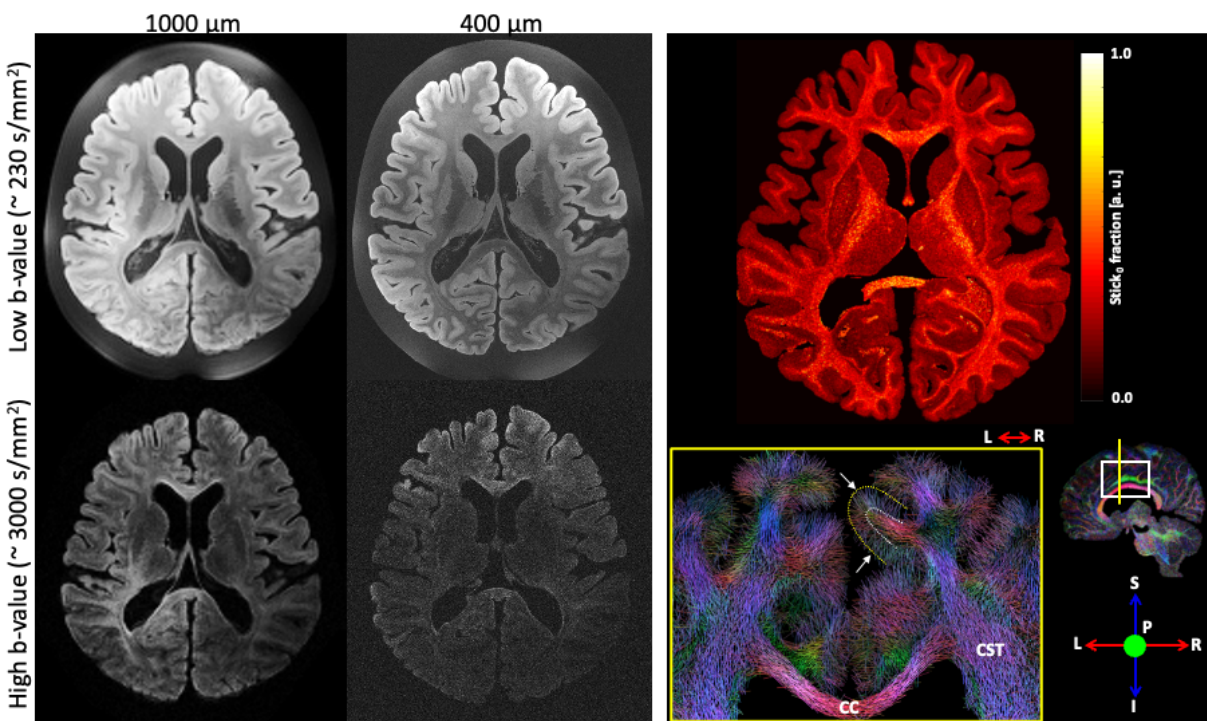


**Figure 5.** *Ex vivo* imaging of the human brain facilitates high resolution and high SNR dMRI (left), which offers exceptional tractography, mapping and creation of templates for small structures, and investigation of gray matter laminar structures (right). Images adapted from (Fritz et al. 2019).

### 2.3.4 Other models

While murine and NHP models are the most widely used models in biomedical imaging research with dMRI (in particular for brain applications), several other models have proven useful to the diffusion community. Examples include the pig brain, which is comparable to the human brain in growth, myelination, and development (Sauleau et al. 2009; Ryan et al. 2018), and has been used with *ex vivo* dMRI for tractography validation (Sauleau et al. 2009; Bech et al. 2020; Dyrby et al. 2007), and even to optimize strategies for *ex vivo* diffusion acquisitions (Dyrby et al. 2011). Other gyrencephalic brains have been used *ex vivo* to study diseases or to validate tractography include ferrets (Hutchinson et al. 2018, 2016; Delettre et al. 2019), sheep (Looij et al. 2012; Pieri et al. 2019; Quezada et al. 2020), dogs (Jacqmot et al. 2013), and cats (Takahashi et al. 2011). One study scanned 123 mammalian species, with brains ranging in size from 0.1-1000mL, to study the evolution of mammalian brain connectivity (Assaf et al. 2020).

Further, various non-human models of white matter, including cat optic nerves, rabbit peripheral nerves, garfish olfactory nerves, lobster nerves, and spinal cords were used to evaluate sources of anisotropy, and attribute and associate microstructural features to not only anisotropy, but restricted and hindered diffusion, compartmental diffusivities, and insight into pathology (Christian Beaulieu 2002; C. Beaulieu and Allen 1994). Moreover, the simple nervous system with very large neurons of *Aplysia*, a sea slug, has been used to study the relationship between the cellular structure and the diffusion MRI signal, to characterize compartment-specific diffusion properties and to follow diffusion changes induced by neuronal responses to ischemic-like stress or chemical stimulation (Ileana Ozana Jelescu et al. 2014; C. H. Lee et al. 2015; Hsu, Aiken, and Blackband 1997; Grant et al. 2001; Flint et al. 2020).

In general, dMRI studies of perfused viable tissue or cells present different advantages and/or challenges as compared to chemically fixed tissue. As mentioned above, isolated perfused 'live' tissue samples facilitate well controlled perturbation studies, for example controllably changing perfusate tonicity as a model of stroke. Furthermore, the estimation of relative compartment sizes can also be thoroughly explored by controlling tonicity, especially since, without fixative, the tissue does not shrink. For example, the tonicity can be changed to evaluate diffusion signal changes with tissue compartmental size changes. This important model can be used to provide an additional comparison with *in vivo* signal changes.

## 3 Acquisition

### 3.1 Standard Protocol - overview

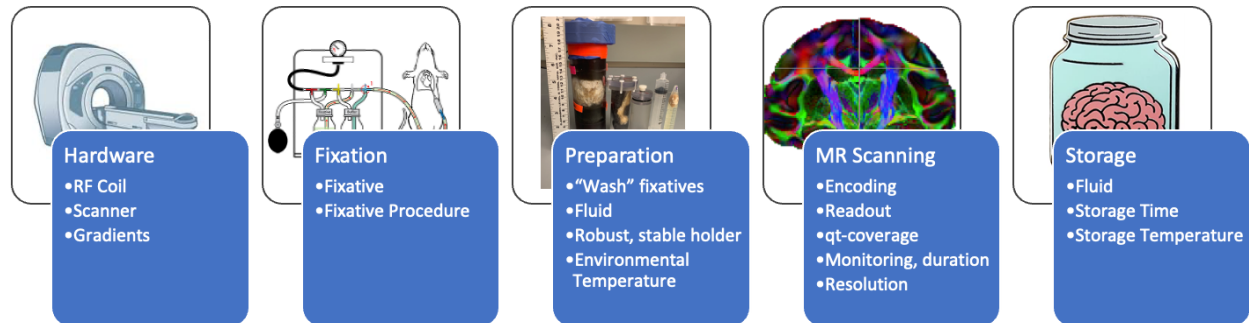


**Figure 6.** For high-quality *ex vivo* diffusion MRI, decisions regarding hardware, fixation, preparation, MR scanning, and tissue storage must be carefully considered. **Hardware:** utilize the smallest coil that fits the sample under investigation, to maximize SNR. **Fixation:** for *ex vivo* tissue to be a good model of *in vivo*, the post-mortem interval to fixation must be as short as possible. **Preparation:** washing out fixative and soaking tissue in a solution of Gadolinium-based contrast agent decreases primarily water-protons  $T_1$  which in turn allows for a favorable trade-off between SNR maximization and TR reduction (i.e., reduced acquisition time), while a robust physical setup eliminates motion during scanning. **MR Scanning:** A multi-shot 3D diffusion-weighted spin echo EPI or multi-shot 3D diffusion-weighted RARE/FSE sequence. While not typically used *in vivo* due to motion sensitivity and long scan time, these sequences combine advantages of high SNR, minimal distortion, and reasonable scan time *ex vivo*. **Storage:** fixed tissue can be stored for many months to several years if stored in fixative or phosphate buffered solution at 5°C.

There are several fundamental decisions that are made when performing *ex vivo* dMRI (Dyrby et al. 2011). Here, we present suggestions and guidelines that should be followed to produce high-quality *ex vivo* dMRI data. We provide recommendations for (1) selecting appropriate hardware including coils and scanners ([Section 3.2](#)), (2) sample fixation ([Section 3.3](#)), (3) sample preparation including sample washing, sample constraint and holders, possible contrast enhancements, and sample immersion solutions ([Section 3.4](#)), (4) MR scanning including diffusion encoding, readouts,  $q$ - $t$  coverage, spatial resolution, and monitoring ([Section 3.5](#)), and (5) long term sample storage ([Section 3.6](#)). Finally, we dedicate a section ([Section 3.7](#)) to challenges, choices, and recommendations related to acquiring ultra-high resolution diffusion images, referred to as ‘magnetic resonance microscopy’ (MRM).

In many sections we defer and reference content in *Part 1* of the series on small animal imaging. We also note that these are general suggestions, and are not always necessary nor optimal depending on experimental goals. For this reason, we discuss trade-offs or alternative choices when appropriate.

## 3.2 Hardware (species/organ specific)

Most investigators are limited to the use of hardware available at their imaging center. The guidelines for *ex vivo* imaging largely follow those suggested for small animal imaging in Part 1. **For RF Coils, the general recommendation is to utilize a coil that will maximize**



**SNR for the sample of interest**, which will typically be the smallest coil that fits the sample under investigation. For *ex vivo* in particular, this is often a volume coil for both excitation and reception, as we typically desire (and have time for) scanning the entire sample field of view. Because volume coils have better homogeneity than surface coils, using a volume coil for both excitation and signal reception avoids the SNR spatial gradient typically observed when using a surface coil. Nevertheless, surface coils for reception can offer higher local SNR so the choice of coil setup depends on the imaging task.

The choice of the MRI scanner is, again, limited to whatever is available at a given research site. If several scanners are available, a recommendation is to **select the scanner with the strongest and fastest gradients, highest field strength, that has a bore and appropriate coil that is large enough for the sample to be imaged**. Higher static magnetic field strengths provide higher SNR, but are challenged by changes in relaxation rates, for example increases in  $T_1$  (Rooney et al. 2007) and decreased  $T_2$  (de Graaf et al. 2006) (see *Sample Preparation* for discussion on techniques to alter both longitudinal and transverse relaxation, and see *Diffusion sequences*: Readout for discussion on taking advantage of altered relaxation rates).

**Finally, stronger and faster gradients are almost always advantageous for *ex vivo* imaging**, enabling to reach strong diffusion weightings at shorter diffusion times, while minimizing readout and echo times. However, stronger gradients present challenges including calibration, gradient nonlinearities, and eddy currents, which must either be reduced, empirically measured, or corrected for in processing.

### 3.3 Fixation

After death, tissues begin a self-degeneration process called autolysis, due to their own autogenous enzymes. This process, intuitively, degrades tissue quality, potentially altering several of the microstructural features we wish to quantify and/or validate against. Chemical fixation stops autolytic processes and preserves tissue structure by cross-linking proteins (Fox et al. 1985). The postmortem interval (PMI) - i.e. the time between death and chemical fixation - is crucial for tissue quality. Anatomical and radiological changes signs of autolysis, such as myelin loosening, decreased anisotropy and decreased diffusivities, may be observed as rapidly as four to six hours postmortem, dependent upon tissue temperature, and continue to be altered with longer times between death and fixation (Shepherd, Thelwall, et al. 2009; H. D'Arceuil and de Crespigny 2007; Fox et al. 1985). Thus, rapid tissue fixation is recommended to maintain its integrity.

For laboratory animals, the method of choice is fixation using intracardiac perfusion, which consists of using the active vascular system to flush fixatives throughout the tissue upon animal sacrifice. This comes with the advantage of a mostly homogenized fixative distribution throughout the tissues and an efficient removal of blood.

For human tissues or in the case where perfusion-fixation is not possible for animals, perfusion fixation can sometimes be performed on post-mortem brain tissue using mechanical means (Roebroek, Miller, and Aggarwal 2019; Grinberg et al. 2008). In an optimal case, a syringe would be inserted into the femoral artery of a non-refrigerated (refrigeration introduces

MRI artifacts) cadaver after a short PMI, via which mannitol 20% (wash step) and subsequently a fixative are pumped at a low pressure to avoid microstructural damage.

Alternatively, tissue may be immersion-fixed, i.e. immersed in a fixative solution where fixative will passively diffuse throughout the tissue over a period of time (estimated at ~1 mm/hr at 25°C (Fox et al. 1985), or longer for refrigerated samples). For example, at least 20 days are needed for enough formaldehyde to diffuse to the core of a human brain to cause fixation (Dawe et al. 2009). Other tissue types may require different fixation durations, since the diffusion dynamics of the fixative solution are not the same as for the brain (e.g., 124 days for 4% formaldehyde to penetrate 30 mm into the whole human spleen, and 62 days for the fixative to diffuse over the same distance into mammalian liver tissue) (Dawe et al. 2009). As a major pitfall, immersion fixation introduces the risk of autolytic effects, especially seen as myelin loosening, as well as microbial degradation and breakdown of cellular membranes (McFadden et al. 2019) due to the PMI and/or delay in penetration of deep tissue in larger samples (Dawe et al. 2009). As autolytic processes are temperature dependent, refrigerating the tissue as soon as possible after death, and during immersion fixation is recommended. Furthermore, this technique yields a transient concentration gradient of the fixative, and hence spatially inhomogeneous tissue integrity with varying MR characteristics (e.g., apparent  $T_1$  and  $T_2$ ). As a result, immersion fixed samples may exhibit lower anisotropy and diffusivity than their perfusion-fixed counterparts, in which case the differences may correlate with tissue degeneration. A rule of thumb to check the quality of fixed tissue (perfusion and immersion fixed) is that FA values should be the same as in vivo, e.g. as measured in the midsagittal corpus callosum. Nonetheless, immersion fixation holds the advantage of not relying on an intact neurovascular system, such that the most peripheral parts of the brain tissue can undergo good fixation even in the case of clogged blood vessels and/or brain trauma. Furthermore, perfusion-fixed tissues may additionally be post-fixed through the immersion process as well, often in a different concentration of the fixative.

**In brief, we recommend minimizing the PMI to minimize autolytic changes in the tissue, refrigerating samples before and during immersion fixation and, whenever possible, sacrificing the animals using perfusion-fixation, which practically reduces the PMI to zero.**

There are a number of fixatives to choose from, the most common being formaldehyde, prepared using liquid formalin or powdered paraformaldehyde (PFA). For an overview of formaldehyde fixatives, see (Vučković et al. 2020; Kiernan 2000). Notably, the type and concentration of fixative can have a considerable impact on tissue relaxation properties ((Shepherd, Thelwall, et al. 2009; H. D'Arceuil and de Crespigny 2007)), leading to differences in image SNR for diffusion MRI. Neutral buffered formalin (NBF; formalin buffered with PBS) at 10% concentration can be used at room temperature and is most commonly used for immersion fixation in large samples (where higher temperature speeds up the penetration), while PFA at 4% in buffered solution should be kept cold and is standard for perfusion fixation (both resulting in a 4% formaldehyde solution). Buffered fixatives (NBF or buffered PFA) may be preferred to their unbuffered versions. For example, brains fixed with NBF have higher  $T_2$  values than brains fixed with standard formalin ((Tendler et al. 2021) - Figure 5), which leads to higher SNR diffusion data. Reducing these fixative concentrations by half has been shown to also prolong  $T_2$

and improve SNR in fixed tissue (Birkl et al. 2018; Barrett et al., n.d.). Further, it has been observed that brains stored in formaldehyde-based fixatives may continually shrink during storage (de Guzman et al. 2016), with different structures experiencing differing rates of morphometric change and with different extents over time (J. Zhang et al. 2010; de Guzman et al. 2016). The addition of glutaraldehyde to the fixative solution has been shown to provide improved ultrastructural brain tissue preservation in the case of immersion-fixation (Morin et al. 1997), a mandatory requirement particularly for electron microscopy cross-validation studies. The use of a fixative solution combining glutaraldehyde and paraformaldehyde has been shown to be MRI compatible while providing a better preservation of the cytoskeletal structures than paraformaldehyde fixative alone (Schwartz et al. 2005), while also better preserving membrane permeability (Shepherd et al. 2009). However, high glutaraldehyde concentrations can reduce the immunogenicity of antigens for immunohistochemistry analyses (Kiernan 2000), but concentrations in the 0.05% range are acceptable, while slightly improving tissue morphology preservation (Welikovitch et al. 2018). For an extensive discussion on other types of fixatives, as well as a comprehensive review on fixation in brain banking, see McFadden et al. 2019.

Even using the recommended procedures and concentrations for perfusion-fixation, there is discrepancy in the literature as to the degree of microstructural changes that the tissue undergoes. Studies mention for example variable levels of **preferential shrinkage** of certain compartments (e.g. the extracellular space) (Korogod, Petersen, and Knott 2015). It should be noted though that shrinkage due to chemical fixation is less than that during dehydration and tissue preparation for electron microscopy, for example (Dyrby et al. 2018; Fox et al. 1985; Korogod, Petersen, and Knott 2015). At the intracellular level, MR microscopy studies on immersion-fixed, isolated neurons from *Aplysia californica* show fully preserved cellular organization between nucleus and cytoplasm (C. H. Lee et al. 2015), indicating that subcellular compartments are affected evenly by formaldehyde fixation. Notably, compartment models of diffusion *in vivo* have long yielded relative intra- to extracellular fractions of 30/70 (or 50/50 at best in white matter) which are in mismatch with 80/20 histological estimates of intra- vs extracellular compartment volume fractions (Clark and Le Bihan 2000; Ileana O. Jelescu et al. 2016). The latter are however more consistent with *ex vivo* diffusion models, which typically report 70/30 signal fractions (Olesen et al. 2022). This suggests that *ex vivo* fixed tissue used for dMRI is closer to its histological counterpart than *in vivo* tissue. It is unclear though whether the change in relative dMRI compartment sizes between *in vivo* and *ex vivo* is due to non-uniform shrinkage with fixation or to non-uniform changes in compartment  $T_2$ 's, which affect the weighting of compartment signal contributions (Ileana O. Jelescu et al. 2020). Methods such as cryo-fixation used for electron microscopy, which preserves the *in vivo* tissue compartment sizes more faithfully, could help shed light on some of these open questions (Pallotto et al. 2015; Korogod, Petersen, and Knott 2015).

Furthermore, there is still controversy as to whether chemical fixation increases or decreases **cell membrane permeability** (Thelwall et al. 2006; Porea and Webb 2006; Sønderby et al. 2014), which is highly relevant for multi-compartment tissue models (Ileana O. Jelescu et al. 2022; Olesen et al. 2022). Another example of altered microstructure is demonstrated in a number of MRI studies performed on fixed tissue, which have reported an

additional signal component in tissues, such as “isotropically-restricted water” in white matter (sometimes referred to as “still water” or “dot compartment”) that is not observed *in vivo* (Panagiotaki et al. 2012; Grussu et al. 2017; Alexander et al. 2010) except for the cerebellum (Tax et al. 2020). This isotropically-restricted signal trapped component is characterized by an extremely low diffusion coefficient, which gives rise to a non-vanishing diffusion-weighted signal even at high  $b$ -values and appears different from noise (Alexander et al 2010), which is above the noise floor level. The exact origin of such a component is unknown, although it may be related to fixation indicative of tissue overfixation, or vacuoles as visualized using synchrotron imaging (Andersson and Kjer 2020). However, the origin of vacuoles is still unknown and could be related to the fixation process (McInnes 2005) as well exist in healthy tissue (Abdollahzadeh et al. 2019).

In addition, fixation alters the relaxation rates, substantially decreasing  $T_1$  and  $T_2$  (Shepherd, Thelwall, et al. 2009). The decrease in  $T_1$  is understood to be due to the cross-linking of proteins that occurs in the fixation reaction, and is not reversible, whereas  $T_2$  is decreased due to the presence of unbound fixative, and can be increased back closer to its *in vivo* value by washing (Shepherd, Thelwall, et al. 2009). Consequently, tissue washing or rehydration has proven to be beneficial for SNR enhancement and must be considered when designing any *ex vivo* MRI acquisition protocol (see [Section 3.4](#)).

Finally, and crucially, fixation changes the water diffusion coefficient ([Shepherd et al. 2009](#); [D'Arceuil and de Crespigny 2007](#); [Lohr et al. 2020](#); [Tovi and Ericsson 1992](#)), with important implications for acquisition protocols and biophysical models of dMRI, as will be discussed in [Section 3.5.3](#).

## 3.4 Sample Preparation

Recommendations for sample preparation include (1) wash out free fixative (can take days), (2) ensure a robust mechanical setup to eliminate motion during scanning, and (3) verify temperature stabilization prior to acquiring used data. If there is no interest in tissue relaxometry or quantitative diffusion metrics, (4) soaking in a Gadolinium-based solution might help to optimize the trade-off between SNR and acquisition time (H. E. D'Arceuil, Westmoreland, and de Crespigny 2007; Barrett et al., n.d.). We discuss each in detail below, and also consider the solution samples may be scanned in.

First, prior to imaging fixed tissues that have been stored in the fixation fluid, **we recommend PBS ‘washes’ to rehydrate the sample and wash out free fixatives**. A ‘wash’ is simply placing your sample in a PBS solution and replacing the PBS regularly. It is very important during wash out to add an antibacterial/antifungal product such as sodium azide to avoid tissue degeneration. Fixatives have a high transverse molar relaxivity, and washing out has been shown to substantially increase the  $T_2$ , as mentioned above. While the  $T_2$  rises quickly, the washing time required for it to stabilize is dependent on sample size, geometry, volume and temperature of PBS solution, fixative concentration and previous time in fixative ([Barrett et al.](#) ), with a wide variety of wash times noted in the literature (**Table 1**). To maximize  $T_2$  and reduce the time to its stabilization, we recommend using as large a volume of PBS solution relative to the sample volume as practical, and replacing the solution several times, more frequently in the

first few hours/days/weeks of washing (e.g., every 12 – 72 hours), depending on sample size. To maximize tissue quality, we recommend refrigerating samples throughout the washing period. Of course, the larger human brain may require several weeks or more to fully wash, and are indeed often not washed due to the prohibitive length of time required and possible inhomogeneity of washing effects throughout the brain.

Specimen	Approximate sample thickness	Soaking time	Fixative	PBS vol	Temperature	Number of solution changes	Reference
Ghost erythrocytes	80 $\mu$ l	12 hours	various	100 x sample vol		3	Thelwall et al., 2006, MRM
Rat cortical slices	0.5 mm	12 hours	4% formaldehyde		Room temperature	4-5	Shepherd et al., MRM, 2009; Shepherd et al., NI, 2009
Rat spinal cord	~2 mm	Overnight	4% formaldehyde				Shepherd et al., NI, 2009
Marmoset brain sections	2.5 mm	4 days	10% formaldehyde	10 x sample vol	4°C	0	D'Arceuil et al., 2007, NI
Marmoset brain	~ 20 mm	4-6 weeks	4% formaldehyde		4°C	0	Blezer et al., 2007, NMR Biomed
Rat brain in situ	~ 25 mm	$\geq$ 20 days	2% formaldehyde	50 mL	4°C	0	Barrett et al., 2022
		$\geq$ 47 days	4% formaldehyde	50 mL	4°C	0	Barrett et al., 2022
Macaque brain	~ 40 mm	$\geq$ 25 days	10% formaldehyde	1 L	4°C	0	D'Arceuil et al., 2007, NI
		3 weeks	4% formaldehyde				Schilling et al., 2018, NI
Sheep brain	~ 50 mm	$\geq$ 3 weeks	4% formaldehyde				Leprince et al., Proc ISMRM, 2015

**Table 1.** Examples of soaking times in PBS prior to MR imaging, depending on specimen size, fixative, etc.

**To further increase SNR and CNR, gadolinium-based contrast agents are often added during the rehydration (washing) step.** Gd is a paramagnetic contrast agent in the form of a chelate that facilitates longitudinal relaxation (reduces  $T_1$ ), which allows TR minimization, particularly in 3D imaging sequences, thus maximizing the SNR per unit time. Alternatively, Gd can be introduced during the perfusion step for small animals, in a technique referred to as ‘active staining’ (G. Allan Johnson et al. 2002). If this is done, we still recommend immersing the sample in a Gd solution as well. Typically,  $T_1$  decreases are observed in the sample within 2-3 days in larger brains (macaque brain) (D'Arceuil 2007, NI), although we recommend soaking for 1-2 weeks in Gd solution depending on brain size. Notably, a higher concentration of Gd results in continually faster relaxation (reducing both  $T_1$  both  $T_2$ ) (Barrett et al., n.d.; H. E. D'Arceuil, Westmoreland, and de Crespigny 2007). The optimal concentration to use depends on minimum TE, maximum TR of the acquisition protocol and method of staining

(active staining typically uses a higher concentration than soaking), as well as field strength. For example, a low Gd concentration is more appropriate for longer TE and/or TR protocols, whereas higher concentrations are optimal for short TE and/or TR protocols, as less signal is lost from transverse relaxation, and the gains from speeding up longitudinal relaxation are more worthwhile. Examples in the literature are shown in **table 2**, where a range of Gd contrasts and concentrations are utilized with different acquisition choices (TE/TR) at varying field strengths.

Concentration (mM)	Contrast agent	TE (ms)	TR (ms)	Magnet (T)	Reference
1	Gd-DTPA	32	240	4.7	D'Arceuil et al., 2007
1	Gd-DTPA	40	1000	4.7	Dai et al., 2016
1	Gd-DTPA	41	410	9.4	Schilling et al., 2019, NMR Biomed
0.5/0.5	Gd-DTPA	26	1000	9.4	Hamaide et al., 2016
5	Gadoteridol	11-15	125-150	11.7	Tyszka et al., 2006; Tyszka & Frank, 2009
5/2.5	Gd-DTPA	21	100	7	Johnson et al., 2012
15-Jan	Gd-DTPA	27	250	9.4	Barrett et al., 2022
50/5	Gd-DTPA	15	100	9.4	Calabrese et al., 2015, Cereb Cortex

**Table 2.** Examples of the concentration of gadolinium contrast agent used in ex vivo dMRI studies from the literature. Where two concentration values are given, the first refers to the active staining concentration (contrast agent added in perfusion fixation), the second to passive staining (soaking post-fixation). A single concentration value refers to passive staining only.

As a caveat, care must be taken when using Gd-soaked tissue for quantitative dMRI studies, as the effects of gadolinium on specific tissue compartments are not well understood.  $T_1$  longitudinal evaluation after Gd-doping exhibited a complex behavior of  $T_1$  variation within different regions (Sébillé et al. 2019). Gd-soaking is thus best suited for tractography acquisitions. Gd staining to optimize SNR has been used without detrimental effects on histology or immunohistochemistry analysis (Spencer et al. 2006; Barrett et al., n.d.).

Our second recommendation is to **ensure a robust mechanical setup to eliminate motion** during MRI data acquisition (**Figure 7**). The sample must be tightly constrained inside the imaging container, to prevent motion within the immersion fluid. This is critical to address both bulk motion and non-linear deformities that may arise over the duration of a long ex vivo scan (for example, bending of the brain stem). Notably, non-linear deformations are particularly challenging to correct when considering the importance of directional information in diffusion MRI. Sample-holders may be as simple as test tubes, or the cylinder of syringes (which may help remove air bubbles described later), as well as holders custom-made to fit within specific volume coils, often made with clear polycarbonate materials. In addition, some fluids that the sample is immersed in (see below), may have high densities, causing the sample to float if not properly constrained. Constraints are often applied through inserting foam pieces, where several groups have suggested very heavily reticulated foam to facilitate removal of air bubbles. Pieces of agar can also be used to stabilize tissue in a container, though agar is MR visible (see considerations on immersion fluids below). If the above options are not feasible, post mortem

brains can also be placed in a plastic bag. Here, the brain is wrapped with a thin layer of gaze in minimal fluid to reduce air bubbles and susceptibility effects, and the bag is slowly compressed until fluid is expelled to fully remove air bubbles, and tied tightly to ensure no leakage. Finally, very fragile tissue specimens, such as embryonic mouse brains, can be immersed in either agar gels, or kept within the skull, for increased mechanical support and to avoid deformation.

To minimize field inhomogeneities, ideally the holder will consist of a simple geometric shape (without sharp boundaries), with the sample immersed in a susceptibility matched fluid (see below). The holder can be designed considering the shape of the coil in mind to minimize coil-to-sample distance, and place samples in a consistent position to facilitate analysis and eliminate any orientation effects.

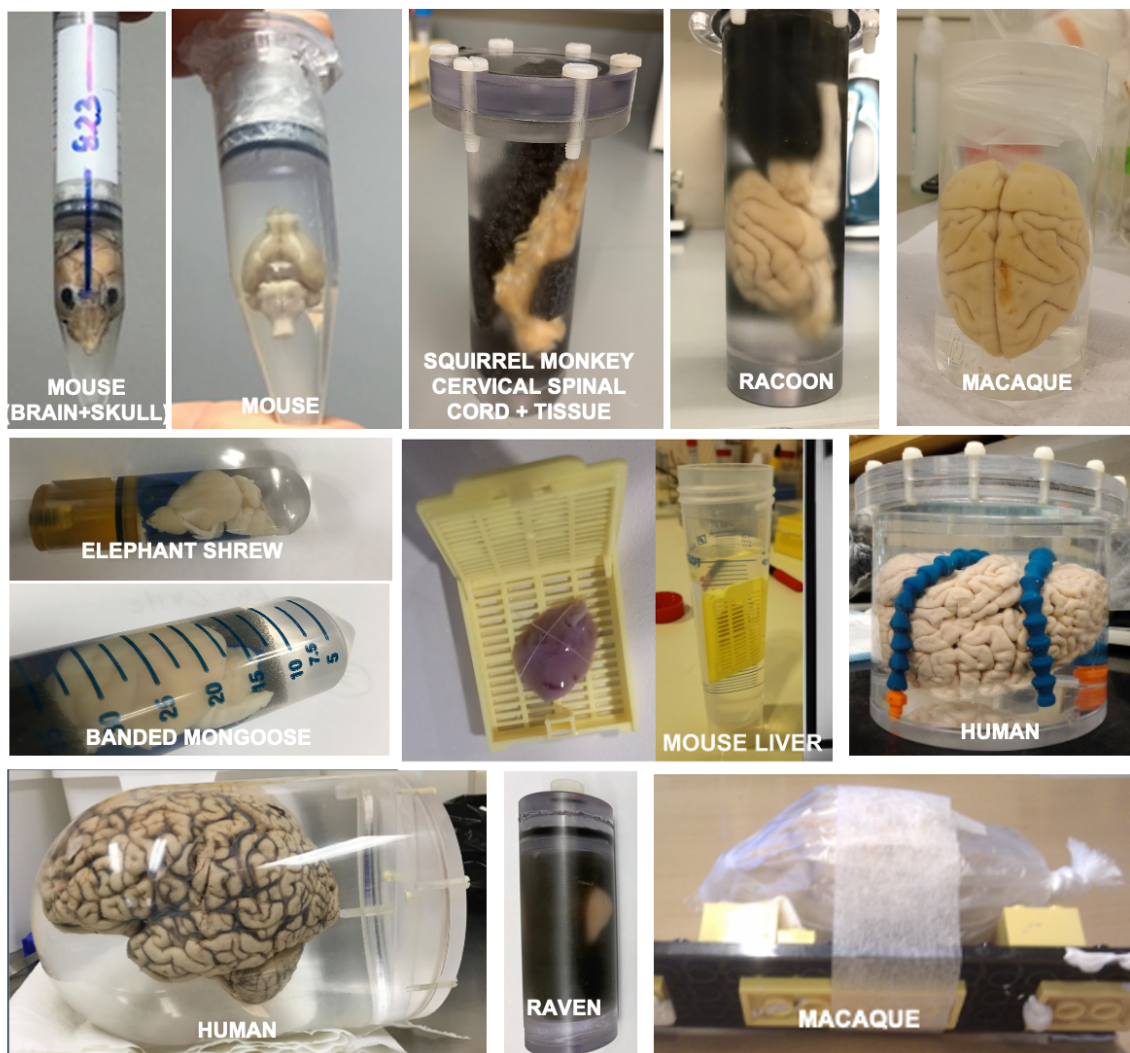


**Figure 7.** Examples of *ex vivo* samples prepared for dMRI acquisitions. Sample holders may be syringes or test tubes/falcon tubes, custom-made or 3D printed holders with ventilation valves, or simply placement within a plastic bag robustly secured to a platform. Photos courtesy of

Daniel Colvin, Kurt Schilling, Luisa Ciobanu, Stijn Michielse, Francesco Grussu, Raquel Perez-Lopez, Ileana Jelescu, Tim Dyrby.

Finally, recent advances allow 3D printing dedicated sample holders for minimizing motion/vibration, larger holders for human brains, and the ability to load multiple samples for simultaneous imaging (although with the disadvantage of requiring larger FOV and limited spatial resolution).

For data acquisition, samples are typically immersed in either PBS or fluorinated oil. **In general, we suggest using a fluorinated oil, these are susceptibility-matched, inert compounds that do not have  $^1\text{H}$  protons.** Thus, they lead to no signal in  $^1\text{H}$  MR images, alleviating ghosting artifacts, facilitating image masking, and allowing a smaller, tighter FOV. There are a variety of fluorinated oils that are suitable: perfluoropolyethers such as Fomblin (Solvay) or Galden (Solvay) or perfluorocarbons such as Fluorinert (3M), and these can even be reused repeatedly instead of throwing out the solution after every scan. While studies have not explicitly looked at the effects of these oils on conventional or immuno-histology, it is our experience that they do not compromise nor interfere with this analysis (Iglesias et al. 2018). However, it is recommended that after the MRI scan, excess oil be removed off the sample using absorbent paper, followed by several PBS washes to remove any residual oil in the cavities of the tissue sample. While these compounds are inert, the effect of long term storage of tissue in them is not known and thus not recommended.

During the transfer from the storage container to the imaging container, air bubbles can get trapped in cavities such as brain sulci and ventricles. Due to the strong difference in magnetic susceptibility, air bubbles will result in substantial image distortions and should be carefully removed during sample preparation. Removing air bubbles can be done by slightly turning, shaking and agitating the tissue. Alternatively, some groups have utilized a vacuum setup to remove trapped air bubbles. It is unclear how much the tissue quality is affected by vacuuming too heavily, but the vacuum pressure should nonetheless be decreased gradually. When using vacuum one must be aware that due to the extremely low pressure, bubble size is expanded substantially, and the tissue and fluid can appear as 'boiling'. Lastly, a fine paintbrush may also be used to remove air bubbles while the sample is immersed.

Finally, to remove unwanted time-dependent signal contributions due to tissue temperature changing during scanning (from the cold storage to bore-temperature), **we advise placing the sample at the desired temperature for at least 4-8 hours prior to scanning** (Dyrby 2011, HBM). In fact, it may be beneficial to actually run a dummy dMRI scan during these hours of temperature regularization (as suggested by Dyrby et al) accounting for possible temperature changes caused by gradient coil heating. The time period also secures the reduction of non-linear motion of the tissue that can appear after physically handling the brain setup when placing it in the magnet. Timing should be kept consistent to avoid bias in group comparisons. During the scanning, the use of strong or varying diffusion weightings can influence the temperature environment of the tissue hence the diffusion coefficient. However, having a constant airflow around the tissue during scanning can reduce the unwanted temperature effect.



## 3.5 MR Scanning

### 3.5.1 Encoding

Just as for *in vivo* small animal imaging (Part 1), a number of possible **diffusion encoding**, or sensitization, schemes are feasible, although the unique changes of decreased diffusivities and increased relaxation rates must be considered. For *ex vivo* dMRI, the two most common encoding schemes are the **pulsed gradient spin echo (PGSE)** and **steady-state free-precession (SSFP)** with diffusion preparation. For **PGSE** encoding, strong diffusion-sensitization gradients are applied on either side of a 180° refocusing pulse, resulting in a mathematically elegant way to describe diffusion weighting through the *b*-value,  $b = (\gamma G \delta)^2 (\Delta - \delta/3)$ , (where  $\gamma$  is the gyromagnetic ratio,  $G$  is the gradient strength,  $\delta$  is the pulse duration, and  $\Delta$  pulse separation). Because of its simplicity, PGSE is the most widespread diffusion weighting in both *in vivo* and *ex vivo* experiments.

Additionally, SSFP has been heavily utilized *ex vivo*. **SSFP** acquisitions are composed of rapid repeats of pulse-encode-readout cycles, sampling or reading out signals every tens of milliseconds. Thus, the signal is retained over multiple repetition times, acquiring both spin echoes and stimulated echoes simultaneously. This results in both strong diffusion weighting and high SNR, with the possibility of very short echo times. The primary disadvantage of SSFP is increased sensitivity to motion, limiting its use *in vivo*, but easily overcome *ex vivo*, with the added benefit of acquiring high resolution high SNR images with great efficiency. However, unlike PGSE, the signal becomes a complicated function of flip angle, TR,  $T_1$ ,  $T_2$ , and the diffusion encoding, requiring specialized modeling to quantify diffusion coefficients.

Other encodings are also possible *ex vivo*, and described in more detail in Part 1. Briefly, **stimulated echo acquisition mode (STEAM)** sequences enable probing very long diffusion times with the disadvantage of a lower SNR compared to PGSE (for equal echo times). **Oscillating gradient spin echoes (OGSE)**, uses periodic sinusoidal gradients to probe much shorter times and length scales, which become particularly smaller with reduced diffusivity *ex vivo*, with limitations associated with attaining higher *b*-values. Finally, diffusion encoding can be applied along multiple spatial directions in **multi-dimensional diffusion encoding** experiments, which offers potential contrasts related to compartmental kurtosis, compartmental exchange, microscopic anisotropy, or heterogeneity of structural sizes/diameters.

### 3.5.2 Readout

For *ex vivo* imaging, readouts can be extremely diverse due to lack of sample motion and long available scan time. Our recommended starting protocol is a **multi-shot 3D EPI sequence**. Echo planar imaging uses rapidly oscillating phase gradients to generate multiple gradient echoes to fill out *k*-space. A 'single-shot' EPI sequence (with PGSE encoding) is far and away the most common *in vivo* readout in both humans and small animals, where 2D *k*-space is acquired within a full TR. This type of acquisition is great to reduce scan time and motion artifacts, but faces challenges including susceptibility distortion due to field

inhomogeneity that causes not only geometric warping but also signal intensity stretching and pileup. This can be especially challenging at high field strengths, and when acquiring large acquisition matrix sizes (for high spatial resolution or field of view). To alleviate this, it is possible to acquire data with a segmented readout, where  $k$ -space is read out in multiple shots. This comes at the cost of increased scan time and possible ghosting artifacts due to physiological motion that are typically corrected for using phase navigation techniques. Conveniently, *ex vivo* MRI is not limited by scan time nor motion, hence the recommendation for a multi-shot 3D EPI sequence.

Here, two features have been changed from the typical *in vivo* protocol: from single to multi-shot, and from 2D multi-slice to a 3D sequence. 3D EPI sequences are capable of achieving substantially higher SNR than 2D EPI sequences (Rane and Duong 2011; Saleem et al. 2021). This SNR gain is due to averaging effects from Fourier encoding the entire tissue volume (i.e., collecting signal from the entire 3D tissue volume). SNR increases as the square root of the number of datapoints in the third spatial dimension, also referred to as second phase-encode direction, and which corresponds to the slice dimension in 2D multi-slice experiments (Bernstein M. A. 2004). For this reason, the primary advantage of increased SNR of 3D sequences is bolstered by the large number of datapoints in the phase encode and second phase encode directions, so it is advantageous to increase these, at the expense of increased scan time (although if a small number of data points in the third dimension are required, 2D sequences may be more suitable). The rationale for going from single to multi-shot is that a strong segmentation of the 3D EPI read-out is necessary to prevent image distortions and prohibitively long echo times, especially if high spatial resolution is desired. For this reason, it is not uncommon to see 4-12 shots, or more. 3D EPI also comes with the advantage of enabling acquisitions with truly isotropic resolution. Indeed, very high spatial resolutions in the third dimension may not be achievable in 2D multi-slice acquisitions, as very thin slices may not be feasible depending on the slice-selection gradient strength.

Despite the intrinsically higher SNR of 3D images, they suffer from suboptimal temporal utilization of  $T_1$  relaxation. The TR with optimal SNR per time unit depends on the  $T_1$  value of the tissue and can be determined by means of Bloch simulations or using the following relationship:  $SNR_t \sim M_0 (1 - e^{-TR/T_1}) e^{-TE/T_2}$ . This equation can be used to determine the optimal TR in terms of **SNR efficiency** (SNR per unit time), where SNR efficiency (SNR / square root of total imaging time) can be modeled as  $SNR_{efficiency} \sim (1/\sqrt{TR})(1 - e^{-TR/T_1})$ . Conveniently, *ex vivo* imaging enables the addition of Gadolinium-based contrast agents to the sample to shorten  $T_1$ , and thus the optimal TR, facilitating high SNR efficiency. Example SNR efficiency curves are shown in **Figure 8**, where the optimal TR is  $\sim 1.25$  times the estimated  $T_1$  (for examples of optimizing TE, TR, and diffusion weighting see *Other Considerations* in [Section 3.5.3 q-t coverage](#); for a discussion of advantages and limitations of contrast agents, see *Sample Preparation* [Section 3.4](#)). It should be noted however that short TR's may introduce  $T_1$  weighting and affect the relative contributions of different compartments to the overall signal, in a similar manner to  $T_2$  weighting.

Alternative readouts are also possible *ex vivo*. This includes the **2D EPI** and **spiral** readouts as *in vivo* (described in detail Part 1), and many *ex vivo* studies have taken advantage of the multiple RF echo trains of **RARE/FSE**, or **GRASE**, which often offers a good trade-off between scan time and image quality with high SNR and immunity to distortions. At the extreme end of acquisition is a **line-scan** readout, which traverses a single line of  $k$ -space per excitation. While this offers excellent robustness to susceptibility artifacts, it has a low SNR efficiency and may require excessively long scan times, or a tradeoff between spatial and angular resolutions.  $B_0$  drift may also become problematic when the scan time is on the order of several days, and should be corrected for. Acquisitions can for example be split into 2-3 hour blocks, with the frequency readjusted before each block. This also allows retrieving at least partial data in the event the scanner crashes during the long acquisition.

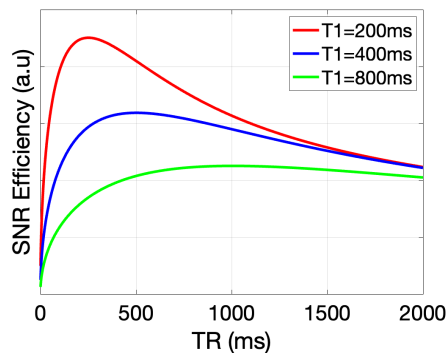


**Figure 8.** Plots showing how SNR efficiency varies with T1. Curves are based on the SNR-efficiency equation given in Section 3.5.2 based on a spin echo sequence. The optimal TR is  $\sim 1.25$  times the sample T1, although there is a wide range of near-maximum efficiency. Similar optimization can be performed for TE, and diffusion weightings (see *Other Considerations* in Section 3.5.3 *q-t coverage* for examples)

### 3.5.3 q-t coverage

The beauty of *ex vivo* imaging, and preclinical small animal imaging in general, is the ability to cover a wide range of  $q$ - $t$  space, sampling multiple  $b$ -values, at potentially multiple diffusion times, and in many diffusion directions. Before setting up diffusion parameters, it is important to understand the theoretical requirements of the chosen data analysis framework which will be used to process the data - this might include requirements of short gradient pulses, long/short diffusion times,  $b$ -value regimes, or number of unique sampling directions.

The primary differences between *in vivo* (described in Part 1) and *ex vivo* is the consideration in changes due to the slower diffusion, which often requires high  $b$ -value and/or longer diffusion times to ensure adequate signal attenuation and spin displacement (we assume here that the sample has been washed to restore  $T_2$  values, otherwise short  $T_2$  are another consideration for fixed tissue). Indeed, *ex vivo* diffusivities of fixed tissue remain lower than *in vivo* even at 37°C, the degree depending on the fixation method (perfusion-fixation or immersion) and postmortem interval (Miller et al. 2011; Shepherd, Thelwall, et al. 2009; H. E. D'Arceuil, Westmoreland, and de Crespigny 2007; Pfefferbaum et al. 2004; Roebroek, Miller,

and Aggarwal 2019; Dyrby et al. 2011). Moreover, scanning is often performed at room temperature, resulting in further reduction of diffusivity (change of -1–3% per °C). As a result,  $b$ -values should be adapted accordingly to ensure sufficient signal decay and sensitivity to parameter estimation ( $\sim$ constant  $bD$  product) (H. E. D’Arceuil, Westmoreland, and de Crespigny 2007; Roebroek, Miller, and Aggarwal 2019). Selected examples are given in **table 3**, where considerable decreases in diffusivity are observed across species in perfusion and immersion fixed brains, as well as in fresh *ex vivo* tissue.

	T1	T2	D	Specimen	Reference
<b>Fixation (% change from in vivo to fixed)</b>			↓ 80% ADC	macaque brain 2.5mm sections, immersion fixed	D’Arceuil et al., 2007, NI
			↓ 64% Trace	mouse brain perfusion fixed	Sun et al, 2003 MRM
			↓ 55% MD	Rat spinal cord perfused fixed	Madi et al, 2005, MRM
			↓ 72% Trace	mouse brain perfusion fixed	Sun et al, 2005, MRM
			↓ 50% MD	squirrel monkey, perfusion fixed	Schilling et al, 2017, MRI
			↓ 62% MD	rat brain, perfusion fixed	Wang et al., Eur Radiol Exp, 2018
	↓ 22%	↓ 5%	↓ 48% MD	Marmoset brain, immersion	Haga et al., Magn Res Med Sci, 2019
	↓ 40%	↓ 3%		mouse brain perfusion fixed	Guilfoyle et al, 2003, NMR Biomed
	↓ 63%	↓ 35%		human immersion fixed	Pfefferbaum et al, 2004, NI
	↓ 69%	↓ 27%		human immersion fixed	BirkI et al, 2016, NMR Biomed
<b>Ex vivo fresh (% change from in vivo to ex vivo)</b>			↓ 65-88% MD, AD, RD	fresh pig brain	Walker et al, 2019, PLoS One
			↓ 50% ADC	fresh monkey brain	D’Arceuil et al., 2007, NI
<b>PBS washing (% change from fixed to washed)</b>	↑ 7%	↑ 30%	↑ 30% ADC	macaque brain 2.5mm sections, immersion fixed	D’Arceuil et al., 2007, NI
	↑ 7%	↑ 3%	↑ 11% MD	human immersion fixed	Leprince et al, 2015, Proc ISMRM
	↑ 3%	↑ 72%	↑ 2% MD	rat brain, perfusion fixed	Barrett et al n.d.
			Reported no difference	Cat spinal cord, immersion fixed	Pattany et al, 1997, AJNR
	Reported no difference	↑ 516% (cortex)		rat cortical slices, immersion fixed	Shepherd et al., 2009, MRM
	↓ 14%	↑ 24%		Marmoset brain	Blezer et al, 2007, NMR Biomed

**Table 3.** Changes in T1, T2 and D reported in the literature due to fixation and washing in PBS. Data is included from samples fixed with 10% Formalin or 4% PFA, scanned at room temperature. Measurements from WM only are included, unless otherwise noted.

Thus, for both fresh *ex vivo* and fixed tissue the drop in diffusivity is typically on the order of  $\sim$ 2-5 at room temperature, which corresponds to increasing the  $b$ -value by a similar factor to match the attenuation expected from an *in vivo* dMRI protocol. For postmortem human samples,

however, due to non-negligible post-mortem interval and an extended duration of immersion fixation needed to preserve cell and tissue components, the diffusivity is often on the order of 85% lower than *in vivo* (Foxley et al. 2014; Miller et al. 2012), also in agreement with animal studies with extended PMI (H. D’Arceuil and de Crespigny 2007), and which corresponds to a much larger increase in *b*-value needed to match an *in vivo* dMRI protocol. Consequently, beyond DTI protocols, including DKI and other advanced dMRI methods are sometimes challenging on postmortem human tissue due to the prohibitively high *b*-values required. For DTI, an adjusted *b*-value to about 4000 s/mm<sup>2</sup> (H. E. D’Arceuil, Westmoreland, and de Crespigny 2007) has been shown to result in similar signal attenuation as for an *in vivo* *b*=1000 s/mm<sup>2</sup> scan, and provide the angular contrast needed to resolve crossing fibers for tractography (Dyrby et al. 2011). It should however be noted that the optimal *b*-value for post-mortem acquisitions is a function of tissue fixation and scanning temperature and should be evaluated for each experiment individually. Notably, for tissue that has been suitably perfusion-fixed, the impact of fixation on the diffusivity is relatively comparable across subjects.

Because of changes in diffusivity, it is important to consider spatial scales that are being probed. As diffusivity drops, diffusion distances proportional to  $\sqrt{Dt}$  drop as well - unless the diffusion time is prolonged accordingly - which results in different interactions between water molecules and the microscopic features they are able to probe. This may be beneficial when interested in probing geometry on small scales and also extends the limit of the narrow pulse approximation validity (Alexander et al 2010). This is additionally important in MR microscopy, where the resolutions start to approach the diffusion length scales and a significant amount of water may diffuse out of the imaging voxels in the echo time such that the spatial resolution is no longer ‘real’ (see [Section 3.7](#) for more details).

Below, we provide guidelines for common applications of ex vivo imaging: signal representations (DTI/DKI), tractography, and biophysical signals models.

**Diffusion tensor imaging (DTI)** requires one non-zero shell with 6 non-collinear directions, but, just as for in vivo acquisitions, 20-30 directions are usually required to mitigate effects of noise and anisotropy. To maximize precision, the *b*-value should be chosen such that the signal decay is substantial, for example so that the product  $bD \simeq 1$ . In vivo, this is approximately a *b*-value of  $b = 1000$  s/mm<sup>2</sup>. Ex vivo, this cut-off value will be higher by a factor of 2-5, depending on the drop in diffusivity values. Similarly, Diffusion Kurtosis Imaging (DKI), which estimates the non-Gaussian characteristics of diffusion in tissue (i.e., how much the tissue differs from a Gaussian medium with matching diffusivities as derived from DTI), requires two non-zero shells with 21 (6+15) non-collinear directions, but is typically acquired with 20-30 directions per shell. The highest recommended *b*-value in vivo is typically  $b = 2000$ - $2500$  s/mm<sup>2</sup> to maximize precision while staying within the radius of convergence of the cumulant expansion; ex vivo this translates into the highest *b*-value typically around  $b = 6000$  s/mm<sup>2</sup> (Kelm et al. 2016; Aggarwal, Smith, and Calabresi 2020; Henriques, Jespersen, and Shemesh 2020; Chuhutin, Hansen, and Jespersen 2017).

For **tractography**, ex vivo guidelines again follow closely those of both small animal (Part 1) and human scans in vivo - our recommended protocol includes acquiring 50-60 directions at a moderate-to-high *b*-value, where again, a greater diffusion weighting (particularly

for *ex vivo*) leads to a higher angular contrast and ability to resolve complex fiber architectures - for example Dyrby et al. (Dyrby et al. 2011) found a  $b$ -value of  $\sim 4000$  s/mm<sup>2</sup> to lead to consistent fiber reconstructions with a high angular contrast, although a much larger range of  $b$ -values has also been utilized *ex vivo* with high angular accuracy and subsequent accurate tractography (Maffei et al. 2022b; R. Jones et al. 2020; H. Wang et al. 2014; K. G. Schilling et al. 2018; Grisot, Haber, and Yendiki 2021b).

Regarding **compartment modeling**, it is critical to consider the data requirements of the intended biophysical model, specifically as it relates to diffusion times and diffusion weightings. Acquisitions for various models are often introduced and optimized for *in vivo* imaging, for example based on expected diameters and expected displacements in certain diffusion time regimes, yet, *ex vivo* imaging requires considerably increased diffusion times to probe the same distances, which must be accounted for when designing sequences. Similarly, if diffusion-relaxometry experiments are intended, altered  $T_1$  and  $T_2$  depending on fixation and subsequent washing must be considered. While it is impossible to give recommendations that will apply to all biophysical models, it is usually advantageous to minimize TE to maximize SNR, especially with significantly reduced  $T_2$  *ex vivo*. This is usually accomplished by minimizing diffusion times, maximizing gradient strengths, along with other potential sequence modifications (multi-shot imaging, partial Fourier, in-plane acceleration) if the acquisition allows, although again, care must be taken to ensure this does not violate modeling assumptions.

### **Other practical considerations**

A great benefit in *ex vivo* imaging is the ability to conduct multiple experiments on the same tissue. It is particularly advantageous to measure  $T_1$ ,  $T_2$ , and diffusivity throughout the sample, and **SNR efficiency** can be optimized and tuned for both 2D and 3D sequences through changes in TE, TR, and diffusion weightings. For example, several studies (Barrett et al., n.d.; H. E. D'Arceuil, Westmoreland, and de Crespigny 2007) present a comprehensive approach: measuring combined effects of tissue preparation strategies, including rehydration time, fixative, fixative concentration, and contrast agent concentration to manipulate acquisition parameters and maximize SNR (**Figure 9**). This can be done for any 2D or 3D sequence, with any choice of readout strategy.

Other practical suggestions, as described in detail in Part 1 and also apply to *ex vivo* scans are to: (1) use an optimally distributed set of diffusion-encoding directions that cover the full sampling sphere (2) randomize ordering of acquisition of DWI images, especially across  $b$ -values to reduce or enable correction of temporal biases, reduce duty cycle, and allow analysis on partial acquisitions (3) intersperse several/many  $b=0$  images throughout the scan to enable controlling for temporal drifts (Vos et al. 2017a), (4) use the effective  $b$ -matrix (i.e., the realized  $b$ -matrix taking into account other sequence gradients — rather than the nominal value entered into the scanner) which can be measured and validated in phantoms (Fieremans and Lee 2018), and (5) perform high order shimming which may be critical for image quality, particularly at high field strengths due to their increased inhomogeneities.

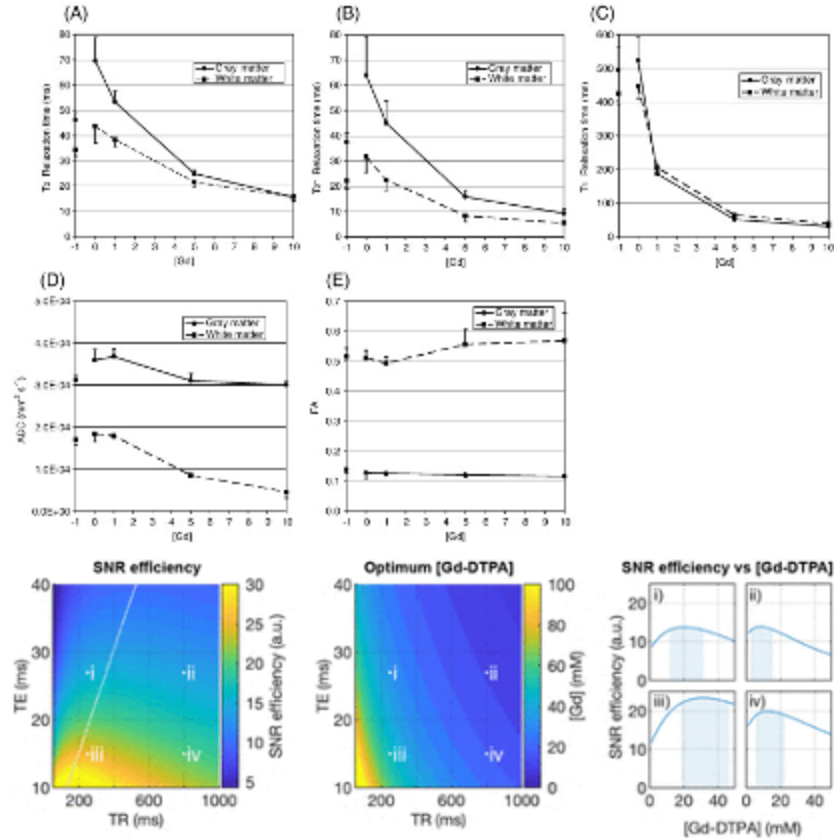


**Figure 9.** Approach to optimizing ex vivo diffusion protocols. Relaxometry (top) and diffusion (middle) can be measured as a function of contrast concentration, or fixative solution, for both white and gray matter tissue types, and SNR efficiency can be optimized (bottom) by manipulating sequence parameters and gadolinium contrast agent concentration. Images are adapted and modified from (H. E. D’Arceuil, Westmoreland, and de Crespiigny 2007) (top) and (Barrett et al., n.d.) (bottom).

### 3.5.4 MR Scanning, Monitoring, scan duration

During long ex vivo scanning, it is important to minimize artifacts using several acquisition strategies. First, it is recommended that each image or volume be collected within as short a time period as possible, i.e., inner-most loops should cover k-space sampling while outer-most loops should cover q-space sampling. Some default vendor sequences acquire a single phase encoding line (inner-most loop) for each of the diffusion encodings before looping through all phase encoding steps, which leads to potential long delays between data composing a single image. A preferred approach, one that is not necessarily implemented by vendors, is to acquire the whole image or volume for a given diffusion encoding before moving on to the next diffusion encoding. Furthermore, if more than a single acquisition is performed using averaging, it is preferred to acquire each image separately split into repetitions, while saving the complex-valued data. Averaging repetitions in complex space rather than magnitude space is beneficial for lowering the noise floor to its theoretical zero-value, as opposed to being affected by the Rician noise floor; however, the advantage of initially saving these volumes as individual

repetitions gives the opportunity to omit severely corrupted individual images, if needed. Phase corrections prior to averaging are mandatory, and may need to be implemented by the user if not addressed well by the scanner reconstruction directly ([Bammer et al. 2010](#); [Pizzolato et al. 2020](#)).

As discussed for *in vivo* protocols, shuffling the order of acquisition of various  $b$ -values, directions, diffusion times, and interspersing  $b=0$  images throughout helps identify and reduce systematic biases related to drift, heating and slow motion (e.g. sample sagging in the coil), and also makes it possible to use “partial data” in case of scanner crash midway through a multiple-day acquisition. Notably, this “evaluation” approach to detect systemic biases only works if one image volume has been acquired at a time i.e. all  $k$ -space lines are acquired per volume and not spread out between image volumes.

A stable temperature throughout the protocol is warranted to limit undesired signal drift due to  $T_1$ -weighting and diffusivity variations. Potential sample temperature changes over time should therefore be prevented for example by ensuring an air flow around the tissue with constant temperature, as it is not easy to compensate for temperature drift in the post-processing pipeline. As a temperature control, a water vial can be placed next to the tissue and monitor its diffusivity over time, although it is important to carefully consider where the vial will appear within the field of view due to the addition of possible susceptibility, ringing, or ghosting artifacts. Of note, a temperature increase may also occur *in vivo*, though the effect may be less pronounced thanks to active thermal regulation of the animal.

Collectively, these strategies do not prevent the artifacts, but at least make them more correctable with subsequent post-processing. Altogether, these considerations and approaches serve to minimize the likelihood that potential artifacts will corrupt entire datasets.

### 3.5.5 Spatial resolution

For *in vivo* human or small animal imaging, spatial resolution is a balance between the available SNR and scan time, where resolution should be as high as permissible for the available SNR and scan time. However, *ex vivo* scans require different considerations when choosing a spatial resolution, due to the substantially increased scan time. Overnight and multi-day scans are common-place in *ex vivo* studies, with some *ex vivo* studies scanning for 1-2 weeks. While signal drift and temperature stability issues indeed arise, resolution can be pushed quite extensively, with recent protocols nearly pushing the boundaries where resolution limits are set by the diffusion process itself, e.g. below 10 microns.

In short, there is no single set of guidelines, or consensus, on image resolution for specific species, nor for specific experimental designs. Rather than providing specific recommendations for resolution, below we give typical volumes of brains, and compute what the equivalent voxel size (i.e, the **volume equivalent resolution**) would be given the ratio of volumes, and a 2-mm isotropic human brain scan, typical of *in vivo* studies (**Table 4**). Further, we give examples of *ex vivo* scans that are **pushing the boundaries of resolution** - we note that these are not always feasible at every institution, and are not for any specific tractographic or modeling purposes, but only to highlight high resolution scans that have been performed.



### 3.5.5.1 Volume equivalent resolutions and pushing the boundaries

Species	Brain Volume (mL)	Matching spatial resolution (isotropic)	Reported in literature ( <i>ex vivo</i> )
Human	1200	2 mm	<p>730-<math>\mu\text{m}</math> isotropic (<math>b=3000 \text{ s/mm}^2</math>, 64 directions, 4 days, 3D-EPI) (Miller et al. 2011)</p> <p>940-<math>\mu\text{m}</math> isotropic (<math>b\sim 4500 \text{ s/mm}^2</math>, 54 directions, 1m15s per volume, repeated 10 times, DW-SSFP) (Miller et al. 2012)</p> <p>1000-<math>\mu\text{m}</math> isotropic (<math>b\sim 5175\text{-}8550 \text{ s/mm}^2</math>, 49-52 directions, DW-SSFP, 10-11 minutes per volume) (Foxley et al. 2014)</p> <p>500-<math>\mu\text{m}</math> isotropic (<math>b\sim 1700\text{-}5000 \text{ s/mm}^2</math>, 120 directions, DW-SSFP, 45 minutes per volume) (<a href="#">Tendler et al. 2022</a>)</p> <p>400-<math>\mu\text{m}</math> isotropic (<math>b\sim 3000 \text{ s/mm}^2</math>, 2h23m/volume); 500-<math>\mu\text{m}</math> isotropic (<math>b\sim 2000/4000 \text{ s/mm}^2</math>, 53m/volume); 1000-<math>\mu\text{m}</math> isotropic (<math>b\sim 1000 \text{ s/mm}^2</math>, 23m/volume) - kT-dSTEAM (Fritz et al. 2019)</p>
Mouse	0.4	140 $\mu\text{m}$	<p>25-<math>\mu\text{m}</math> isotropic (<math>b=4000 \text{ s/mm}^2</math>, 61 directions, 95h scan, 3D-SE) (N. Wang et al. 2020)</p> <p>43-<math>\mu\text{m}</math> isotropic (<math>b=4000 \text{ s/mm}^2</math>, 120 directions, 235h scan, 3D-SE) (Calabrese, Badea, et al. 2015)</p> <p>100-<math>\mu\text{m}</math> isotropic (<math>b=2000/5000 \text{ s/mm}^2</math>, 60 directions, 12h scan, 3D-SE) (Liang et al. 2022)</p>
Rat	0.6	160 $\mu\text{m}$	<p>50-<math>\mu\text{m}</math> isotropic (<math>b=3000 \text{ s/mm}^2</math>, 61 directions, 289h scan, 3D-SE) (G. Allan Johnson et al. 2021)</p> <p>150-<math>\mu\text{m}</math> isotropic (<math>b=3000/6000 \text{ s/mm}^2</math>, 30/30 directions, 21h scan, 3D-DW-GRASE) (Chary et al. 2021)</p> <p>88-<math>\mu\text{m}</math> isotropic (<math>b=800 \text{ s/mm}^2</math>, 12 directions, 18h scan, 3D-SE) (Veraart et al. 2011)</p> <p>78-<math>\mu\text{m}</math> isotropic (<math>b=1500 \text{ s/mm}^2</math>, 6 directions) (Papp et al. 2014) (<math>b=4000 \text{ s/mm}^2</math>, 30 directions) (Papp et al. 2014)</p>
Squirrel monkey	35	600 $\mu\text{m}$	<p>300-<math>\mu\text{m}</math> isotropic (<math>b=3000/6000/9000/12000 \text{ s/mm}^2</math>, 100 directions each, 48hr scan, 3D-EPI) (K. G. Schilling et al. 2018)</p>
Mini-Pig	64	750 $\mu\text{m}$	<p>500-<math>\mu\text{m}</math> isotropic (<math>b=4009 \text{ s/mm}^2</math>), 61 directions, 28 hrs, 2D-SE) (Dyrby et al. 2007)</p>
Macaque	80	800 $\mu\text{m}$	<p>390x540x520 <math>\mu\text{m}</math> (<math>b=1000 \text{ s/mm}^2</math>, 8 directions, 45hr scan, 3D multiple echo SE) (Feng et al. 2017)</p> <p>500-1000 <math>\mu\text{m}</math> isotropic (<math>b=1477 - 9500 \text{ s/mm}^2</math>, 20-180 directions, up to 19 days scan, 2D-SE) (Dyrby et al. 2013, 2014; Ambrosen et al. 2020)</p> <p>600-<math>\mu\text{m}</math> isotropic (<math>b=4000 \text{ s/mm}^2</math>, 60 directions, 2D-SE single echo) (Mars et al. 2016)</p> <p>200-<math>\mu\text{m}</math> isotropic (<math>b=100\text{-}10,000 \text{ s/mm}^2</math>, 3-36 directions, 93hr scan, 3D-EPI) (Mars et al. 2016; Saleem et al. 2021)</p> <p>200-<math>\mu\text{m}</math> isotropic (<math>b=500, 1000, 4000, 10\ 000 \text{ s/mm}^2</math>, 8- 16-32-64 directions respectively, 73hr scan, 3D-EPI) (Sébille et al. 2019).</p> <p>300-<math>\mu\text{m}</math> isotropic (<math>b=6000 \text{ s/mm}^2</math>, 101 directions, 3D-EPI) (K. Schilling, Gao, Janve, et al. 2017)</p> <p>250-<math>\mu\text{m}</math> isotropic (<math>b=4800 \text{ s/mm}^2</math>, 121 directions, 71hr scan, 3D-EPI) (Thomas et al. 2014b)</p> <p>600-<math>\mu\text{m}</math> isotropic (<math>b = 4000 \text{ s/mm}^2</math>, 128 gradient directions, DW-SE multi-slice) (<a href="#">Howard et al. 2022</a>)</p>

			1000- $\mu\text{m}$ isotropic ( $b = 4000, 7000$ and $10000$ $\text{s}/\text{mm}^2$ , 250-1000-1000 directions respectively + spherical tensor encoding, DW-SE multi-slice) ( <a href="#">Howard et al. 2022</a> )
Macaque	35	600 $\mu\text{m}$	80- $\mu\text{m}$ isotropic ( $b=2400$ $\text{s}/\text{mm}^2$ , 64 directions, 15 days 3D-EPI) (Liu et al. 2020)

**Table 4.** Summary of brain volumes of various species, matching spatial resolutions to the typical one for human dMRI, and ranges of spatial resolutions reported in the literature, *ex vivo*. The references provided are not comprehensive.

### 3.6 Storage

*Ex vivo* offers the advantage that repeated scans of fixed brains can be performed, enabling longer scans, multiple sessions, and optimization of the sequences and contrasts over time. **Here, if tissue storage is necessary, we recommend storing the samples in either a PBS solution with Sodium Azide to inhibit bacterial and fungal growth, or in a weak fixative solution (1% formalin in PBS), at low temperature (4-5°C).** Long-term storage at room temperature is also possible in 4% formaldehyde, although it is associated with an increase in formic acid and methanol which may have a dehydrating effect, and a slow decline in T1 and T2 relaxation times ([Raman et al. 2017](#); [Shatil et al. 2018](#)). These effects can be mitigated by regularly refreshing the formaldehyde solution and by sufficient rehydration prior to scanning. Several studies have investigated the effects of storage time on diffusion metrics, and concluded that with appropriate care, tissue can be rescanned over several years with negligible variability in results (Dyrby et al. 2011; Xiao et al. 2021). Once fixed, the tissue quality should be inspected periodically (Dyrby et al. 2011, 2018) to ensure tissue integrity and absence of bacterial or fungal growth.

### 3.7 Specifics of ultra-high resolution MRI and MR microscopy

MR microscopy is defined as MR imaging with a spatial resolution in the micrometer range, which makes it possible to even image individual cells. Indeed, with dedicated setups that allow sufficiently high SNR, MRI with a resolution of a few  $\mu\text{m}$  becomes feasible (Flint et al. 2010, 2012, 2009; C. H. Lee et al. 2015; Portnoy et al. 2013). By convention, MRI transforms to MR microscopy (MRM) when the voxel side lengths are less than 100  $\mu\text{m}$  (Benveniste and Blackband 2006). One might think that MRM is merely MRI with higher resolution. But this would be equivalent to thinking that optical microscopy is photography at higher resolution – this is clearly not the case. A number of effects and considerations are encountered in MR microscopy that must be considered with respect to hardware, sequences, diffusion dispersion, and data processing. For an introduction to MRM emphasizing practical aspects relevant to high magnetic fields see (Ciobanu 2017).

For diffusion experiments, the initial SNR (at  $b=0$ ) needs to be substantial so that the SNR does not deteriorate completely at higher diffusion weighting. The typical way to achieve the required surplus of SNR for ultra-high resolution has been through the use of stronger

magnets. A discussion on the challenges inherent to working at ultra-high field are discussed in *Part 1: In vivo imaging*. For MR microscopy in particular, the decrease in  $T_2$  at high field which calls for short echo times reinforces the need for strong gradients, especially in the context of a large imaging matrix to be sampled during read-out. Since high resolution imaging already requires a large gradient integral, the overall gradient requirements for high resolution dMRI /dMRM are considerable.

For the reasons outlined above, the combination of high magnetic field strength and strong, linear, and fast switching gradients and generally small RF coils required for MRM. As touched upon in *Part 1*, this poses challenges for gradient design, gradient power amplifier construction, active shielding and magnet design to minimize the influence of eddy currents. An overview of these topics is provided in (Winkler et al. 2018), while details of microscale nuclear magnetic resonance hardware are given in (Anders and Korvink 2018). However we note that the gradient strength requirements become much easier to attain in terms of power as the gradient coil size scales down. Although human gradient coils require hundreds of amperes to attain even just a few tens of mT/m, small diameter coils (10 cm or less) can be made to achieve tens of T/m with only tens of amperes, and additionally due to lower impedance, much faster gradient switching times (tens of milliseconds rather than hundreds).

In terms of RF coil considerations, the recommendation for imaging of microscopic structures is also to use the smallest coil that will fit the sample. The SNR dependency on hardware and sample properties is covered in detail in e.g. (van Benthum, Janssen, and Kentgens 2004). In the case where the noise figure is dominated by coil resistance and sample loss (i.e. negligible preamplifier noise) the circuit Q-factor is of little importance and the achievable SNR is dictated mostly by constants of nature, experimental conditions e.g. field strength, bandwidth, system noise factor and a few sample properties such as spin density, temperature, and sample volume. The typical MRM coil is a simple solenoid or micro surface coil (50-500  $\mu\text{m}$  diameter). Micro surface coils have pronounced transmit/receive inhomogeneity so that accurate sample placement is crucial; alternatively, sample geometry can be controlled to minimize this issue, for example using slices of brain tissue that are thin compared to the coil diameter. This is somewhat alleviated with arrays of these small coils but these are not commonly encountered. Taken together, the optimal MR microscope operates at a very high magnetic field strength, has gradients that are small diameter and thus fast, strong, linear and efficiently cooled, and employs small (microscopic) RF-coils. The abundant SNR from the whole sample produced by this setup can then be sacrificed in return for high spatial resolution with modest SNR in each voxel. This potential was realized already by the pioneers of MRI (Mansfield and Morris 1982) and was soon after demonstrated using a biological cell (frog egg) in (Aguayo et al. 1986). Direct resolution of cells in plant systems was demonstrated a few years later in (Bowtell et al. 1990; Eccles and Callaghan 1986). The interested reader is referred to (Haber-Pohlmeier, Blumich, and Ciobanu 2022).

Uniquely, diffusion can influence MRM even when dMRI is not performed as such. This happens e.g. through broadening of the line shape caused by diffusion during the signal readout (Callaghan and Eccles 1988). To avoid this, gradients need to be sufficiently strong that nominal resolution is not deteriorated by spin diffusion between voxels within the time window of the measurement (Cho et al. 1988). This effect can be reduced by half-Fourier imaging (Cho et al.

1988). Similarly, diffusion may also influence the imaging point-spread function (McFarland 1992). In some cases, special sequences can mitigate these effects. This is the case for instance in high resolution relaxometry where the high spatial resolution (i.e. sampling of a large portion of  $k$ -space) causes very long  $k$ -space trajectories to be traveled resulting in severe, echo time-dependent diffusion weighting. For this reason, a modified spin echo sequence is needed for high spatial resolution  $T_2$  mapping using variable echo time (Hsu et al. 1995; Schoeniger et al. 1994).

## 4 Data Processing

In this paper we refer to *pre-processing* as steps that come before any diffusion fitting (tensors, biophysical models, etc.). Pre-processing thus includes data conversion (e.g. DICOM to NIfTI), noise reduction, artifact correction/mitigation or any step that aims at improving data quality. Processing refers to diffusion data fitting and normalization to standard space. See **Figure 10** for possible preprocessing steps.

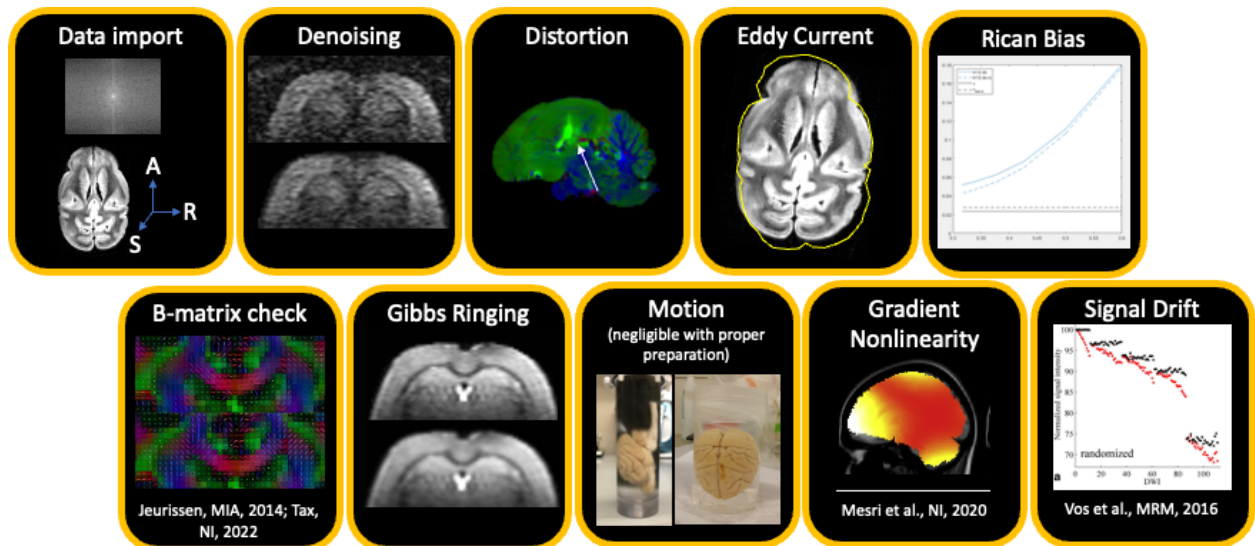


**Figure 10.** There are many artifacts that must be corrected for in preprocessing. These are not necessarily presented in order, and correction may not be necessary in all cases. Nevertheless, the most common order for pre-processing steps is: (i) Thermal noise reduction (referred to as denoising), (ii) Gibbs ringing correction, (iii) Susceptibility distortion + motion + eddy current corrections (+ gradient non-linearity, if applicable), (iv) Rician bias correction and (v) Signal drift correction. Figures kindly provided by Ileana Jelescu, Kurt Schilling, or reproduced from (Mesri et al. 2020; Vos et al. 2017a).

### 4.1 Pre-processing pipeline

Ex vivo diffusion MRI suffers from many of the same artifacts that in vivo imaging of both small animals and humans are susceptible to. This includes thermal noise, Gibbs ringing, signal drift, eddy current and susceptibility distortions, and sample motion. Below, we detail the steps

associated with a typical pre-processing pipeline, stressing in particular what may differentiate implementations of *ex vivo* imaging from *in vivo*, and how available tools can/should be modified accordingly.

While most pipelines are designed for, and most heavily used in, the brain, similar artifacts occur in all dMRI images. Our recommendations are generically applicable for all organs scanned *ex vivo*, although most details below are specific to brain imaging.

Any pipeline, regardless of sample, begins with **data importation and reconstruction**. Here, it is important that the MRI signal is properly organized in *k*-space and/or transformed into the image domain - which is typically performed at the console by the vendor software. While preclinical vendor software may output data in vendor-specific formats, common diffusion preprocessing software is most easily compatible with NIFTI or DICOM data, which stores not only the image matrix but also header information that includes information such as spatial resolution, sample orientation, and often acquisition parameters. With diffusion data, the diffusion weighting and diffusion directions are often stored as accompanying *b*-value and *b*-vector text files. The orientation of the images with respect to the applied diffusion directions is important, particularly for tractography, and should be quality checked carefully (Jeurissen, Leemans, and Sijbers 2014; K. G. Schilling, Yeh, et al. 2019). Tools for importation, reconstruction, conversion, and b-table quality control are given in [Section 5.1.1](#).

A prerequisite for many preprocessing steps is generating a **brain mask**. The mask is often used to save computation time or optimize areas on the image to focus corrections on. While the brain mask is particularly challenging for small animal models - because most brain extraction tools are optimized for and validated on the human brain - *ex vivo* images, particularly if the sample was immersed in fomblin, are easily extracted from the background using simple thresholding techniques from the non-diffusion weighted image. Other species-agnostic algorithms that use thresholding based on diffusion weighted images, followed by subsequent iterative dilation/eroding and removal of non-connected components (Tournier et al. 2019), often perform well on *ex vivo* images.

Next, **denoising** aims to reduce thermal noise in diffusion-weighted images. Most denoising approaches, and requirements for these approaches, are un-changed for *ex vivo* diffusion MRI. For example, a common approach based on principal component analysis (PCA) (Manjón et al. 2013) and automated identification of signal and noise-carrying components (MP-PCA) ([Veraart et al. 2016](#)) has proven useful in dMRI and is therefore recommended. The requirements here are that the noise level is constant across all diffusion images and that the number of diffusion images is large, where we suggest the use of >30 images. Other methods, for example total variation minimization (Rudin, Osher, and Fatemi 1992) or non-local means denoising (Rudin, Osher, and Fatemi 1992; Coupe et al. 2008) are also applicable to *ex vivo* images. Several algorithms and packages are also provided in [Section 5.1.1](#).

The next suggested step is **Gibbs ringing correction**, which is an artifact that appears as parallel lines next to high contrast tissue interfaces and can interfere with model fitting in e.g. corpus callosum (Dyrby et al. 2013). Correction techniques include the methods described in (Kellner et al. 2016) when a full Fourier acquisition is acquired and that of (H.-H. Lee, Novikov, and Fieremans 2021) when partial-Fourer acquisition is used (both for 2D multi-slice imaging).

Gibbs ringing correction, while not dramatically affecting tractography, is important for microstructure modeling, particularly near voxels neighboring CSF.

Next, **susceptibility distortion, eddy current correction, and sample motion** need to be corrected. While susceptibility distortion in *ex vivo* scans can be mitigated through a multi-shot acquisition, or alternative readouts with a high phase encoding bandwidth, and motion should be minimal (with proper sample preparation), we still recommend correction for these potential artifacts. Pipelines and algorithms, such as those implemented within FSL (using the `topup` and `eddy` tools) or within TORTOISE (using the DR BUDDI tool) utilize a reverse phase encode scan to estimate the distortion field, and may utilize this field while correcting all three artifacts simultaneously. Regardless of software, care should be taken when using these pipelines with default parameters, for example some require configuration files or tunable parameters (for example knot-spacing to estimate distortion/warping fields) that may need changed for high resolution imaging. Additionally, practical compromises may need to be made (for example when choosing the number of iterations to run, or downsampling factors within the pipeline) for time considerations, particularly with ultra-high resolution images with many directions.

**Rician bias correction** consists in correcting the diffusion signal decay by subtracting the non-zero Rician floor. Typical methods will assume the Gaussian noise standard deviation to be known, for example as previously estimated using MP-PCA on low  $b$ -value data. For software and methods, see (Ades-Aron et al. 2018; Koay and Basser 2006) and Section 5.1.1]. Preclinical dMRI data, both *in vivo* and *ex vivo*, is fortunately often single-channel which is by design characterized by Gaussian noise. Further, Rician bias can be minimized by denoising in complex space, and complex data is more easily retrievable from preclinical scanners (Ilanuş et al. 2022).

Finally, **temporal instability** on the scanner can cause signal drift, especially for diffusion sequences where strong gradients are employed for extended periods of time, even more so on preclinical scanners and especially for multi-day *ex vivo* experiments. This decrease in signal intensity over time can cause mis-estimates of derived parameters and also affect tractography (Vos et al. 2017b). While randomized diffusion gradient directions and  $b$ -values may alleviate this to some extent by randomizing directionality of this bias, this presence of signal drift can be examined, and corrected by collecting multiple  $b=0$  images throughout the scan to determine correction factors (typically linear or quadratic) to minimize this effect. Although this is not commonly done in the literature, we advocate for its use, and methodology and code to do so is described in (Vos et al. 2017b) and in [Section 5.1.1](#).

## 4.2 Processing pipelines

After pre-processing, the act of processing data includes data fitting, normalization to a standard space, and tractography analysis.

Diffusion analysis differences between *in vivo* and *ex vivo* are along the same lines as differences outlined for setting up the acquisition protocol, i.e., all changes are a direct result of potential differences/alterations in compartment sizes, diffusivities and relaxivities that are affected by chemical fixation and temperature.

For first-order and second-order cumulant approximation validity, i.e., validity of **DTI and DKI**, the rule of thumb is that  $bD \sim 1$  (DTI limit), and  $bD \sim 2 - 3$  (DKI limit) (Kiselev 2010). Maximum recommended  $b$ -values depend on the diffusivity and thus on the temperature at which the data were acquired. In general, diffusion tensor estimation *ex vivo* can/should be performed based on  $b$ -values  $\leq 2000$  s/mm<sup>2</sup>, and diffusion and kurtosis tensors should be estimated jointly from at least two shells with  $b$ -values  $\leq 6000$  s/mm<sup>2</sup>. It should be noted that DKI estimation is affected by the choice of  $b$ -values and post-processing (fitting procedures) and that optimal DKI  $b$ -values in GM are not necessarily optimal for DKI estimation in WM (Chuhutin, Hansen, and Jespersen 2017). To help researchers plan their experiments, densely sampled dMRI data sets from human brain and fixed rodent brain have been made available (Hansen and Jespersen 2016), and *ex vivo* also comes with the advantage that cursory scans can be used to investigate signal attenuation at different  $b$ -values.

For **biophysical models**, recommended  $b$ -values for optimal accuracy and precision of parameter estimation should also be adjusted *ex vivo*. At the parameter estimation level, priors on diffusivities for instance should be adapted to match *ex vivo* values, as well as potential admitted bounds on parameter values and algorithm initialization values. A typical example of this is an ‘*ex vivo* flag’ in the original implementation and source code of the NODDI model (H. Zhang et al. 2012) which changed the assumed fixed diffusivity from 1.7E-6 mm<sup>2</sup>/s to 0.6E-6 mm<sup>2</sup>/s. Importantly, biophysical models may need to be adapted dramatically by the inclusion of additional compartments, such as the “dot” compartment (trapped water with extremely low diffusion coefficient, see previous [Section 2.2](#) *Ex vivo*: Translation and validation considerations”) (Alexander et al. 2010), for which *in vivo* evidence is limited to the cerebellum (Tax et al. 2020; Dhital et al. 2018) and *ex vivo* more widespread to the cerebrum (Panagiotaki et al. 2012; Veraart et al. 2020), spinal cord (Grussu et al. 2017) and optic nerve (Stanisz et al. 1997).

Once parametric maps of various diffusion metrics are available in native space, it is common to use registration either to import atlas-based segmentation of brain regions for ROI analysis or to bring individual maps into a common space for voxel-based comparisons. For this **registration/normalization** step, typical tools used in human data also work well for animal data, both *in vivo* and *ex vivo*, with some customization. For non-linear registration for instance, default physical dimensions of warp and smoothing kernels should be scaled to those of small-animal brains. Common MRI atlases, including brain segmentation, for a variety of species are provided in [Section 5.1.2](#).

#### 4.2.1 *Ex vivo* MRI-histology correlations

One of the main advantages of the ideal experimental conditions in *ex vivo* MRI (e.g., lack of motion and image distortions; high-resolution) is the possibility of deriving detailed histological information at accurate radiographic position (X. Wang et al. 2014; Khan et al. 2015; K. G. Schilling et al. 2018; Budde et al. 2011; Grussu et al. 2017). This can then be used to validate MRI maps against histological indices quantifying similar biological features, or, more generally, to assess the correlation between MRI markers and a variety of histopathological markers. An example of this is given in **Figure 11**, illustrating co-localised MRI and histological

information from two published studies, i.e. i) in multiple sclerosis human spinal cord tissue (Grussu et al. 2017) (top), and ii) in a mouse liver (Grussu et al. 2022). The Figure shows that deriving 2D histological cuts along a direction that is consistent with the MRI slice direction, enables good MRI-histology alignment (Duval et al. 2019), especially if 3D-printed molds customized to the specimen's anatomy are used to guide histological sectioning (Bourne et al. 2017). 3D histology is also possible (K. Schilling et al. 2016; Khan et al. 2015), although it is usually limited to much smaller fields-of-view as compared to sample-wide 2D histological cutting, or requires very specialized protocols such as CLARITY (Morawski et al. 2018).

Importantly, it should be noted that digitized optical images of stained histological sections are typically acquired at a resolution that is hundreds of times higher than the MRI voxel size. For example, typical resolutions on 2D slide scanner microscopes are of the order of 0.25-1.0  $\mu\text{m}$ , while typical *ex vivo* dMRI resolutions are of the order of 100-500  $\mu\text{m}$ . A common strategy to tackle the resolution mismatch is to partition the histological images in patches matching the in-plane MRI resolution, and derive per-patch descriptors of histological properties (e.g., per-patch staining fractions, fiber orientation descriptors, or cell size distribution statistics (Grussu et al. 2017; Budde and Annese 2013; Grussu et al. 2022; Veraart et al. 2020)). This provides histological parametric maps at a spatial scale that is comparable to that of diffusion MR images, which can be warped to MRI space by means of non-linear co-registration for detailed voxel-by-voxel MRI-histology comparisons. Nevertheless, it is important to remember that in most cases the resolution mismatch not only relates to the in-plane resolution, but also to the slice direction: microtome cut thicknesses are of the order of 5-20  $\mu\text{m}$ , while slice thickness in *ex vivo* dMRI is of the order of 200-1000  $\mu\text{m}$ . This implies that 2D histology only provides a partial picture of the microscopic characteristics underlying an MRI scan, since there are considerable portions of tissue that contribute to the observed MRI signals but that are not sampled in histology. This is an intrinsic limitation of studies relating 2D histological data to 3D MRI, therefore one should consider using 3D imaging techniques such as 3D EM, 3D Confocal Imaging, (Khan et al. 2015; K. Schilling et al. 2016), 3D optical coherence tomography (H. Wang et al. 2014), or synchrotron-based tomographic imaging (Andersson and Kjer 2020), or small-angle X-ray scattering tensor tomography (Georgiadis et al. 2020). From these one can segment a more complete 3D microstructure environment that "3D" dMRI detects within a voxel.



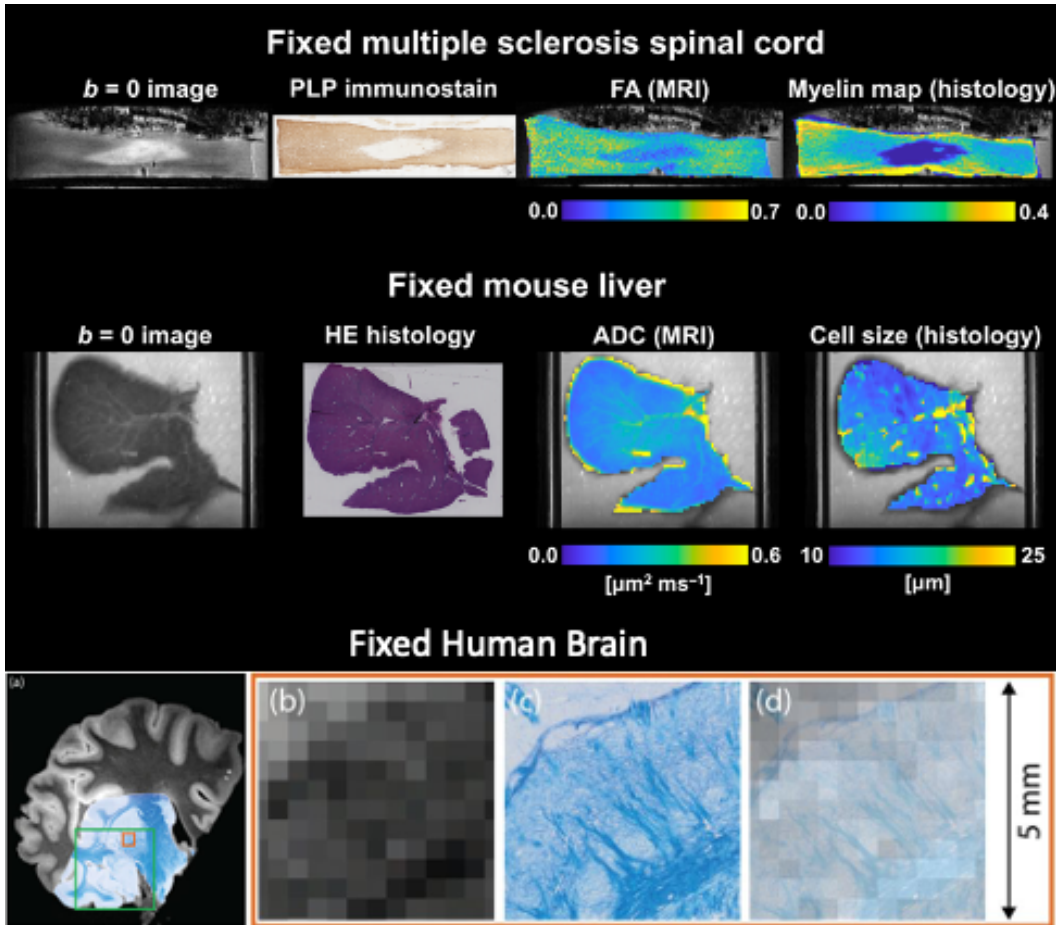


**Figure 11.** Examples of co-localised MRI and histological data. Top: fixed multiple sclerosis human spinal cord; bottom: fixed mouse liver. From left to right:  $b = 0$  image; whole-sample histological section taken within the tissue corresponding to the MRI slice (proteolipid protein (PLP) immunostain for the spinal cord; hematoxylin and eosin (HE) staining for the mouse liver); dMRI parametric map (fractional anisotropy (FA) for the spinal cord; apparent diffusion coefficient (ADC) for the mouse liver); histological parametric maps co-registered to dMRI space (myelin staining fraction for the spinal cord, and volume-weighted cell size statistics for the mouse liver, evaluated within histological image patches matching the in-plane MRI resolution). The data reproduced in this figure with kind permission from C. A. M. Gandini Wheeler-Kingshott, G. C. DeLuca and R. Perez-Lopez refer to previous dMRI studies (Grussu et al. 2017, 2022).

#### 4.2.2 Ex vivo MRI-histology alignment

Finally, there are several ways to **align MRI and histology** for quantitative comparison and validation. As described above, a 3D printed mold may be created to facilitate registration. Here, an *in vivo* or *ex vivo* structural scan is quickly performed to create a 3D segmentation of the object (i.e. brain, prostate, spinal cord). Then, a mold is designed which not only holds the sample, but also has cutting guides, or slots, for cutting. Some guides may be nicely made to fit within specialized sample holders as well. Further scans can be performed *ex vivo*, where the

FOV may be aligned with the cutting guide, so that there is a direct correspondence between the subsequent 2D histology and a slice (or slices) of the MRI image. This technique has been used for MRI imaging and histology alignment of multiple species and various organs (Baldi et al. 2019; Luciano et al. 2016; Bourne et al. 2017; Guy et al. 2016), but, as of yet, not for diffusion validation directly.

A second option is to utilize an intermediate modality, usually referred to as block-face images, that are digital photographs of the tissue block as it is being sectioned. These block-face images can be stacked into a 3D volume and registered to the 3D MRI. Because each 2D digital photograph can be mapped directly to a specific 2D histological slice, 2D registration can be performed to align histology to block-face, and subsequent 3D registration can be performed to align blockface to MRI (**Figure 12**). This technique has been performed in human, mice, and monkeys, with dedicated pipelines and software (Mancini et al. 2020; Annese et al. 2006; Lebenberg et al. 2010), and has been shown to provide accurate alignment (Choe et al. 2011). Moreover, it has been used to validate tractography, fiber orientation, and tissue microstructure measures (Choe et al. 2011; K. G. Schilling et al. 2018; K. G. Schilling, Gao, et al. 2019; Dauguet et al. 2007, 2006).

Finally, a more simple, and arguably more common, approach is to manually select corresponding regions of interest in MRI and histology for quantitative analysis (Jespersen et al. 2010; Leergaard et al. 2010; Hansen et al. 2011) (Jespersen et al. 2010; Leergaard et al. 2010), especially suited for the small field-of-view of electron microscopy and similar techniques that are necessary for axon diameter and volume fraction quantification (Kelm et al. 2016; Alexander et al. 2010).

We also note that in some special cases, especially with small samples imaged using planar surface coils, the entire RF coil, holder and sample can be removed for optical microscopy, providing a direct comparison as demonstrated on onion plant cells (Glover et al. 1994) and in mammalian brain slices and muscle fibers (Flint et al. 2010, 2012, 2009; C. H. Lee et al. 2015; Portnoy et al. 2013).

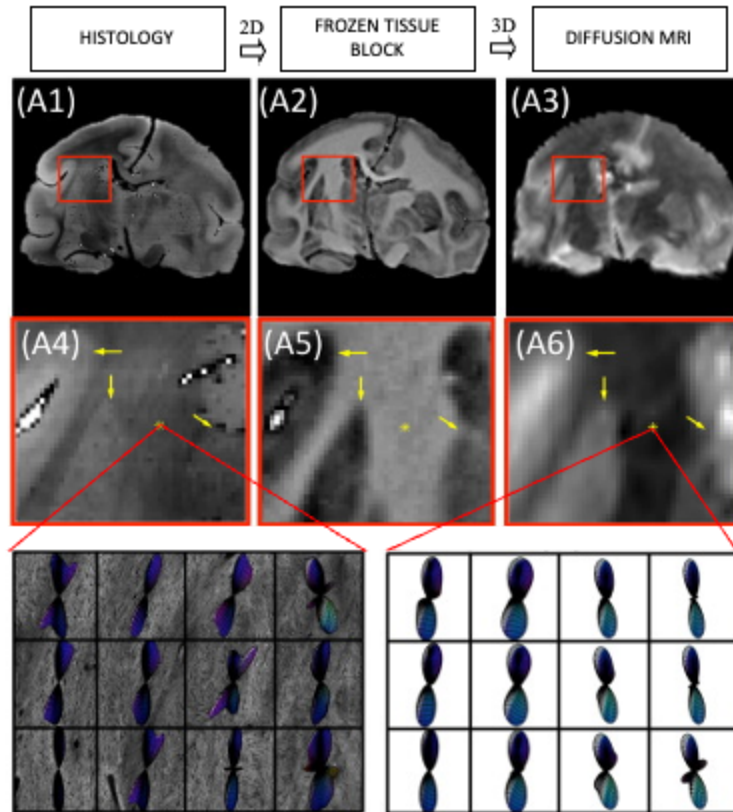


**Figure 12.** Histology to diffusion MRI alignment example using the intermediate modality, block-face images. 2D histology (A1) can be mapped to specific 2D block-face images (A2), which can be stacked into a 3D volume and mapped directly to 3D diffusion MRI data/derived data (A3). In this example, fiber orientation distribution from histology is aligned with similar measures estimated from diffusion MRI for validation purposes (K. Schilling et al. 2016; K. G. Schilling et al. 2018). Insets (A4-A5) zoom in to show alignment across modalities, with final panels showing histology-derived (left) and MRI derived (right) fiber orientation distributions.

#### 4.2.3 Where future work should lie

Currently, there is strong heterogeneity in terms of processing pipelines in *ex vivo* dMRI. This is due to the fact that a variety of signal representations/biophysical models can be fitted to dMRI images, and even when the same representation/model is considered, a variety of custom/open source fitting implementation can be used. Additional heterogeneity is also due to the variety of approaches used for co-localised histology. These depend, in turn, on the specific procedures followed for tissue processing and on the technique used for histological imaging (e.g., optical vs synchrotron; 2D vs 3D). Future work of the community should focus on harmonizing this variety of approaches, as this would enhance study reproducibility and would facilitate the comparability of findings from different studies. Free online sharing of processing tools can accelerate this harmonization process, and several efforts are already going in this direction (see also [Section 5.1.1 Code/Software](#)). Moreover, systematic comparisons of

preprocessing pipelines as well as prospective harmonization studies (Immonen et al. 2019) are also required.

Finally, with the advent of 3D large field of view microscopy with potential tissue clearing methods, it may be advantageous to perform direct 3D to 3D registration from histology to MRI for voxel-wise comparison and validation. However, due to large differences in resolution, contrasts, and geometric tissue distortions, substantial work is needed to make these comparisons feasible.

### 4.3 Tractography

The application and use of fiber tractography as a tool to study the fiber pathways and wiring diagram of the brain remain largely the same for *ex vivo* as for *in vivo* small animal and human dMRI (Jillings et al. 2020), as fixation preserves the structure of axon bundles. In general, a measure of fiber orientation is estimated for each voxel, which is used to create continuous space curves (i.e., streamlines) which are thought of as representations of groups of axons traveling throughout the tissue. For these reasons, the fundamentals of tractography (deterministic and probabilistic algorithms) also remain the same, and guidelines follow that of human data.

For **acquisition**, we recommend acquiring data with isotropic resolution, as anisotropic voxel size can introduce bias in estimates of fractional anisotropy and hinder the ability of algorithms to deal with branching/bending pathways (Neher et al. 2013). Higher angular resolution and strong diffusion weightings are likely to benefit tractography, particularly for small pathways, pathways near CSF or gray matter boundaries, or pathways with high curvature. For most reconstruction techniques, we recommend acquiring greater than 30 diffusion-weighted directions (and commonly 60-100+, especially with little-to-no scan time limits). Example acquisitions with subsequent validation that have demonstrated reliable tractography results include the *ex vivo* mouse (0.1-mm resolution, 60 directions,  $b=5000$  (Moldrich et al. 2010)), *ex vivo* ferret (0.24-mm resolution, 200 directions,  $b=4000$  (Delettre et al. 2019)), *ex vivo* squirrel monkey (0.3-mm resolution, 30-100 directions,  $b=1000-12'000$  (Delettre et al. 2019; K. G. Schilling, Gao, et al. 2019; K. Schilling et al. 2018)), *ex vivo* macaque (0.25-mm resolution,  $b=4900$ , 114 directions (Thomas et al. 2014b); 0.5-mm resolution,  $b=1477-8040$ , 180 directions (Girard et al. 2020b; Ambrosen et al. 2020)), and *ex vivo* pig (0.5-mm resolution,  $b=4000$ , 61 directions (Knösche et al. 2015)) — all  $b$ -values given in units of  $s/mm^2$ .

The next step in the tractography process is estimating a **fiber orientation** for every voxel in the image. For *ex vivo* imaging, very little changes occur for this step, as most reconstruction techniques, including DTI, spherical deconvolution, ball & sticks models, and q-ball imaging, will result in a field of orientation estimates that can be used for tractography.

The **tractography** process itself is also largely unchanged *ex vivo*. As described in Part 1, it is still important to consider, and adapt, parameters that can be tuned, for example the step-size (the size of steps when propagating streamlines), curvature threshold (which stops streamlines if curvature is too high), or length thresholds (only allowing streamlines that are between a minimum and maximum total length) - which should be considered based on acquired resolution, expected curvature of pathways under investigation, and length/size of the

brain. For these reasons, most software packages for tractography (MRTrix3, DSI Studio, DIPY, FSL, ExploreDTI) are able to easily be used for *ex vivo* dMRI with few modifications.

Applications of tractography include bundle segmentation - the process of virtually selecting and dissecting pathways to study - and connectome analysis - assessing streamlines throughout the full brain to determine network properties, typically using graph-theoretic measures. Recommendations for these are identical to that for *in vivo* imaging (see Part 1), where the primary challenges associated with small animals are the lack of automated bundle dissection tools in different species, and a lack of (or challenges in identifying) cortical parcellation schemes to use for connectome analysis.

## 5 Perspectives

### 5.1 Open science

#### 5.1.1 Code/Software

Challenges with pre-processing and processing pipelines highlighted in the previous sections could start to be overcome through code sharing and harmonization of implementations. Sharing combined knowledge and experience of many groups is valuable as it generates a lower barrier to entry and an excellent opportunity to evaluate robustness and reproducibility. We provide a (non-comprehensive) list of available software dedicated for acquisition and processing *ex vivo* diffusion MRI data at (<https://github.com/Diffusion-MRI/awesome-preclinical-diffusion-mri>) where updates on available software and tools can be shared by developers and where users can ask questions/advice for implementation, etc.

We also provide some guidelines for code sharing:

Code can be hosted on platforms such as GitHub, GitLab, Zenodo, NITRC etc. Hosting code via these tools is not only beneficial for the community, but also for the code developers themselves (and their respective research groups). Indeed, this ensures code safekeeping, retrieving and versioning. Nevertheless, code sharing platforms are not scratchpads for any code. Sharing code also comes with the responsibilities of documenting, cleaning, packaging, testing and versioning the code. These duties come at a (high) cost of requiring an in situ software engineer. Initiatives aimed at allocating special resources for software maintenance via funding bodies would be much welcome.

In terms of licensing open source code, there exist different options. Some of the most permissive licenses include MIT and BSD licenses. It means that the code can be reused by any entity (person or company), and importantly to note, is that the modified code can be distributed as closed source. If you wish to enforce the disclosure of your open source code, there are so-called 'copyleft' licenses, such as the GNU GPLv3 and the Mozilla Public License 2.0. For more details, see <https://choosealicense.com/licenses/>.

## 5.1.2 Data Sharing & Databases

Platforms that could serve as a repository for *ex vivo* dMRI datasets include OSF, OpenNeuro, Zenodo, NITRC, or other center resources (e.g. US National High Magnetic Field Laboratory). To promote data sharing and reuse, we compiled a (non-comprehensive) list of existing freely shared small-animal or *ex vivo* diffusion-weighted datasets, available on a public repository: <https://github.com/Diffusion-MRI/awesome-preclinical-diffusion-mri.git>. As for code sharing, the repository will enable a regular update of this database by the community.

## 5.2 The future: what should we strive to achieve?

As a field, we should continually strive to achieve reduced barriers to entry for new imaging centers, new scientists, and new industries who aim to use dMRI in a preclinical setting. Towards this end, as a community, we should promote dissemination of knowledge, code, and datasets to achieve high standards of data quality and analysis, reproducibility, transparency and foster collaborations, as well as reduce globally the time and cost of research in this field.

By design, *ex vivo* dMRI enables a more direct comparison / validation with invasive or destructive techniques such as histological stainings or electron microscopy. This potential can be exploited to its fullest to characterize and understand the biology behind a variety of diseases and injuries, thus contributing immensely to the translational value of dMRI.

Notwithstanding, for the translational circle to be complete, more research is needed to bridge *ex vivo* with *in vivo* measurements. So far, the extrapolation of *ex vivo* measurements to their *in vivo* counterpart has been hampered by open questions regarding the changes that the tissue undergoes during fixation and how those affect NMR-based measurements. Examples include the impact of partial volume effects between tissue types in high spatial resolution (*ex vivo*) imaging vs moderate resolution (*in vivo*) imaging, changes in compartment relaxation times, in membrane permeability, in relative compartment sizes, etc. Tissue fixation techniques such as cryofixation enable electron microscopy imaging of biological tissues where the *in vivo* structure was preserved to a greater extent than with regular chemical fixation (Knott and Genoud 2013) — which would provide a more realistic “ground truth” or comparative method for dMRI-derived *in vivo* microstructure, and for relative compartment sizes in particular. New preparation techniques have also recently enabled joint imaging using light microscopy (immunofluorescence) and electron microscopy on cryofixed tissue, with full hydration for light microscopy imaging (Tsang et al. 2018); the exploration of MR imaging of cryofixed rehydrated samples would certainly be worthwhile.

From a **hardware** perspective, ever stronger magnets and gradients, ever faster slew rates will keep pushing the capabilities of *ex vivo* dMRI forward. This progress in magnet and gradient designs should also be paralleled with progress in transmit-receive coil designs for good  $B_1^+$  transmit homogeneity at high field and high reception sensitivity.

As far as **diffusion acquisition** is concerned, the flexibility associated with preclinical MRI scanners will hopefully foster further developments in terms of novel diffusion encoding and acquisition techniques to bring dMRI ever closer to *in vivo* histology. On a more practical level,

the randomized order of acquisition for different  $b$ -values and diffusion times, along with interspersed  $b=0$  images to control for drifts and/or temperature changes should be increasingly adopted; this effort would be greatly supported by enabling this option in vendor default sequences, as opposed to users creating and loading custom files with such a random design. The harmonization of acquisition protocols (e.g. as to the choice of  $b_{\max}$  for DTI and for DKI *ex vivo*, at a certain sample temperature) may help multi-site reproducibility and comparison studies. Notwithstanding, encouraging the community to acquire richer datasets by default (e.g. multi-shell at minimum, but even for multiple diffusion times) can open up many avenues for testing new models retrospectively on public datasets, in a variety of animal models, healthy and diseased. Within such rich datasets, it is recommended to adopt a consistent echo time for all diffusion-weighted images, since accounting for variable  $T_2$ -weighting considerably complicates the data analysis.

**Pre-processing** steps are far from being optimized and integrated into a seamless pipeline for *ex vivo* dMRI, so an initiative in this direction, ideally for each species, would highly benefit the community. We note this is not unique to *ex vivo* dMRI, nor preclinical dMRI, as there is no consensus or full understanding of the effects of different steps in preprocessing human *in vivo* data.

Transparent **processing** pipelines should also become the norm in the near future, though given the diversity and complexity of possible dMRI analyses, harmonization may be out of reach or even unjustified. We encourage new community members to search for existing tools in our GitHub database and expand/build on that.

New **biophysical models** of tissue are typically initially tested in a preclinical imaging setting. We underline that the development of new models should uphold high standards in terms of accuracy and precision of microstructural features estimated, and be validated using complementary techniques such as light or electron microscopy.

Rather than debate or controversy, most of the lack of **tractography** guidelines comes from a sparsity of resources dedicated to this application in the animal models. Future work could thus lie in creating resources that allow whole brain tractography in various species, followed by atlas-based labeling and bundle dissection for pathways of interest. As for biophysical models of microstructure, tractography is often validated in a preclinical setting. Thus, another path for future efforts is to understand and quantify differences between tractography and tracer, and to relate these to situations that may occur in the human brain.

To remain consistent with  $b$ -value units of  $\text{s}/\text{mm}^2$  typically set at the scanner console and with “common language”, we have reported  $b$ -values in  $\text{s}/\text{mm}^2$  and diffusivities in  $\text{mm}^2/\text{s}$  throughout this work. However, we would like to encourage the community to gradually adopt units that are more suitable for dMRI of biological tissue, where diffusion lengths are on the order of a few microns and diffusion times on the order of a few ms. Hence diffusivities expressed in  $\mu\text{m}^2/\text{ms}$  and  $b$ -values expressed in  $\text{ms}/\mu\text{m}^2$  are much more “natural” and enable to juggle numbers close to unity vs thousands (e.g.  $b=1 \text{ ms}/\mu\text{m}^2$  vs  $b=1000 \text{ s}/\text{mm}^2$ ) or decimals (e.g.  $D=1 \mu\text{m}^2/\text{ms}$  vs  $D=10^{-3} \text{ mm}^2/\text{s}$ ). Some of the recent literature on dMRI microstructure models have adopted this new convention, and we hope it will prevail in the near future.

**Open science:** One of the main challenges and goals for the preclinical dMRI community is to responsibly share code and data, and develop transparent and comprehensive analysis frameworks that promote reproducibility. In order to provide a useful resource and starting point, we have created a dedicated github repository where publicly available datasets, software and tools are collected, and which will be updated regularly.

## 6 Acknowledgements and Support

The authors acknowledge financial support from: the National Institutes of Health (K01EB032898, R01AG057991, R01NS125020, R01EB017230, R01EB019980, R01EB031954, R01CA160620, R01NS109090), the National Institute of Biomedical Imaging and Bioengineering (R01EB031765, R56EB031765), the National Institute on Drug Abuse (P30DA048742), the Secretary of Universities and Research (Government of Catalonia) Beatriu de Pinós postdoctoral fellowship (2020 BP 00117), “la Caixa” Foundation Junior Leader fellowship (LCF/BQ/PR22/11920010), the Research Foundation Flanders (FWO: 12M3119N), the Belgian Science Policy Prodex (Grant ISLRA 2009–1062), the  $\mu$ NEURO Research Center of Excellence of the University of Antwerp, the Institutional research chair in Neuroinformatics (Sherbrooke, Canada), the NSERC Discovery Grant, the European Research Council Consolidator grant (101044180), the Canada Research Chair in Quantitative Magnetic Resonance Imaging [950-230815], the Canadian Institute of Health Research [CIHR FDN-143263], the Canada Foundation for Innovation [32454, 34824], the Fonds de Recherche du Québec - Santé [322736], the Natural Sciences and Engineering Research Council of Canada [RGPIN-2019-07244], the Canada First Research Excellence Fund (IVADO and TransMedTech), the Courtois NeuroMod project, the Quebec BioImaging Network [5886, 35450], the Mila - Tech Transfer Funding Program and the Swiss National Science Foundation (Eccellenza Fellowship PCEFP2\_194260).

## 7 References

- Abdollahzadeh, Ali, Ilya Belevich, Eija Jokitalo, Jussi Tohka, and Alejandra Sierra. 2019. “Automated 3D Axonal Morphometry of White Matter.” *Scientific Reports* 9 (1): 6084.
- Ades-Aron, Benjamin, Jelle Veraart, Peter Kochunov, Stephen McGuire, Paul Sherman, Elias Kellner, Dmitry S. Novikov, and Els Fieremans. 2018. “Evaluation of the Accuracy and Precision of the Diffusion Parameter Estimation with Gibbs and Noise Removal Pipeline.” *NeuroImage* 183 (December): 532–43.
- Adil, Syed M., Evan Calabrese, Lefko T. Charalambous, James J. Cook, Shervin Rahimpour, Ahmet F. Atik, Gary P. Cofer, et al. 2021. “A High-Resolution Interactive Atlas of the Human Brainstem Using Magnetic Resonance Imaging.” *NeuroImage* 237 (August): 118135.
- Aggarwal, Manisha, David W. Nauen, Juan C. Troncoso, and Susumu Mori. 2015. “Probing Region-Specific Microstructure of Human Cortical Areas Using High Angular and Spatial Resolution Diffusion MRI.” *NeuroImage* 105 (January): 198–207.
- Aggarwal, Manisha, Matthew D. Smith, and Peter A. Calabresi. 2020. “Diffusion-Time Dependence of Diffusional Kurtosis in the Mouse Brain.” *Magnetic Resonance in Medicine*:



- Official Journal of the Society of Magnetic Resonance in Medicine / Society of Magnetic Resonance in Medicine* 84 (3): 1564–78.
- Aggarwal, Manisha, Jiangyang Zhang, and Susumu Mori. 2011. “Magnetic Resonance Imaging-Based Mouse Brain Atlas and Its Applications.” *Methods in Molecular Biology* 711: 251–70.
- Aggarwal, Manisha, Jiangyang Zhang, Olga Pletnikova, Barbara Crain, Juan Troncoso, and Susumu Mori. 2013. “Feasibility of Creating a High-Resolution 3D Diffusion Tensor Imaging Based Atlas of the Human Brainstem: A Case Study at 11.7 T.” *NeuroImage* 74 (July): 117–27.
- Aguayo, J. B., S. J. Blackband, J. Schoeniger, M. A. Mattingly, and M. Hintermann. 1986. “Nuclear Magnetic Resonance Imaging of a Single Cell.” *Nature* 322 (6075): 190–91.
- Alexander, Daniel C., Penny L. Hubbard, Matt G. Hall, Elizabeth A. Moore, Maurice Ptito, Geoff J. M. Parker, and Tim B. Dyrby. 2010. “Orientationally Invariant Indices of Axon Diameter and Density from Diffusion MRI.” *NeuroImage* 52 (4): 1374–89.
- Ambrosen, Karen S., Simon F. Eskildsen, Max Hinne, Kristine Krug, Henrik Lundell, Mikkel N. Schmidt, Marcel A. J. van Gerven, Morten Mørup, and Tim B. Dyrby. 2020. “Validation of Structural Brain Connectivity Networks: The Impact of Scanning Parameters.” *NeuroImage* 204 (January): 116207.
- Anders, Jens, and Jan G. Korvink. 2018. *Micro and Nano Scale NMR: Technologies and Systems*. John Wiley & Sons.
- Andersson, M., and H. M. Kjer. 2020. “Axon Morphology Is Modulated by the Local Environment and Impacts the Noninvasive Investigation of Its Structure–function Relationship.” *Proceedings of the*. <https://www.pnas.org/content/117/52/33649.short>.
- Annese, J., D. M. Sforza, M. Dubach, D. Bowden, and A. W. Toga. 2006. “Postmortem High-Resolution 3-Dimensional Imaging of the Primate Brain: Blockface Imaging of Perfusion Stained Tissue.” *NeuroImage* 30 (1): 61–69.
- Assaf, Yaniv, Tamar Blumenfeld-Katzir, Yossi Yovel, and Peter J. Basser. 2008. “AxCaliber: A Method for Measuring Axon Diameter Distribution from Diffusion MRI.” *Magnetic Resonance in Medicine: Official Journal of the Society of Magnetic Resonance in Medicine / Society of Magnetic Resonance in Medicine* 59 (6): 1347–54.
- Assaf, Yaniv, Arieli Bouznach, Omri Zomet, Assaf Marom, and Yossi Yovel. 2020. “Conservation of Brain Connectivity and Wiring across the Mammalian Class.” *Nature Neuroscience* 23 (7): 805–8.
- Baldi, D., M. Aiello, A. Duggento, M. Salvatore, and C. Cavaliere. 2019. “MR Imaging-Histology Correlation by Tailored 3D-Printed Slicer in Oncological Assessment.” *Contrast Media & Molecular Imaging* 2019 (May): 1071453.
- Barrett, Rachel L. C., Diana Cash, Camilla Simmons, Eugene Kim, Tobias C. Wood, Richard Stones, Anthony C. Vernon, Marco Catani, and Flavio Dell’Acqua. n.d. “Tissue Optimisation Strategies for High Quality Ex Vivo Diffusion Imaging.” <https://doi.org/10.1101/2021.12.13.472113>.
- Beaulieu, C., and P. S. Allen. 1994. “Water Diffusion in the Giant Axon of the Squid: Implications for Diffusion-Weighted MRI of the Nervous System.” *Magnetic Resonance in Medicine: Official Journal of the Society of Magnetic Resonance in Medicine / Society of Magnetic Resonance in Medicine* 32 (5): 579–83.
- Beaulieu, Christian. 2002. “The Basis of Anisotropic Water Diffusion in the Nervous System - a Technical Review.” *NMR in Biomedicine*. <https://doi.org/10.1002/nbm.782>.
- Bech, Johannes, Dariusz Orlowski, Andreas N. Glud, Tim B. Dyrby, Jens Christian H. Sørensen, and Carsten R. Bjarkam. 2020. “Ex Vivo Diffusion-Weighted MRI Tractography of the

- Göttingen Minipig Limbic System." *Brain Structure & Function* 225 (3): 1055–71.
- Bentum, Jan van, J. Janssen, and A. Kentgens. 2004. "Towards Nuclear Magnetic Resonance  $^2$ -Spectroscopy and  $^2$ -Imaging." *The Analyst* 129 (October): 793–803.
- Benveniste, Helene, and Stephen J. Blackband. 2006. "Translational Neuroscience and Magnetic-Resonance Microscopy." *Lancet Neurology* 5 (6): 536–44.
- Bernstein M. A., King K. F. And Zhou X. J. 2004. *Handbook of MRI Pulse Sequences*. Elsevier.
- Birkel, Christoph, Martin Soellradl, Anna Maria Toeglhofer, Stefanie Krassnig, Marlene Leoni, Lukas Pirpamer, Thomas Vorauer, et al. 2018. "Effects of Concentration and Vendor Specific Composition of Formalin on Postmortem MRI of the Human Brain." *Magnetic Resonance in Medicine: Official Journal of the Society of Magnetic Resonance in Medicine / Society of Magnetic Resonance in Medicine* 79 (2): 1111–15.
- Bourne, Roger M., Colleen Bailey, Edward William Johnston, Hayley Pye, Susan Heavey, Hayley Whitaker, Bernard Siow, et al. 2017. "Apparatus for Histological Validation of In Vivo and Ex Vivo Magnetic Resonance Imaging of the Human Prostate." *Frontiers in Oncology* 7 (March): 47.
- Bowtell, R. W., G. D. Brown, P. M. Glover, M. McJury, P. Mansfield, J. M. Pope, R. E. Ratcliffe, J. Waterton, and W. E. Timms. 1990. "Resolution of Cellular Structures by NMR Microscopy at 11.7 T." *Philosophical Transactions. Physical Sciences and Engineering* 333 (1632): 457–67.
- Budde, Matthew D., and Jacopo Annese. 2013. "Quantification of Anisotropy and Fiber Orientation in Human Brain Histological Sections." *Frontiers in Integrative Neuroscience* 7 (February): 3.
- Budde, Matthew D., and Joseph A. Frank. 2012. "Examining Brain Microstructure Using Structure Tensor Analysis of Histological Sections." *NeuroImage* 63 (1): 1–10.
- Budde, Matthew D., Lindsay Janes, Eric Gold, Lisa Christine Turtzo, and Joseph A. Frank. 2011. "The Contribution of Gliosis to Diffusion Tensor Anisotropy and Tractography Following Traumatic Brain Injury: Validation in the Rat Using Fourier Analysis of Stained Tissue Sections." *Brain: A Journal of Neurology* 134 (Pt 8): 2248–60.
- Budde, and Song. n.d. "Insights into Diffusion Tensor Imaging from Animal Models of White Matter Pathology." *Diffusion MRI: Theory, Methods and Applications*.
- Calabrese, Evan, Alexandra Badea, Gary Cofer, Yi Qi, and G. Allan Johnson. 2015. "A Diffusion MRI Tractography Connectome of the Mouse Brain and Comparison with Neuronal Tracer Data." *Cerebral Cortex* 25 (11): 4628–37.
- Calabrese, Evan, Patrick Hickey, Christine Hulette, Jingxian Zhang, Beth Parente, Shivanand P. Lad, and G. Allan Johnson. 2015. "Postmortem Diffusion MRI of the Human Brainstem and Thalamus for Deep Brain Stimulator Electrode Localization." *Human Brain Mapping* 36 (8): 3167–78.
- Callaghan, P. T., and C. D. Eccles. 1988. "Diffusion-Limited Resolution in Nuclear Magnetic Resonance Microscopy." *Journal of Magnetic Resonance* 78 (1): 1–8.
- Chary, Karthik, Omar Narvaez, Raimo A. Salo, Isabel San Martín Molina, Jussi Tohka, Manisha Aggarwal, Olli Gröhn, and Alejandra Sierra. 2021. "Microstructural Tissue Changes in a Rat Model of Mild Traumatic Brain Injury." *Frontiers in Neuroscience*.  
<https://doi.org/10.3389/fnins.2021.746214>.
- Choe, Ann S., Yurui Gao, Xia Li, Keegan B. Compton, Iwona Stepniewska, and Adam W. Anderson. 2011. "Accuracy of Image Registration between MRI and Light Microscopy in the Ex Vivo Brain." *Magnetic Resonance Imaging* 29 (5): 683–92.
- Cho, Z. H., C. B. Ahn, S. C. Juh, H. K. Lee, R. E. Jacobs, S. Lee, J. H. Yi, and J. M. Jo. 1988. "Nuclear Magnetic Resonance Microscopy with 4-Microns Resolution: Theoretical Study

- and Experimental Results.” *Medical Physics* 15 (6): 815–24.
- Chuhutin, Andrey, Brian Hansen, and Sune Nørhøj Jespersen. 2017. “Precision and Accuracy of Diffusion Kurtosis Estimation and the Influence of B-Value Selection.” *NMR in Biomedicine* 30 (11): e3777.
- Ciobanu, Luisa. 2017. *Microscopic Magnetic Resonance Imaging: A Practical Perspective*. Jenny Stanford Publishing.
- Clark, C. A., and D. Le Bihan. 2000. “Water Diffusion Compartmentation and Anisotropy at High B Values in the Human Brain.” *Magnetic Resonance in Medicine: Official Journal of the Society of Magnetic Resonance in Medicine / Society of Magnetic Resonance in Medicine* 44 (6): 852–59.
- Coupe, P., P. Yger, S. Prima, P. Hellier, C. Kervrann, and C. Barillot. 2008. “An Optimized Blockwise Nonlocal Means Denoising Filter for 3-D Magnetic Resonance Images.” *IEEE Transactions on Medical Imaging*. <https://doi.org/10.1109/tmi.2007.906087>.
- D’Arceuil, Helen, and Alex de Crespigny. 2007. “The Effects of Brain Tissue Decomposition on Diffusion Tensor Imaging and Tractography.” *NeuroImage* 36 (1): 64–68.
- D’Arceuil, Helen E., Susan Westmoreland, and Alex J. de Crespigny. 2007. “An Approach to High Resolution Diffusion Tensor Imaging in Fixed Primate Brain.” *NeuroImage* 35 (2): 553–65.
- Dauguet, Julien, Sharon Peled, Vladimir Berezovskii, Thierry Delzescaux, Simon K. Warfield, Richard Born, and Carl-Fredrik Westin. 2006. “3D Histological Reconstruction of Fiber Tracts and Direct Comparison with Diffusion Tensor MRI Tractography.” *Medical Image Computing and Computer-Assisted Intervention – MICCAI 2006*. [https://doi.org/10.1007/11866565\\_14](https://doi.org/10.1007/11866565_14).
- . 2007. “Comparison of Fiber Tracts Derived from in-Vivo DTI Tractography with 3D Histological Neural Tract Tracer Reconstruction on a Macaque Brain.” *NeuroImage* 37 (2): 530–38.
- Dawe, Robert J., David A. Bennett, Julie A. Schneider, Sunil K. Vasireddi, and Konstantinos Arfanakis. 2009. “Postmortem MRI of Human Brain Hemispheres: T2 Relaxation Times during Formaldehyde Fixation.” *Magnetic Resonance in Medicine: Official Journal of the Society of Magnetic Resonance in Medicine / Society of Magnetic Resonance in Medicine* 61 (4): 810–18.
- Delettre, Céline, Arnaud Messé, Leigh-Anne Dell, Ophélie Foubet, Katja Heuer, Benoit Larrat, Sebastien Meriaux, et al. 2019. “Comparison between Diffusion MRI Tractography and Histological Tract-Tracing of Cortico-Cortical Structural Connectivity in the Ferret Brain.” *Network Neuroscience (Cambridge, Mass.)* 3 (4): 1038–50.
- Dhital, Bibek, Elias Kellner, Valerij G. Kiselev, and Marco Reisert. 2018. “The Absence of Restricted Water Pool in Brain White Matter.” *NeuroImage* 182 (November): 398–406.
- Does, Mark D., Edward C. Parsons, and John C. Gore. 2003. “Oscillating Gradient Measurements of Water Diffusion in Normal and Globally Ischemic Rat Brain.” *Magnetic Resonance in Medicine: Official Journal of the Society of Magnetic Resonance in Medicine / Society of Magnetic Resonance in Medicine* 49 (2): 206–15.
- Donahue, Chad J., Stamatios N. Sotiropoulos, Saad Jbabdi, Moises Hernandez-Fernandez, Timothy E. Behrens, Tim B. Dyrby, Timothy Coalson, et al. 2016. “Using Diffusion Tractography to Predict Cortical Connection Strength and Distance: A Quantitative Comparison with Tracers in the Monkey.” *The Journal of Neuroscience*. <https://doi.org/10.1523/jneurosci.0493-16.2016>.
- Duval, Tanguy, Ariane Salianni, Harris Nami, Antonio Nanci, Nikola Stikov, Hugues Leblond, and Julien Cohen-Adad. 2019. “Axons Morphometry in the Human Spinal Cord.” *NeuroImage*

- 185 (January): 119–28.
- Dyrby, Tim B., William F. C. Baaré, Daniel C. Alexander, Jacob Jelsing, Ellen Garde, and Lise V. Søgaard. 2011. “An Ex Vivo Imaging Pipeline for Producing High-Quality and High-Resolution Diffusion-Weighted Imaging Datasets.” *Human Brain Mapping* 32 (4): 544–63.
- Dyrby, Tim B., Giorgio M. Innocenti, Martin Bech, and Henrik Lundell. 2018. “Validation Strategies for the Interpretation of Microstructure Imaging Using Diffusion MRI.” *NeuroImage* 182 (November): 62–79.
- Dyrby, Tim B., Henrik Lundell, Mark W. Burke, Nina L. Reisle, Olaf B. Paulson, Maurice Ptito, and Hartwig R. Siebner. 2014. “Interpolation of Diffusion Weighted Imaging Datasets.” *NeuroImage* 103 (December): 202–13.
- Dyrby, Tim B., Lise V. Søgaard, Matt G. Hall, Maurice Ptito, and Daniel C. Alexander. 2013. “Contrast and Stability of the Axon Diameter Index from Microstructure Imaging with Diffusion MRI.” *Magnetic Resonance in Medicine: Official Journal of the Society of Magnetic Resonance in Medicine / Society of Magnetic Resonance in Medicine* 70 (3): 711–21.
- Dyrby, Tim B., Lise V. Søgaard, Geoffrey J. Parker, Daniel C. Alexander, Nanna M. Lind, William F. C. Baaré, Anders Hay-Schmidt, et al. 2007. “Validation of in Vitro Probabilistic Tractography.” *NeuroImage* 37 (4): 1267–77.
- Eccles, C. D., and P. T. Callaghan. 1986. “High-Resolution Imaging. The NMR Microscope.” *Journal of Magnetic Resonance* 68 (2): 393–98.
- Feng, Lei, Tina Jeon, Qiaowen Yu, Minhui Ouyang, Qinmu Peng, Virendra Mishra, Mihovil Pletikos, et al. 2017. “Population-Averaged Macaque Brain Atlas with High-Resolution Ex Vivo DTI Integrated into in Vivo Space.” *Brain Structure & Function* 222 (9): 4131–47.
- Fieremans, Els, and Hong-Hsi Lee. 2018. “Physical and Numerical Phantoms for the Validation of Brain Microstructural MRI: A Cookbook.” *NeuroImage* 182 (November): 39–61.
- Flint, Jeremy J., Brian Hansen, Michael Fey, Daniel Schmidig, Michael A. King, Peter Vestergaard-Poulsen, and Stephen J. Blackband. 2010. “Cellular-Level Diffusion Tensor Microscopy and Fiber Tracking in Mammalian Nervous Tissue with Direct Histological Correlation.” *NeuroImage* 52 (2): 556–61.
- Flint, Jeremy J., Brian Hansen, Sharon Portnoy, Choong-Heon Lee, Michael A. King, Michael Fey, Franck Vincent, Greg J. Stanisz, Peter Vestergaard-Poulsen, and Stephen J. Blackband. 2012. “Magnetic Resonance Microscopy of Human and Porcine Neurons and Cellular Processes.” *NeuroImage* 60 (2): 1404–11.
- Flint, Jeremy J., Choong H. Lee, Brian Hansen, Michael Fey, Daniel Schmidig, Jonathan D. Bui, Michael A. King, Peter Vestergaard-Poulsen, and Stephen J. Blackband. 2009. “Magnetic Resonance Microscopy of Mammalian Neurons.” *NeuroImage* 46 (4): 1037–40.
- Flint, Jeremy J., Kannan Menon, Brian Hansen, John Forder, and Stephen J. Blackband. 2015. “A Microperfusion and In-Bore Oxygenator System Designed for Magnetic Resonance Microscopy Studies on Living Tissue Explants.” *Scientific Reports* 5 (December): 18095.
- . 2020. “Visualization of Live, Mammalian Neurons during Kainate-Infusion Using Magnetic Resonance Microscopy.” *NeuroImage* 219 (October): 116997.
- Fox, C. H., F. B. Johnson, J. Whiting, and P. P. Roller. 1985. “Formaldehyde Fixation.” *The Journal of Histochemistry and Cytochemistry: Official Journal of the Histochemistry Society* 33 (8): 845–53.
- Foxley, Sean, Saad Jbabdi, Stuart Clare, Wilfred Lam, Olaf Ansorge, Gwenaëlle Douaud, and Karla Miller. 2014. “Improving Diffusion-Weighted Imaging of Post-Mortem Human Brains: SSFP at 7T.” *NeuroImage*. <https://doi.org/10.1016/j.neuroimage.2014.08.014>.
- Fritz, F. J., S. Sengupta, R. L. Harms, D. H. Tse, B. A. Poser, and A. Roebroek. 2019.

- “Ultra-High Resolution and Multi-Shell Diffusion MRI of Intact Ex Vivo Human Brains Using K-dSTEAM at 9.4T.” *NeuroImage* 202 (November): 116087.
- Georgiadis, Marios, Aileen Schroeter, Zirui Gao, Manuel Guizar-Sicairos, Dmitry S. Novikov, Els Fieremans, and Markus Rudin. 2020. “Retrieving Neuronal Orientations Using 3D Scanning SAXS and Comparison with Diffusion MRI.” *NeuroImage* 204 (January): 116214.
- Girard, Gabriel, Roberto Caminiti, Alexandra Battaglia-Mayer, Etienne St-Onge, Karen S. Ambrosen, Simon F. Eskildsen, Kristine Krug, et al. 2020a. “On the Cortical Connectivity in the Macaque Brain: A Comparison of Diffusion Tractography and Histological Tracing Data.” *NeuroImage* 221 (November): 117201.
- . 2020b. “On the Cortical Connectivity in the Macaque Brain: A Comparison of Diffusion Tractography and Histological Tracing Data.” *NeuroImage* 221 (November): 117201.
- Glover, P. M., R. W. Bowtell, G. D. Brown, and P. Mansfield. 1994. “A Microscope Slide Probe for High Resolution Imaging at 11.7 Tesla.” *Magnetic Resonance in Medicine: Official Journal of the Society of Magnetic Resonance in Medicine / Society of Magnetic Resonance in Medicine* 31 (4): 423–28.
- Graaf, Robin A. de, Peter B. Brown, Scott McIntyre, Terence W. Nixon, Kevin L. Behar, and Douglas L. Rothman. 2006. “High Magnetic Field Water and Metabolite Proton T1 and T2 Relaxation in Rat Brain in Vivo.” *Magnetic Resonance in Medicine: Official Journal of the Society of Magnetic Resonance in Medicine / Society of Magnetic Resonance in Medicine* 56 (2): 386–94.
- Grant, S. C., D. L. Buckley, S. Gibbs, A. G. Webb, and S. J. Blackband. 2001. “MR Microscopy of Multicomponent Diffusion in Single Neurons.” *Magnetic Resonance in Medicine: Official Journal of the Society of Magnetic Resonance in Medicine / Society of Magnetic Resonance in Medicine* 46 (6): 1107–12.
- Grinberg, Lea T., Edson Amaro Jr, Stefan Teipel, Denis Dionizio dos Santos, Carlos Augusto Pasqualucci, Renata E. P. Leite, Celia Regina Camargo, et al. 2008. “Assessment of Factors That Confound MRI and Neuropathological Correlation of Human Postmortem Brain Tissue.” *Cell and Tissue Banking* 9 (3): 195–203.
- Grisot, Giorgia, Suzanne N. Haber, and Anastasia Yendiki. 2021a. “Diffusion MRI and Anatomic Tracing in the Same Brain Reveal Common Failure Modes of Tractography.” *NeuroImage* 239 (October): 118300.
- . 2021b. “Diffusion MRI and Anatomic Tracing in the Same Brain Reveal Common Failure Modes of Tractography.” *NeuroImage* 239 (October): 118300.
- Grussu, Francesco, Kinga Bernatowicz, Irene Casanova-Salas, Natalia Castro, Paolo Nuciforo, Joaquin Mateo, Ignasi Barba, and Raquel Perez-Lopez. 2022. “Diffusion MRI Signal Cumulants and Hepatocyte Microstructure at Fixed Diffusion Time: Insights from Simulations, 9.4T Imaging, and Histology.” *Magnetic Resonance in Medicine: Official Journal of the Society of Magnetic Resonance in Medicine / Society of Magnetic Resonance in Medicine*, February. <https://doi.org/10.1002/mrm.29174>.
- Grussu, Francesco, Torben Schneider, Carmen Tur, Richard L. Yates, Mohamed Tachrount, Andrada Ianuş, Marios C. Yiannakas, et al. 2017. “Neurite Dispersion: A New Marker of Multiple Sclerosis Spinal Cord Pathology?” *Annals of Clinical and Translational Neurology* 4 (9): 663–79.
- Grussu, Francesco, Torben Schneider, Hui Zhang, Daniel C. Alexander, and Claudia A. M. Wheeler-Kingshott. 2015. “Neurite Orientation Dispersion and Density Imaging of the Healthy Cervical Spinal Cord in Vivo.” *NeuroImage* 111 (May): 590–601.
- Gutierrez, Carlos Enrique, Henrik Skibbe, Ken Nakae, Hiromichi Tsukada, Jean Lienard, Akiya Watakabe, Junichi Hata, et al. 2020. “Optimization and Validation of Diffusion MRI-Based

- Fiber Tracking with Neural Tracer Data as a Reference.” *Scientific Reports* 10 (1): 21285.
- Guy, Joseph R., Pascal Sati, Emily Leibovitch, Steven Jacobson, Afonso C. Silva, and Daniel S. Reich. 2016. “Custom Fit 3D-Printed Brain Holders for Comparison of Histology with MRI in Marmosets.” *Journal of Neuroscience Methods* 257 (January): 55–63.
- Guzman, A. Elizabeth de, Michael D. Wong, Jacqueline A. Gleave, and Brian J. Nieman. 2016. “Variations in Post-Perfusion Immersion Fixation and Storage Alter MRI Measurements of Mouse Brain Morphometry.” *NeuroImage* 142 (November): 687–95.
- Haber-Pohlmeier, Sabina, Bernhard Blumich, and Luisa Ciobanu. 2022. *Magnetic Resonance Microscopy: Instrumentation and Applications in Engineering, Life Science, and Energy Research*. John Wiley & Sons.
- Hansen, Brian, Jeremy J. Flint, Choong Heon-Lee, Michael Fey, Franck Vincent, Michael A. King, Peter Vestergaard-Poulsen, and Stephen J. Blackband. 2011. “Diffusion Tensor Microscopy in Human Nervous Tissue with Quantitative Correlation Based on Direct Histological Comparison.” *NeuroImage* 57 (4): 1458–65.
- Hansen, Brian, and Sune Nørhøj Jespersen. 2016. “Data for Evaluation of Fast Kurtosis Strategies, B-Value Optimization and Exploration of Diffusion MRI Contrast.” *Scientific Data*. nature.com.
- Henriques, Rafael Neto, Sune Nørhøj Jespersen, and Noam Shemesh. 2020. “Correlation Tensor Magnetic Resonance Imaging.” *NeuroImage* 211 (May): 116605.
- Hsu, E. W., N. R. Aiken, and S. J. Blackband. 1997. “A Study of Diffusion Isotropy in Single Neurons by Using NMR Microscopy.” *Magnetic Resonance in Medicine: Official Journal of the Society of Magnetic Resonance in Medicine / Society of Magnetic Resonance in Medicine* 37 (4): 624–27.
- Hsu, E. W., J. S. Schoeniger, R. Bowtell, N. R. Aiken, A. Horsman, and S. J. Blackband. 1995. “A Modified Imaging Sequence for Accurate T2 Measurements Using NMR Microscopy.” *Journal of Magnetic Resonance. Series B* 109 (1): 66–69.
- Hutchinson, Elizabeth B., Susan C. Schwerin, Kryslaine L. Radomski, Mustafa O. Irfanoglu, Sharon L. Juliano, and Carlo M. Pierpaoli. 2016. “Quantitative MRI and DTI Abnormalities During the Acute Period Following CCI in the Ferret.” *Shock* 46 (3 Suppl 1): 167–76.
- Hutchinson, Elizabeth B., Susan C. Schwerin, Kryslaine L. Radomski, Neda Sadeghi, Michal E. Komlos, M. O. Irfanoglu, Sharon L. Juliano, and Carlo Pierpaoli. 2018. “Detection and Distinction of Mild Brain Injury Effects in a Ferret Model Using Diffusion Tensor MRI (DTI) and DTI-Driven Tensor-Based Morphometry (D-TBM).” *Frontiers in Neuroscience* 12 (August): 573.
- Ianuș, Andrada, Joana Carvalho, Francisca F. Fernandes, Renata Cruz, Cristina Chavarrias, Marco Palombo, and Noam Shemesh. 2022. “Soma and Neurite Density MRI (SANDI) of the in-Vivo Mouse Brain and Comparison with the Allen Brain Atlas.” *NeuroImage* 254 (July): 119135.
- Ianuș, Andrada, Sune N. Jespersen, Teresa Serradas Duarte, Daniel C. Alexander, Ivana Drobnjak, and Noam Shemesh. 2018. “Accurate Estimation of Microscopic Diffusion Anisotropy and Its Time Dependence in the Mouse Brain.” *NeuroImage* 183 (December): 934–49.
- Iglesias, Juan Eugenio, Shauna Crampsie, Catherine Strand, Mohamed Tachrount, David L. Thomas, and Janice L. Holton. 2018. “Effect of Fluorinert on the Histological Properties of Formalin-Fixed Human Brain Tissue.” *Journal of Neuropathology and Experimental Neurology* 77 (12): 1085–90.
- Immonen, Riikka, Gregory Smith, Rhys D. Brady, David Wright, Leigh Johnston, Neil G. Harris, Eppu Manninen, et al. 2019. “Harmonization of Pipeline for Preclinical Multicenter MRI

- Biomarker Discovery in a Rat Model of Post-Traumatic Epileptogenesis.” *Epilepsy Research* 150 (February): 46–57.
- Jacqmot, Olivier, Bert Van Thielen, Yves Fierens, Martha Hammond, Inneke Willekens, Peter Van Schuerbeek, Filip Verhelle, et al. 2013. “Diffusion Tensor Imaging of White Matter Tracts in the Dog Brain.” *Anatomical Record* 296 (2): 340–49.
- Jelescu, Ileana O., Marco Palombo, Francesca Bagnato, and Kurt G. Schilling. 2020. “Challenges for Biophysical Modeling of Microstructure.” *Journal of Neuroscience Methods* 344 (October): 108861.
- Jelescu, Ileana O., Alexandre de Skowronski, Françoise Geffroy, Marco Palombo, and Dmitry S. Novikov. 2022. “Neurite Exchange Imaging (NEXI): A Minimal Model of Diffusion in Gray Matter with Inter-Compartment Water Exchange.” *NeuroImage* 256 (August): 119277.
- Jelescu, Ileana Ozana, Luisa Ciobanu, Françoise Geffroy, Pierre Marquet, and Denis Le Bihan. 2014. “Effects of Hypotonic Stress and Ouabain on the Apparent Diffusion Coefficient of Water at Cellular and Tissue Levels in Aplysia.” *NMR in Biomedicine* 27 (3): 280–90.
- Jelescu, Ileana O., Magdalena Zurek, Kerryanne V. Winters, Jelle Veraart, Anjali Rajaratnam, Nathanael S. Kim, James S. Babb, et al. 2016. “In Vivo Quantification of Demyelination and Recovery Using Compartment-Specific Diffusion MRI Metrics Validated by Electron Microscopy.” *NeuroImage* 132 (May): 104–14.
- Jespersen, Sune N., Carsten R. Bjarkam, Jens R. Nyengaard, M. Mallar Chakravarty, Brian Hansen, Thomas Vosegaard, Leif Østergaard, Dmitriy Yablonskiy, Niels Chr Nielsen, and Peter Vestergaard-Poulsen. 2010. “Neurite Density from Magnetic Resonance Diffusion Measurements at Ultrahigh Field: Comparison with Light Microscopy and Electron Microscopy.” *NeuroImage* 49 (1): 205–16.
- Jeurissen, Ben, Alexander Leemans, and Jan Sijbers. 2014. “Automated Correction of Improperly Rotated Diffusion Gradient Orientations in Diffusion Weighted MRI.” *Medical Image Analysis* 18 (7): 953–62.
- Jillings, S., J. Morez, N. Vidas-Guscic, J. Van Audekerke, F. Wuyts, M. Verhoye, J. Sijbers, and B. Jeurissen. 2020. “Multi-Tissue Constrained Spherical Deconvolution in a Murine Brain.” In *Proc Intl Soc Mag Reson Med* 28, 900.
- Johnson, G. A., H. Benveniste, R. D. Black, L. W. Hedlund, R. R. Maronpot, and B. R. Smith. 1993. “Histology by Magnetic Resonance Microscopy.” *Magnetic Resonance Quarterly* 9 (1): 1–30.
- Johnson, G. Allan, Alexandra Badea, Jeffrey Brandenburg, Gary Cofer, Boma Fubara, Song Liu, and Jonathan Nissanov. 2010. “Waxholm Space: An Image-Based Reference for Coordinating Mouse Brain Research.” *NeuroImage* 53 (2): 365–72.
- Johnson, G. Allan, Gary P. Cofer, Sally L. Gewalt, and Laurence W. Hedlund. 2002. “Morphologic Phenotyping with MR Microscopy: The Visible Mouse.” *Radiology* 222 (3): 789–93.
- Johnson, G. Allan, Rick Laoprasert, Robert J. Anderson, Gary Cofer, James Cook, Forrest Pratson, and Leonard E. White. 2021. “A Multicontrast MR Atlas of the Wistar Rat Brain.” *NeuroImage* 242 (November): 118470.
- Jones, D. K., D. C. Alexander, R. Bowtell, M. Cercignani, F. Dell’Acqua, D. J. McHugh, K. L. Miller, et al. 2018. “Microstructural Imaging of the Human Brain with a ‘Super-Scanner’: 10 Key Advantages of Ultra-Strong Gradients for Diffusion MRI.” *NeuroImage* 182 (November): 8–38.
- Jones, Robert, Giorgia Grisot, Jean Augustinack, Caroline Magnain, David A. Boas, Bruce Fischl, Hui Wang, and Anastasia Yendiki. 2020. “Insight into the Fundamental Trade-Offs of Diffusion MRI from Polarization-Sensitive Optical Coherence Tomography in Ex Vivo

- Human Brain." *NeuroImage* 214 (July): 116704.
- Kellner, Elias, Bibek Dhital, Valerij G. Kiselev, and Marco Reisert. 2016. "Gibbs-Ringing Artifact Removal Based on Local Subvoxel-Shifts." *Magnetic Resonance in Medicine: Official Journal of the Society of Magnetic Resonance in Medicine / Society of Magnetic Resonance in Medicine* 76 (5): 1574–81.
- Kelm, Nathaniel D., Kathryn L. West, Robert P. Carson, Daniel F. Gochberg, Kevin C. Ess, and Mark D. Does. 2016. "Evaluation of Diffusion Kurtosis Imaging in Ex Vivo Hypomyelinated Mouse Brains." *NeuroImage* 124 (Pt A): 612–26.
- Khan, Ahmad Raza, Anda Cornea, Lindsey A. Leigland, Steven G. Kohama, Sune Nørhøj Jespersen, and Christopher D. Kroenke. 2015. "3D Structure Tensor Analysis of Light Microscopy Data for Validating Diffusion MRI." *NeuroImage* 111 (May): 192–203.
- Kiernan, John A. 2000. "Formaldehyde, Formalin, Paraformaldehyde and Glutaraldehyde: What They Are and What They Do." *Microscopy Today* 8 (1): 8–13.
- Kiselev, Valerij G. 2010. "The Cumulant Expansion: An Overarching Mathematical Framework for Understanding Diffusion NMR." *Diffusion MRI*, 152–68.
- Kjonigsen, Lisa J., Sveinung Lillehaug, Jan G. Bjaalie, Menno P. Witter, and Trygve B. Leergaard. 2015. "Waxholm Space Atlas of the Rat Brain Hippocampal Region: Three-Dimensional Delineations Based on Magnetic Resonance and Diffusion Tensor Imaging." *NeuroImage* 108 (March): 441–49.
- Kleinnijenhuis, Michiel. 2014. *Imaging Fibres in the Brain*. Michiel Kleinnijenhuis.
- Knösche, Thomas R., Alfred Anwander, Matthew Liptrot, and Tim B. Dyrby. 2015. "Validation of Tractography: Comparison with Manganese Tracing." *Human Brain Mapping* 36 (10): 4116–34.
- Knott, Graham, and Christel Genoud. 2013. "Is EM Dead?" *Journal of Cell Science* 126 (Pt 20): 4545–52.
- Koay, Cheng Guan, and Peter J. Basser. 2006. "Analytically Exact Correction Scheme for Signal Extraction from Noisy Magnitude MR Signals." *Journal of Magnetic Resonance* 179 (2): 317–22.
- Korogod, Natalya, Carl C. H. Petersen, and Graham W. Knott. 2015. "Ultrastructural Analysis of Adult Mouse Neocortex Comparing Aldehyde Perfusion with Cryo Fixation." *eLife* 4 (August). <https://doi.org/10.7554/eLife.05793>.
- Lebenberg, J., A-S Hérard, A. Dubois, J. Dague, V. Frouin, M. Dhenain, P. Hantraye, and T. Delzescaux. 2010. "Validation of MRI-Based 3D Digital Atlas Registration with Histological and Autoradiographic Volumes: An Anatomofunctional Transgenic Mouse Brain Imaging Study." *NeuroImage* 51 (3): 1037–46.
- Lee, Choong H., Jeremy J. Flint, Brian Hansen, and Stephen J. Blackband. 2015. "Investigation of the Subcellular Architecture of L7 Neurons of *Aplysia Californica* Using Magnetic Resonance Microscopy (MRM) at 7.8 Microns." *Scientific Reports* 5 (June): 11147.
- Lee, Hong-Hsi, Dmitry S. Novikov, and Els Fieremans. 2021. "Removal of Partial Fourier-Induced Gibbs (RPG) Ringing Artifacts in MRI." *Magnetic Resonance in Medicine: Official Journal of the Society of Magnetic Resonance in Medicine / Society of Magnetic Resonance in Medicine* 86 (5): 2733–50.
- Leergaard, Trygve B., Nathan S. White, Alex de Crespigny, Ingeborg Bolstad, Helen D'Arceuil, Jan G. Bjaalie, and Anders M. Dale. 2010. "Quantitative Histological Validation of Diffusion MRI Fiber Orientation Distributions in the Rat Brain." *PloS One* 5 (1): e8595.
- Liang, Zifei, Choong H. Lee, Tanzil M. Arefin, Zijun Dong, Piotr Walczak, Song-Hai Shi, Florian Knoll, Yulin Ge, Leslie Ying, and Jiangyang Zhang. 2022. "Virtual Mouse Brain Histology from Multi-Contrast MRI via Deep Learning." *eLife* 11 (January).



- <https://doi.org/10.7554/eLife.72331>.
- Liu, Cirong, Frank Q. Ye, John D. Newman, Diego Szczupak, Xiaoguang Tian, Cecil Chern-Chyi Yen, Piotr Majka, et al. 2020. "A Resource for the Detailed 3D Mapping of White Matter Pathways in the Marmoset Brain." *Nature Neuroscience* 23 (2): 271–80.
- Liu, Cirong, Frank Q. Ye, Cecil Chern-Chyi Yen, John D. Newman, Daniel Glen, David A. Leopold, and Afonso C. Silva. 2018. "A Digital 3D Atlas of the Marmoset Brain Based on Multi-Modal MRI." *NeuroImage* 169 (April): 106–16.
- Looij, Yohan van de, Yohan van de Looij, Gregory A. Lodygensky, Justin Dean, François Lazeyras, Henrik Hagberg, Ingemar Kjellmer, Carina Mallard, Petra S. Hüppi, and Stéphane V. Sizonenko. 2012. "High-Field Diffusion Tensor Imaging Characterization of Cerebral White Matter Injury in Lipopolysaccharide-Exposed Fetal Sheep." *Pediatric Research*. <https://doi.org/10.1038/pr.2012.72>.
- Luciano, Nicholas J., Pascal Sati, Govind Nair, Joseph R. Guy, Seung-Kwon Ha, Martina Absinta, Wen-Yang Chiang, et al. 2016. "Utilizing 3D Printing Technology to Merge MRI with Histology: A Protocol for Brain Sectioning." *Journal of Visualized Experiments: JoVE*, no. 118 (December). <https://doi.org/10.3791/54780>.
- Lundell, H., M. Nilsson, T. B. Dyrby, G. J. M. Parker, P. L. Hubbard Cristinacce, F-L Zhou, D. Topgaard, and S. Lasič. 2019. "Multidimensional Diffusion MRI with Spectrally Modulated Gradients Reveals Unprecedented Microstructural Detail." *Scientific Reports* 9 (1): 9026.
- Maffei, Chiara, Gabriel Girard, Kurt G. Schilling, Dogu Baran Aydogan, Nagesh Adluru, Andrey Zhylika, Ye Wu, et al. 2022a. "Insights from the IronTract Challenge: Optimal Methods for Mapping Brain Pathways from Multi-Shell Diffusion MRI." *NeuroImage* 257 (August): 119327.
- . 2022b. "Insights from the IronTract Challenge: Optimal Methods for Mapping Brain Pathways from Multi-Shell Diffusion MRI." *NeuroImage* 257 (August): 119327.
- Mancini, Matteo, Adrià Casamitjana, Loic Peter, Eleanor Robinson, Shauna Crampsie, David L. Thomas, Janice L. Holton, Zane Jaunmuktane, and Juan Eugenio Iglesias. 2020. "A Multimodal Computational Pipeline for 3D Histology of the Human Brain." *Scientific Reports* 10 (1): 13839.
- Mandonnet, Emmanuel, Silvio Sarubbo, and Laurent Petit. 2018. "The Nomenclature of Human White Matter Association Pathways: Proposal for a Systematic Taxonomic Anatomical Classification." *Frontiers in Neuroanatomy* 12 (November): 94.
- Manjón, José V., Pierrick Coupé, Luis Concha, Antonio Buades, D. Louis Collins, and Montserrat Robles. 2013. "Diffusion Weighted Image Denoising Using Overcomplete Local PCA." *PLoS ONE*. <https://doi.org/10.1371/journal.pone.0073021>.
- Mansfield, P., and P. G. Morris. 1982. *NMR Imaging in Biomedicine*. Sydney: Academic Press.
- Mars, Rogier B., Sean Foxley, Lennart Verhagen, Saad Jbabdi, Jérôme Sallet, Maryann P. Noonan, Franz-Xaver Neubert, et al. 2016. "The Extreme Capsule Fiber Complex in Humans and Macaque Monkeys: A Comparative Diffusion MRI Tractography Study." *Brain Structure & Function* 221 (8): 4059–71.
- McFadden, Whitney C., Hadley Walsh, Felix Richter, Céline Soudant, Clare H. Bryce, Patrick R. Hof, Mary Fowkes, John F. Crary, and Andrew T. McKenzie. 2019. "Perfusion Fixation in Brain Banking: A Systematic Review." *Acta Neuropathologica Communications* 7 (1): 146.
- McFarland, E. W. 1992. "Time-Independent Point-Spread Function for NMR Microscopy." *Magnetic Resonance Imaging* 10 (2): 269–78.
- McInnes, Elizabeth. 2005. "Artefacts in Histopathology." *Comparative Clinical Pathology* 13 (3): 100–108.
- Mesri, Hamed Y., Szabolcs David, Max A. Viergever, and Alexander Leemans. 2020. "The

- Adverse Effect of Gradient Nonlinearities on Diffusion MRI: From Voxels to Group Studies.” *NeuroImage* 205 (January): 116127.
- Miller, Karla L., Jennifer A. McNab, Saad Jbabdi, and Gwenaëlle Douaud. 2012. “Diffusion Tractography of Post-Mortem Human Brains: Optimization and Comparison of Spin Echo and Steady-State Free Precession Techniques.” *NeuroImage* 59 (3): 2284–97.
- Miller, Karla L., Charlotte J. Stagg, Gwenaëlle Douaud, Saad Jbabdi, Stephen M. Smith, Timothy E. J. Behrens, Mark Jenkinson, et al. 2011. “Diffusion Imaging of Whole, Post-Mortem Human Brains on a Clinical MRI Scanner.” *NeuroImage* 57 (1): 167–81.
- Moldrich, Randal X., Kerstin Pannek, Renee Hoch, John L. Rubenstein, Nyoman D. Kurniawan, and Linda J. Richards. 2010. “Comparative Mouse Brain Tractography of Diffusion Magnetic Resonance Imaging.” *NeuroImage* 51 (3): 1027–36.
- Morawski, Markus, Evgeniya Kirilina, Nico Scherf, Carsten Jäger, Katja Reimann, Robert Trampel, Filippos Gavriilidis, et al. 2018. “Developing 3D Microscopy with CLARITY on Human Brain Tissue: Towards a Tool for Informing and Validating MRI-Based Histology.” *NeuroImage* 182 (November): 417–28.
- Neher, Peter, Bram Stieltjes, Ivo Wolf, Hans-Peter Meinzer, and Klaus Maier-Hein. 2013. *Analysis of Tractography Biases Introduced by Anisotropic Voxels*.
- “Nonhuman Primates and Medical Research.” 1973. <https://doi.org/10.1016/c2013-0-10403-5>.
- Olesen, Jonas L., Leif Østergaard, Noam Shemesh, and Sune N. Jespersen. 2022. “Diffusion Time Dependence, Power-Law Scaling, and Exchange in Gray Matter.” *NeuroImage* 251 (May): 118976.
- Osen, Kirsten K., Jala Imad, Arvind E. Wennberg, Eszter A. Papp, and Trygve B. Leergaard. 2019. “Waxholm Space Atlas of the Rat Brain Auditory System: Three-Dimensional Delineations Based on Structural and Diffusion Tensor Magnetic Resonance Imaging.” *NeuroImage* 199 (October): 38–56.
- Pajevic, S., and C. Pierpaoli. 2000. “Color Schemes to Represent the Orientation of Anisotropic Tissues from Diffusion Tensor Data: Application to White Matter Fiber Tract Mapping in the Human Brain.” *Magnetic Resonance in Medicine: Official Journal of the Society of Magnetic Resonance in Medicine / Society of Magnetic Resonance in Medicine* 43 (6): 921.
- Pallotto, Marta, Paul V. Watkins, Boma Fubara, Joshua H. Singer, and Kevin L. Briggman. 2015. “Extracellular Space Preservation Aids the Connectomic Analysis of Neural Circuits.” *eLife* 4 (December). <https://doi.org/10.7554/eLife.08206>.
- Panagiotaki, Eleftheria, Torben Schneider, Bernard Siow, Matt G. Hall, Mark F. Lythgoe, and Daniel C. Alexander. 2012. “Compartment Models of the Diffusion MR Signal in Brain White Matter: A Taxonomy and Comparison.” *NeuroImage* 59 (3): 2241–54.
- Panesar, Sandip S., and Juan Fernandez-Miranda. 2019. “Commentary: The Nomenclature of Human White Matter Association Pathways: Proposal for a Systematic Taxonomic Anatomical Classification.” *Frontiers in Neuroanatomy*.
- Papp, Eszter A., Trygve B. Leergaard, Evan Calabrese, G. Allan Johnson, and Jan G. Bjaalie. 2014. “Waxholm Space Atlas of the Sprague Dawley Rat Brain.” *NeuroImage* 97 (August): 374–86.
- Pfefferbaum, Adolf, Edith V. Sullivan, Elfar Adalsteinsson, Therese Garrick, and Clive Harper. 2004. “Postmortem MR Imaging of Formalin-Fixed Human Brain.” *NeuroImage*. <https://doi.org/10.1016/j.neuroimage.2003.11.024>.
- Pieri, Valentina, Marco Trovati, Marcello Cadioli, Davide Danilo Zani, Stefano Brizzola, Giuliano Ravasio, Fabio Acocella, et al. 2019. “Diffusion Tensor Magnetic Resonance Tractography of the Sheep Brain: An Atlas of the Ovine White Matter Fiber Bundles.” *Frontiers in Veterinary Science* 6 (October): 345.

- Portnoy, S., J. J. Flint, S. J. Blackband, and G. J. Stanisiz. 2013. "Oscillating and Pulsed Gradient Diffusion Magnetic Resonance Microscopy over an Extended B-Value Range: Implications for the Characterization of Tissue Microstructure." *Magnetic Resonance in Medicine: Official Journal of the Society of Magnetic Resonance in Medicine / Society of Magnetic Resonance in Medicine* 69 (4): 1131–45.
- Purea, Armin, and Andrew G. Webb. 2006. "Reversible and Irreversible Effects of Chemical Fixation on the NMR Properties of Single Cells." *Magnetic Resonance in Medicine: Official Journal of the Society of Magnetic Resonance in Medicine / Society of Magnetic Resonance in Medicine* 56 (4): 927–31.
- Pyatigorskaya, Nadya, Denis Le Bihan, Olivier Reynaud, and Luisa Ciobanu. 2014. "Relationship between the Diffusion Time and the Diffusion MRI Signal Observed at 17.2 Tesla in the Healthy Rat Brain Cortex." *Magnetic Resonance in Medicine: Official Journal of the Society of Magnetic Resonance in Medicine / Society of Magnetic Resonance in Medicine* 72 (2): 492–500.
- Quezada, Sebastian, Yohan van de Looij, Nadia Hale, Shreya Rana, Stéphane V. Sizonenko, Courtney Gilchrist, Margie Castillo-Melendez, Mary Tolcos, and David W. Walker. 2020. "Genetic and Microstructural Differences in the Cortical Plate of Gyri and Sulci during Gyrfication in Fetal Sheep." *Cerebral Cortex* 30 (12): 6169–90.
- Rane, Swati, and Timothy Q. Duong. 2011. "[No Title]." November 18, 2011. <https://doi.org/10.2174/1874440001105010172>.
- Roebroek, Alard, Ralf Galuske, Elia Formisano, Oriana Chiry, Hansjürgen Bratzke, Itamar Ronen, Dae-Shik Kim, and Rainer Goebel. 2008. "High-Resolution Diffusion Tensor Imaging and Tractography of the Human Optic Chiasm at 9.4 T." *NeuroImage* 39 (1): 157–68.
- Roebroek, Alard, Karla L. Miller, and Manisha Aggarwal. 2019. "Ex Vivo Diffusion MRI of the Human Brain: Technical Challenges and Recent Advances." *NMR in Biomedicine* 32 (4): e3941.
- Rooney, William D., Glyn Johnson, Xin Li, Eric R. Cohen, Seong-Gi Kim, Kamil Ugurbil, and Charles S. Springer Jr. 2007. "Magnetic Field and Tissue Dependencies of Human Brain Longitudinal 1H<sub>2</sub>O Relaxation in Vivo." *Magnetic Resonance in Medicine: Official Journal of the Society of Magnetic Resonance in Medicine / Society of Magnetic Resonance in Medicine* 57 (2): 308–18.
- Royo, Julie, Stephanie J. Forkel, Pierre Pouget, and Michel Thiebaut de Schotten. 2021. "The Squirrel Monkey Model in Clinical Neuroscience." *Neuroscience and Biobehavioral Reviews* 128 (September): 152–64.
- Rudin, Leonid I., Stanley Osher, and Emad Fatemi. 1992. "Nonlinear Total Variation Based Noise Removal Algorithms." *Physica D: Nonlinear Phenomena*. [https://doi.org/10.1016/0167-2789\(92\)90242-f](https://doi.org/10.1016/0167-2789(92)90242-f).
- Ryan, Meghann C., Paul Sherman, Laura M. Rowland, S. Andrea Wijtenburg, Ashley Acheson, Els Fieremans, Jelle Veraart, et al. 2018. "Miniature Pig Model of Human Adolescent Brain White Matter Development." *Journal of Neuroscience Methods* 296 (February): 99–108.
- Saleem, Kadharbatcha S., Alexandru V. Avram, Daniel Glen, Cecil Chern-Chyi Yen, Frank Q. Ye, Michal Komlos, and Peter J. Basser. 2021. "High-Resolution Mapping and Digital Atlas of Subcortical Regions in the Macaque Monkey Based on Matched MAP-MRI and Histology." *NeuroImage* 245 (December): 118759.
- Sarubbo, Silvio, Laurent Petit, Alessandro De Benedictis, Franco Chioffi, Maurice Ptito, and Tim B. Dyrby. 2019. "Uncovering the Inferior Fronto-Occipital Fascicle and Its Topological Organization in Non-Human Primates: The Missing Connection for Language Evolution."

- Brain Structure & Function* 224 (4): 1553–67.
- Sauleau, P., E. Lapouble, D. Val-Laillet, and C-H Malbert. 2009. “The Pig Model in Brain Imaging and Neurosurgery.” *Animal*. <https://doi.org/10.1017/s1751731109004649>.
- Schilling, Kurt, Yurui Gao, Vaibhav Janve, Iwona Stepniewska, Bennett A. Landman, and Adam W. Anderson. 2017. “Can Increased Spatial Resolution Solve the Crossing Fiber Problem for Diffusion MRI?” *NMR in Biomedicine* 30 (12). <https://doi.org/10.1002/nbm.3787>.
- . 2018. “Confirmation of a Gyral Bias in Diffusion MRI Fiber Tractography.” *Human Brain Mapping* 39 (3): 1449–66.
- Schilling, Kurt, Yurui Gao, Iwona Stepniewska, Ann S. Choe, Bennett A. Landman, and Adam W. Anderson. 2017. “Reproducibility and Variation of Diffusion Measures in the Squirrel Monkey Brain, in Vivo and Ex Vivo.” *Magnetic Resonance Imaging* 35 (January): 29–38.
- Schilling, Kurt G., Yurui Gao, Iwona Stepniewska, Vaibhav Janve, Bennett A. Landman, and Adam W. Anderson. 2019. “Anatomical Accuracy of Standard-Practice Tractography Algorithms in the Motor System - A Histological Validation in the Squirrel Monkey Brain.” *Magnetic Resonance Imaging* 55 (January): 7–25.
- Schilling, Kurt G., Vaibhav Janve, Yurui Gao, Iwona Stepniewska, Bennett A. Landman, and Adam W. Anderson. 2018. “Histological Validation of Diffusion MRI Fiber Orientation Distributions and Dispersion.” *NeuroImage*. <https://doi.org/10.1016/j.neuroimage.2017.10.046>.
- Schilling, Kurt G., Vishwesh Nath, Colin Hansen, Prasanna Parvathaneni, Justin Blaber, Yurui Gao, Peter Neher, et al. 2019. “Limits to Anatomical Accuracy of Diffusion Tractography Using Modern Approaches.” *NeuroImage* 185 (January): 1–11.
- Schilling, Kurt G., Laurent Petit, Francois Rheault, Samuel Remedios, Carlo Pierpaoli, Adam W. Anderson, Bennett A. Landman, and Maxime Descoteaux. 2020a. “Brain Connections Derived from Diffusion MRI Tractography Can Be Highly Anatomically Accurate-If We Know Where White Matter Pathways Start, Where They End, and Where They Do Not Go.” *Brain Structure & Function* 225 (8): 2387–2402.
- . 2020b. “Brain Connections Derived from Diffusion MRI Tractography Can Be Highly Anatomically Accurate-If We Know Where White Matter Pathways Start, Where They End, and Where They Do Not Go.” *Brain Structure & Function* 225 (8): 2387–2402.
- Schilling, Kurt G., François Rheault, Laurent Petit, Colin B. Hansen, Vishwesh Nath, Fang-Cheng Yeh, Gabriel Girard, et al. 2021. “Tractography Dissection Variability: What Happens When 42 Groups Dissect 14 White Matter Bundles on the Same Dataset?” *NeuroImage* 243 (November): 118502.
- Schilling, Kurt G., Fang-Cheng Yeh, Vishwesh Nath, Colin Hansen, Owen Williams, Susan Resnick, Adam W. Anderson, and Bennett A. Landman. 2019. “A Fiber Coherence Index for Quality Control of B-Table Orientation in Diffusion MRI Scans.” *Magnetic Resonance Imaging* 58 (May): 82–89.
- Schilling, Kurt, Vaibhav Janve, Yurui Gao, Iwona Stepniewska, Bennett A. Landman, and Adam W. Anderson. 2016. “Comparison of 3D Orientation Distribution Functions Measured with Confocal Microscopy and Diffusion MRI.” *NeuroImage* 129 (April): 185–97.
- Schmahmann, Jeremy D., and Deepak Pandya. 2009. *Fiber Pathways of the Brain*. OUP USA.
- Schoeniger, J. S., N. Aiken, E. Hsu, and S. J. Blackband. 1994. “Relaxation-Time and Diffusion NMR Microscopy of Single Neurons.” *Journal of Magnetic Resonance. Series B* 103 (3): 261–73.
- Sébille, Sophie Bernadette, Anne-Sophie Rolland, Marie-Laure Welter, Eric Bardinnet, and Mathieu David Santin. 2019. “Post Mortem High Resolution Diffusion MRI for Large Specimen Imaging at 11.7 T with 3D Segmented Echo-Planar Imaging.” *Journal of*

- Neuroscience Methods* 311 (January): 222–34.
- Seehaus, Arne, Alard Roebroek, Matteo Bastiani, Lúcia Fonseca, Hansjürgen Bratzke, Nicolás Lori, Anna Vilanova, Rainer Goebel, and Ralf Galuske. 2015. “Histological Validation of High-Resolution DTI in Human Post Mortem Tissue.” *Frontiers in Neuroanatomy* 9 (July): 98.
- Sepehrband, Farshid, Daniel C. Alexander, Nyoman D. Kurniawan, David C. Reutens, and Zhengyi Yang. 2016. “Towards Higher Sensitivity and Stability of Axon Diameter Estimation with Diffusion-Weighted MRI.” *NMR in Biomedicine* 29 (3): 293–308.
- Shepherd, Timothy M., Jeremy J. Flint, Peter E. Thelwall, Greg J. Stanisz, Thomas H. Mareci, Anthony T. Yachnis, and Stephen J. Blackband. 2009. “Postmortem Interval Alters the Water Relaxation and Diffusion Properties of Rat Nervous Tissue — Implications for MRI Studies of Human Autopsy Samples.” *NeuroImage*.  
<https://doi.org/10.1016/j.neuroimage.2008.09.054>.
- Shepherd, Timothy M., Peter E. Thelwall, Greg J. Stanisz, and Stephen J. Blackband. 2009. “Aldehyde Fixative Solutions Alter the Water Relaxation and Diffusion Properties of Nervous Tissue.” *Magnetic Resonance in Medicine: Official Journal of the Society of Magnetic Resonance in Medicine / Society of Magnetic Resonance in Medicine* 62 (1): 26–34.
- Sibal, L. R., and K. J. Samson. 2001. “Nonhuman Primates: A Critical Role in Current Disease Research.” *ILAR Journal*. <https://doi.org/10.1093/ilar.42.2.74>.
- Sønderby, Casper K., Henrik M. Lundell, Lise V. Søgaaard, and Tim B. Dyrby. 2014. “Apparent Exchange Rate Imaging in Anisotropic Systems.” *Magnetic Resonance in Medicine: Official Journal of the Society of Magnetic Resonance in Medicine / Society of Magnetic Resonance in Medicine* 72 (3): 756–62.
- Spencer, Richard G., Kenneth W. Fishbein, Aiwu Cheng, and Mark P. Mattson. 2006. “Compatibility of Gd-DTPA Perfusion and Histologic Studies of the Brain.” *Magnetic Resonance Imaging* 24 (1): 27–31.
- Stanisz, G. J., A. Szafer, G. A. Wright, and R. M. Henkelman. 1997. “An Analytical Model of Restricted Diffusion in Bovine Optic Nerve.” *Magnetic Resonance in Medicine: Official Journal of the Society of Magnetic Resonance in Medicine / Society of Magnetic Resonance in Medicine* 37 (1): 103–11.
- Suárez, Laura E., Yossi Yovel, Martijn P. van den Heuvel, Olaf Sporns, Yaniv Assaf, Guillaume Lajoie, and Bratislav Misic. n.d. “A Connectomics-Based Taxonomy of Mammals.”  
<https://doi.org/10.1101/2022.03.11.483995>.
- Sun, Shu-Wei, Jeffrey J. Neil, Hsiao-Fang Liang, Yong Y. He, Robert E. Schmidt, Chung Y. Hsu, and Sheng-Kwei Song. 2005. “Formalin Fixation Alters Water Diffusion Coefficient Magnitude but Not Anisotropy in Infarcted Brain.” *Magnetic Resonance in Medicine: Official Journal of the Society of Magnetic Resonance in Medicine / Society of Magnetic Resonance in Medicine* 53 (6): 1447–51.
- Takahashi, Emi, Guangping Dai, Glenn D. Rosen, Ruopeng Wang, Kenichi Ohki, Rebecca D. Folkerth, Albert M. Galaburda, Van J. Wedeen, and P. Ellen Grant. 2011. “Developing Neocortex Organization and Connectivity in Cats Revealed by Direct Correlation of Diffusion Tractography and Histology.” *Cerebral Cortex* 21 (1): 200–211.
- Tax, Chantal M. W., Filip Szczepankiewicz, Markus Nilsson, and Derek K. Jones. 2020. “The Dot-Compartment Revealed? Diffusion MRI with Ultra-Strong Gradients and Spherical Tensor Encoding in the Living Human Brain.” *NeuroImage* 210 (April): 116534.
- Tendler, Benjamin C., Feng Qi, Sean Foxley, Menuka Pallegage-Gamarallage, Ricarda A. L. Menke, Olaf Ansorge, Samuel A. Hurley, and Karla L. Miller. 2021. “A Method to Remove the Influence of Fixative Concentration on Postmortem T2 Maps Using a Kinetic Tensor

- Model." *Human Brain Mapping* 42 (18): 5956–72.
- Thelwall, Peter E., Timothy M. Shepherd, Greg J. Stanisiz, and Stephen J. Blackband. 2006. "Effects of Temperature and Aldehyde Fixation on Tissue Water Diffusion Properties, Studied in an Erythrocyte Ghost Tissue Model." *Magnetic Resonance in Medicine: Official Journal of the Society of Magnetic Resonance in Medicine / Society of Magnetic Resonance in Medicine* 56 (2): 282–89.
- The Squirrel Monkey in Biomedical and Behavioral Research*. 2000.
- Thomas, Cibu, Frank Q. Ye, M. Okan Irfanoglu, Pooja Modi, Kadharbatcha S. Saleem, David A. Leopold, and Carlo Pierpaoli. 2014a. "Anatomical Accuracy of Brain Connections Derived from Diffusion MRI Tractography Is Inherently Limited." *Proceedings of the National Academy of Sciences of the United States of America* 111 (46): 16574–79.
- . 2014b. "Anatomical Accuracy of Brain Connections Derived from Diffusion MRI Tractography Is Inherently Limited." *Proceedings of the National Academy of Sciences of the United States of America* 111 (46): 16574–79.
- Tournier, J-Donald, Robert Smith, David Raffelt, Rami Tabbara, Thijs Dhollander, Maximilian Pietsch, Daan Christiaens, Ben Jeurissen, Chun-Hung Yeh, and Alan Connelly. 2019. "MRtrix3: A Fast, Flexible and Open Software Framework for Medical Image Processing and Visualisation." *NeuroImage* 202 (November): 116137.
- Tsang, Tin Ki, Eric A. Bushong, Daniela Boassa, Junru Hu, Benedetto Romoli, Sebastien Phan, Davide Dulcis, Chih-Ying Su, and Mark H. Ellisman. 2018. "High-Quality Ultrastructural Preservation Using Cryofixation for 3D Electron Microscopy of Genetically Labeled Tissues." *eLife* 7 (May). <https://doi.org/10.7554/eLife.35524>.
- Ullmann, Jeremy F. P., Charles Watson, Andrew L. Janke, Nyoman D. Kurniawan, and David C. Reutens. 2013. "A Segmentation Protocol and MRI Atlas of the C57BL/6J Mouse Neocortex." *NeuroImage* 78 (September): 196–203.
- Veraart, Jelle, Trygve B. Leergaard, Bjørnar T. Antonsen, Wim Van Hecke, Ines Blockx, Ben Jeurissen, Yi Jiang, et al. 2011. "Population-Averaged Diffusion Tensor Imaging Atlas of the Sprague Dawley Rat Brain." *NeuroImage* 58 (4): 975–83.
- Veraart, Jelle, Dmitry S. Novikov, Daan Christiaens, Benjamin Ades-Aron, Jan Sijbers, and Els Fieremans. 2016. "Denoising of Diffusion MRI Using Random Matrix Theory." *NeuroImage* 142 (November): 394–406.
- Veraart, Jelle, Daniel Nunes, Umesh Rudrapatna, Els Fieremans, Derek K. Jones, Dmitry S. Novikov, and Noam Shemesh. 2020. "Noninvasive Quantification of Axon Radii Using Diffusion MRI." *eLife* 9 (February): e49855.
- Vos, Sjoerd B., Chantal M. W. Tax, Peter R. Luijten, Sebastien Ourselin, Alexander Leemans, and Martijn Froeling. 2017a. "The Importance of Correcting for Signal Drift in Diffusion MRI." *Magnetic Resonance in Medicine*. <https://doi.org/10.1002/mrm.26124>.
- . 2017b. "The Importance of Correcting for Signal Drift in Diffusion MRI." *Magnetic Resonance in Medicine: Official Journal of the Society of Magnetic Resonance in Medicine / Society of Magnetic Resonance in Medicine* 77 (1): 285–99.
- Vučković, Ivan, Tarek Nayfeh, Prasanna K. Mishra, Sigapriya Periyaran, Caroline R. Sussman, Timothy L. Kline, and Slobodan Macura. 2020. "Influence of Water Based Embedding Media Composition on the Relaxation Properties of Fixed Tissue." *Magnetic Resonance Imaging* 67 (April): 7–17.
- Walker, Matthew R., Jidan Zhong, Adam C. Waspe, Thomas Looi, Karolina Piorkowska, James M. Drake, and Mojgan Hodaie. 2019. "Acute Ex Vivo Changes in Brain White Matter Diffusion Tensor Metrics." *PloS One* 14 (9): e0223211.
- Wang, Hui, Junfeng Zhu, Martin Reuter, Louis N. Vinke, Anastasia Yendiki, David A. Boas,

- Bruce Fischl, and Taner Akkin. 2014. "Cross-Validation of Serial Optical Coherence Scanning and Diffusion Tensor Imaging: A Study on Neural Fiber Maps in Human Medulla Oblongata." *NeuroImage* 100 (October): 395–404.
- Wang, Nian, Leonard E. White, Yi Qi, Gary Cofer, and G. Allan Johnson. 2020. "Cytoarchitecture of the Mouse Brain by High Resolution Diffusion Magnetic Resonance Imaging." *NeuroImage* 216 (August): 116876.
- Wang, Xiaojie, Matthew F. Cusick, Yong Wang, Peng Sun, Jane E. Libbey, Kathryn Trinkaus, Robert S. Fujinami, and Sheng-Kwei Song. 2014. "Diffusion Basis Spectrum Imaging Detects and Distinguishes Coexisting Subclinical Inflammation, Demyelination and Axonal Injury in Experimental Autoimmune Encephalomyelitis Mice." *NMR in Biomedicine* 27 (7): 843–52.
- Wehrl, Hans F., Ilja Bezrukov, Stefan Wiehr, Mareike Lehnhoff, Kerstin Fuchs, Julia G. Mannheim, Leticia Quintanilla-Martinez, et al. 2015. "Assessment of Murine Brain Tissue Shrinkage Caused by Different Histological Fixatives Using Magnetic Resonance and Computed Tomography Imaging." *Histology and Histopathology* 30 (5): 601–13.
- Winkler, Simone A., Franz Schmitt, Hermann Landes, Joshua de Bever, Trevor Wade, Andrew Alejski, and Brian K. Rutt. 2018. "Gradient and Shim Technologies for Ultra High Field MRI." *NeuroImage* 168 (March): 59–70.
- Wu, Dan, Lee J. Martin, Frances J. Northington, and Jiangyang Zhang. 2014. "Oscillating Gradient Diffusion MRI Reveals Unique Microstructural Information in Normal and Hypoxia-Ischemia Injured Mouse Brains." *Magnetic Resonance in Medicine: Official Journal of the Society of Magnetic Resonance in Medicine / Society of Magnetic Resonance in Medicine* 72 (5): 1366–74.
- Xiao, Jaclyn, Kathryn J. Hornburg, Gary Cofer, James J. Cook, Forrest Pratson, Yi Qi, and G. Allan Johnson. 2021. "A Time-Course Study of Actively Stained Mouse Brains: Diffusion Tensor Imaging Parameters and Connectomic Stability over 1 Year." *NMR in Biomedicine*, September, e4611.
- Xu, Junzhong, Hua Li, Kevin D. Harkins, Xiaoyu Jiang, Jingping Xie, Hakmook Kang, Mark D. Does, and John C. Gore. 2014. "Mapping Mean Axon Diameter and Axonal Volume Fraction by MRI Using Temporal Diffusion Spectroscopy." *NeuroImage* 103 (December): 10–19.
- Yan, Mingchao, Wenwen Yu, Qian Lv, Qiming Lv, Tingting Bo, Xiaoyu Chen, Yilin Liu, et al. 2022. "Mapping Brain-Wide Excitatory Projectome of Primate Prefrontal Cortex at Submicron Resolution and Comparison with Diffusion Tractography." *eLife* 11 (May). <https://doi.org/10.7554/eLife.72534>.
- Zhang, Hui, Torben Schneider, Claudia A. Wheeler-Kingshott, and Daniel C. Alexander. 2012. "NODDI: Practical in Vivo Neurite Orientation Dispersion and Density Imaging of the Human Brain." *NeuroImage*. <https://doi.org/10.1016/j.neuroimage.2012.03.072>.
- Zhang, Jiangyang, Melina V. Jones, Michael T. McMahon, Susumu Mori, and Peter A. Calabresi. 2012. "In Vivo and Ex Vivo Diffusion Tensor Imaging of Cuprizone-Induced Demyelination in the Mouse Corpus Callosum." *Magnetic Resonance in Medicine*. <https://doi.org/10.1002/mrm.23032>.
- Zhang, Jiangyang, Qi Peng, Qing Li, Neda Jahanshad, Zhipeng Hou, Mali Jiang, Naoki Masuda, et al. 2010. "Longitudinal Characterization of Brain Atrophy of a Huntington's Disease Mouse Model by Automated Morphological Analyses of Magnetic Resonance Images." *NeuroImage* 49 (3): 2340–51.